INVADOPODIA FORMATION ON NANOMETER SCALE PROTEIN PATTERNS

A Thesis Submitted to
The Graduate School of Engineering and Sciences of
Izmir Institute of Technology
in Partial Fulfillment of the Requirements for the Degree of

MASTER OF SCIENCE

in Biotechnology and Bioengineering

by
Gizem BATI

December 2014
IZMIR

We approve the thesis of **Gizem BATI**

Examining Committee Members:

Assoc. Prof. Dr. Devrim PESEN OKVUR
Department of Molecular Biology and Genetics, Izmir Institute of Technology

Prof. Dr. Lütfi ÖZYÜZER
Department of Physics, Izmir Institute of Technology

Assist. Prof. Dr. Gülistan MEŞE ÖZÇİVİCİ
Department of Molecular Biology and Genetics, Izmir Institute of Technology

Prof. Dr. Volga BULMUŞ
Department of Chemical Engineering, Izmir Institute of Technology

Prof. Dr. Ahmet KOÇ
Department of Molecular Biology and Genetics, Izmir Institute of Technology

18 December 2014

Assoc. Prof. Dr. Devrim PESEN OKVUR
Supervisor, Department of Molecular Biology and Genetics, Izmir Institute of Technology

Prof. Dr. Lütfi ÖZYÜZER
Co-Supervisor, Department of Physics, Izmir Institute of Technology

Prof. Dr. Volga BULMUŞ
Head of the Department of Biotechnology and Bioengineering

Prof. Dr. Bilge KARAÇALI
Dean of the Graduated School of Engineering and Sciences

ACKNOWLEDGEMENTS

I would like to express my deepest appreciation and thanks to supervisor Assoc. Prof. Dr. Devrim PESEN OKVUR for her patience, encouragement, understanding, guidance and excellent support throughout this study.

I am thankful to co-supervisor Prof. Dr. Lütfi ÖZYÜZER for Electron Beam Lithography support.

I would like to thank also the members of my thesis defense committee Assist. Prof. Dr. Gülistan MEŞE ÖZÇİVİCİ and Prof. Dr. Volga BULMUŞ for helpful comments and giving suggestions.

As teamwork is essential, I am very thankful to the members of the Controlled *in vitro* Microenvironments (C*iv*Ms) laboratory for their team spirit and support.

I would like to thank to my friends and colleagues Berrin ÖZDİL, Utku HORZUM, Tuğçe CANAVAR, Tutku YARAŞ, Merve TÜRKER, Ece SOMUNCULAR, Emre TARIM, Murat SAĞLAM and İlayda BAĞCI for their support, help and friendship.

I would like to thank to especially Umur AYAZ for his love and support.

Finally, I would like to express my gratitude and love to my family has always supported and encouraged me.

ABSTRACT

INVADOPODIA FORMATION ON NANOMETER SCALE PROTEIN PATTERNS

How the positions of invadopodium in the cell are determined and if they have an adhesivefunction are not known. Using fluorescence microscopy and antibodies that recognize actin, cortactin and MT1-MMP proteins, invadopodia formed by breast cancer cells plated on protein nanopatterns of different geometeries and components after stimulation with epidermal growth factor which is known to induce invadopodia formation, were examined. Invadopodia formation was studied for the first time on nanometer scale, single and double active component, protein patterns with equal distance and gradient spacings. The results show that:

• On K-casein-fibronectin nanopatterns, invadopodia prefer to form on K-casein which blocks cell adhesion rather than on fibronectin nanodots which promote cell adhesion.

• On Laminin-fibronectin nanopatterns, invadopodia prefer to form on laminin rather than on fibronectin nanodots.

• On gradient patterns, invadopodia prefer areas with wide spacings.

These results support the hypotheses that the positions where invadopodia form can be determined by surface protein nanopatterns and that cell adhesion is not required at points where invadopodia will form.

ÖZET

NANOMETRE ÖLÇEĞİNDEKİ PROTEİN DESENLERİ ÜZERİNDE İŞGALCİ AYAK OLUŞUMU

İşgalci-ayakların oluşacakları yerlerin nasıl belirlendiği ve yapışma işlevlerinin olup olmadıkları bilinmemektedir. Farklı geometrilerde ve bileşimlerdeki protein nanodesenleri üzerine ekilen meme kanseri hücreleri, işgalci-ayak oluşumunu sağladığı bilinen epidermal büyüme etkeni ile uyarılması ile oluşturdukları işgalci-ayaklar, aktin, kortaktin ve MT1-MMP proteinlerini tanıyan antikorlarla boyanarak floresan mikroskopta incelenmiştir. İşgalci-ayak oluşumu ilk defa nanometre ölçeğinde hem tek hem de çift aktif bileşenli, hem eşit aralıklı hem de değişken aralıklı protein desenleri üzerinde incelenmiştir. Sonuçlar gösteriyor ki:

• K-kazein-fibronektin nanodesenlerinde, işgalci-ayaklar hücre yapışmasını sağlayanfibronektin nanonoktaları üzerinde değil, hücre yapışmasını engelleyen k-kazein alanlarındaoluşmayı tercih ederler.

• Laminin-fibronektin nanodesenlerinde, işgalci-ayaklar fibronektin nanonoktaları üzerinde değil, laminin alanlarında oluşmayı tercih ederler.

• Değişken aralıklı desenlerde işgalci-ayaklar geniş aralıklı alanları tercih ederler.

Bu sonuçlar, işgalci-ayakların oluşacağı yerlerin yüzeylerdeki protein nanodesenleri ilebelirlenebildiği hipotezini ve işgalci-ayakların oluşacağı noktalarda hücrenin yüzeye yapışmasının gerekli olmadığı hipotezini desteklemektedir.

To my family…

TABLE OF CONTENTS

LIST OF FIGURES

Figure **Page**

LIST OF TABLES

Table **Page**

CHAPTER 1

INTRODUCTION

1.1. Metastasis

The leading cause of death in cancer patients is metastasis. Metastasis defines both the process of spreading of cancer cells from the primary tumor and the resulting secondary tumors. The primary tumor changes its place (meta + statis) and new tumors form at distant sites. During metastasis of carcinoma (cancer of epithelial tissue), tumor cells proliferate in an uncontrolled fashion, induce angiogenesis (new blood vessel formation), degrade the underlying basement membrane and penetrate into the connective tissue, migrate towards blood vessels, intravasate (enterblood vessels), survive in the blood circulation, extravasate (exit blood vessels), and form secondary tumors in distant organs (Figure 1A). Therefore, cancer metastasis is a disease of altered cell adhesion, motility, and invasion.

1.2. Definition of Invadopodia

Under physiological conditions such as bone resorption, cells invade into tissues in a tightly regulated manner. Normal bone osteoclasts form special cellular structurescalled podosomes to degrade and thus remodel the bone matrix. During cancer metastasis, tumor cells perform uncontrolled invasion using cellular structures called invadopodia (Figure 1B). The term invadopodia was firstused by Chen (1989) to describe membrane protrusions involved in the local degradation of the extracellular matrix. After 25 years, the field has grown to be complexand rather complicated even in terms of definitions. There are three major structures in cells, each of which can be definedin terms of their molecular components and the functions they carry out. These are focal adhesions, podosomes, and invadopodia. They do have similarities, but they are also distinct from one another. In attempts to clear up some of the confusion, podosomes and invadopodia have also been collectively called invadosomes. Although focal adhesions do share common protein markers with podosomes, they were thought

to be more distinct from podosomes and invadopodia; however, recently proteolytic activity hasalso been observed for these structures, further blurring the borders between the definitions of these structures (McNiven, 2013). Available data raise the question of whether focal adhesions, podosomes, and invadopodia share a common precursor. A conservative comparison of focal adhesions, podosomes, and invadopodia is presented in the Table 1. There are also several reviews and milestone papers describing in detail various aspects summarized here (Ayala et al., 2006; Gimona and Buccione, 2006; Linder, 2007; Gimona et al., 2008; Caldieriet al., 2009; Linder, 2009; Yilmaz and Christofori, 2009; Linder et al., 2011a, 2011b; Murphy and Courtneidge, 2011; Oser et al., 2011; Yamaguchi, 2012). In particular, there are comprehensive reviews on the signaling mechanisms involved (Stylli et al., 2008; Destaing et al., 2011; Hoshino et al., 2013).

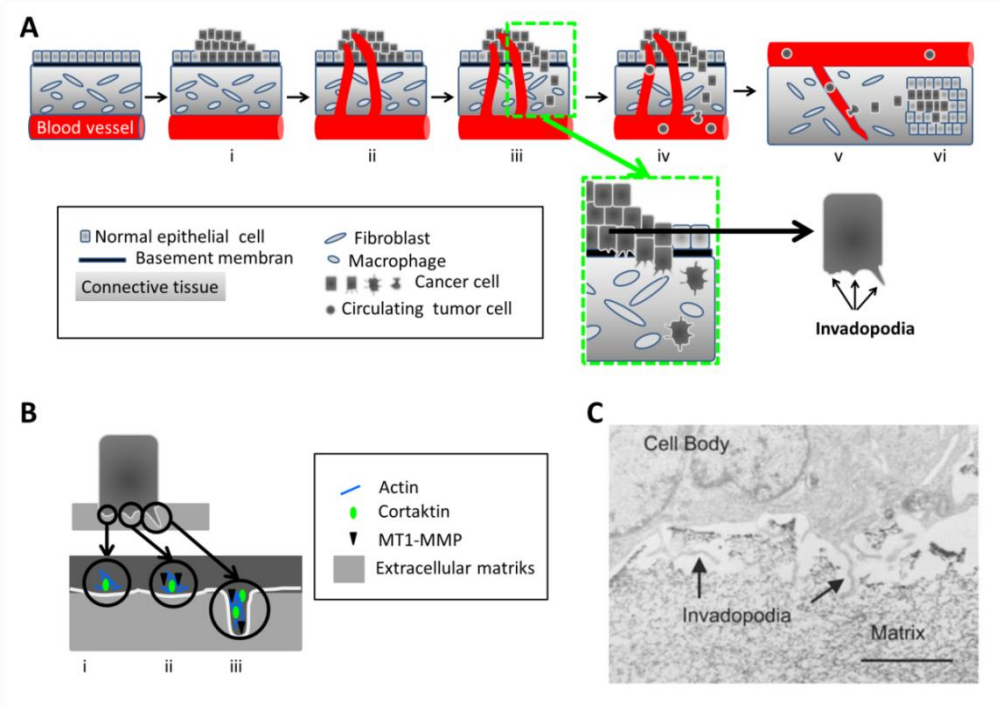

Figure 1.1. Metastasis and Invadopodia
(Source: Batı and Pesen Okvur, 2014)

A. Metastasis comprises (i) uncontrolled proliferation, (ii) angiogenesis, (iii) invasion, (iv) intravasation, (v) extravasation, and (vi) secondary tumor formation. Invasion involves matrix degradation carried out by invadopodia. B. Invadopodiaform and mature atmultiple stages: (i) initiation, (ii) stabilization, and (iii) maturation (see

also Figure 1.3). Initiation involves recruitment of actin and cortactin, MT1-MMP recruitment leads to stabilization. Maturation stage involves matrix degradation. When cells are on a thick matrix, invadopodia appear as membrane protrusions penetrating into the extracellular matrix. C. Electron micrograph of an MDA-MB-231 cell cultured ongelatin. The ultrastructure of invadopodia (arrows) is shown. Reprinted by permission from Macmillan Publishers Ltd: Oncogene (Bowden et al., 1999) copyright 1999.

Invadopodia are relatively dynamic, actin rich proteolytic cellular structures formed by invasive cancer cells (Bowden et al., 2006; Buccione et al., 2009; Linder,2009; Linder and Aepfelbacher, 2003) (Figure 1.2). Invadopodia can be from a few hundred nanometers to several microns wide and can be up to 8 micrometers if the underlying matrix is thick enough (Baldassarre et al.,2003). Invadopodia also form on stiff substrates such as glass and thus they can be studied with high resolution imaging (DesMarais et al., 2009). The molecular markers for invadopodia include actin and its associated proteins cortactin, Arp2/3, N-WASP, Nck1, and cofilin as well as matrix metalloproteinase MT1-MMP (Artym et al., 2006; Stylli et al., 2008; Oser et al., 2009, 2011). In addition, actin filaments, microtubules, and intermediate filaments cooperate during invadopodia elongation (Schoumacheret al., 2010). In melanoma cells, invadopodia contain α3β1 integrin at the core and α5β1 integrin at the periphery (Mueller et al., 1999). Integrins at invadopodia may function to signal and to focus degradation of the extracellular matrix (ECM) (Buccione et al., 2009; Muelleret al., 1999). However, it is unclear if invadopodia havean adhesive function as they lack vinculin (Gimona et al.,2008; Linder, 2009). That is, whether invadopodia require local adhesion at the sites of formation is unknown. Preliminary results from our lab using nano-patterned surfaces suggest that invadopodia do not require local adhesion (unpublished data). Experiments using nano and micro-patterned substrates can present valuable approaches to answer such questions and other aspects of invadopodia/podosome research such as dynamics of mechanical properties (Labernadie et al., 2010). In images of cells forming invadopodia, the Golgi complex appears to be polarized and juxtaposed to the site of invadopodia, suggesting a link between proteolytic activity and membrane transport (Baldassarre et al.,2003; Buccione et al., 2009; Caldieri and Buccione, 2010). However, if and how the spatial positioning of invadopodia is controlled is not known. In addition, the position and orientation of the Golgi can be modulated by micrometer scale surface patterns (Thery et al., 2006). Therefore, if invadopodia are positionally linked to the Golgi, changing the position of

the Golgi by culturing cells on different micrometer scale surface patterns should also change the localization of invadopodia. Thus micropatterned substrates present themselves as valuable tools for the question at hand.

	Focal adhesions	**Podosomes**	**Invadopodia**
Cell type	virtually all cells	osteoclasts, macrophages, endothelial cells, smooth muscle cells	cancer cells
Function	adhesion, matrix degradation?	matrix degradation	matrix degradation
Cellular localization	cell periphery	distributed	leading edge and proximal to golgi
Composition	Actin Vinculin Talin Paxillin Focal adhesion kinase Integrin	Actin Vinculin WASP Grb2 MT1-MMP	Actin Arp2/3 Cortactin N-WASP Nck1 Cofilin Tks5 MT1-MMP
Shape	ellipse	ring	dot
Size	< 20 μm	< 1 μm x 4 μm	< 8 μm x 5 μm
Number per cell	< 400	20-100	1-40
Stability/ Persistance	stable/ several hours	highly dynamic/ 2 – 12 min	dynamic/ up to 3 hrs

Table 1.1. Comparison of Focal Adhesions, Podosomes, and Invadopodia. (Source: Batı and Pesen Okvur, 2014)

1.3. Upstream of Invadopodia

Growth factors act as intercellular signaling molecules that promote various processes such as cell growth, proliferation, differentiation, and motility. In addition, growth factor receptors and integrins are known to crosstalk (Moro et al., 2002; Yamada and Even-Ram, 2002; Alamet al., 2007; Gilcrease, 2007). Growth factors can be soluble, transmembrane, or ECM bound proteins (Ruoslahti et al.,1992; Massague and Pandiella, 1993; Taipale and Keski-Oja,1997). Epidermal growth factor (EGF) is 1 of the 7 ligandsof EGF receptor (EGFR also known as ErbB1), which is in turn the most studied member of the ErbB receptor family (Cohen, 1962; Carpenter and Cohen, 1990; Harriset al., 2003; Singh and Harris, 2005). Furthermore, EGFR expression correlates with poor prognosis in breast cancer (Sainsbury et al., 1985; Lewis et al., 1990; Memon et al.,2006). EGF is known to induce motility and invadopodia formation in breast cancer cells (Yamaguchi et al., 2005). However, whether EGFR is present at invadopodia and acts directly and locally or not is not known. In terms of signal transduction, growth factor receptor tyrosine kinase and integrin initiated upstream events have been shown to promote invadopodia formation through phosphorylation of cortactin via a Src and Arg dependent pathway (Stylli et al., 2008; Oser et al., 2010; Destainget al., 2011; Mader et al., 2011; MacGrath and Koleske,2012). β1 integrin has been shown to promote metastasis, invadopodia maturation, and matrix degradation through Arg (Beaty et al., 2013). Local changes in pH induced by NHE1 are also shown to regulate cortactin phosphorylation (Magalhaes et al., 2011). Furthermore, small GTPases are shown to be spatiotemporally regulated at invadopodia where RhoC is inactivated at the center ofinvadopodia and is activated at its periphery so that cofilin is active at the center and is inactive at the periphery (Bravo-Cordero et al., 2011, 2012). Here, RhoC is shown to act through ROCK, which phosphorylates LIMK, which in turn phosphorylates and inactivates cofilin.

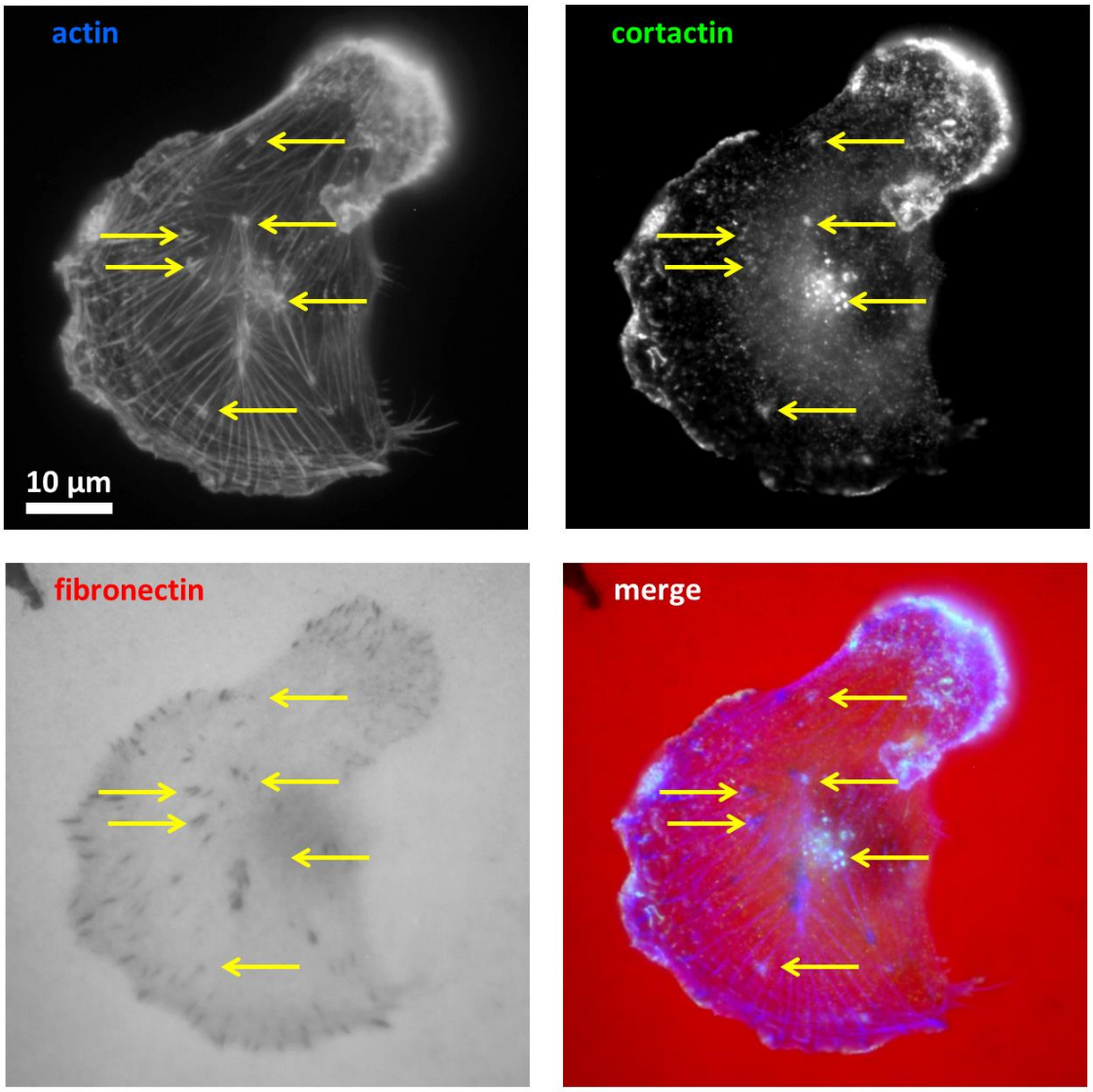

Figure 1.2. Immunofluorescence Images of Invadopodia in MDA-MB-231 Breast Cancer Cells Cultured on Fibronectin, An Extracellular Matrix Protein. (Source: Batı and Pesen Okvur, 2014)

Yellow arrows point to invadopodia. Cortactin and actin colocalize at invadopodia. At mature invadopodia, the underlying matrix of fibronectin is also degraded. Cortactin (green), actin (blue), fibronectin (red).

1.4. An Integrated Model of Invadopodia

Over the years, valuable research has produced models that describe invadopodia. An integrated model is presented in Figure 1.3. One of the early studies classified invadopodia formation into 4 stages: I. Invadopodia initiation, II. Preinvadopodia, III. Mature invadopodia, and IV. Late invadopodia. Cortactin levels are at their maximum atstages II and III and subside afterwards, while actin levelsreach a peak at stage III. MT1-MMP reaches a maximum at stage II and is stable thereafter, while matrix degradation saturates at stage III (Artym et al., 2006). Later on, a more detailed model was presented by Oser et al. (2009), pointing out the central role of cortactin in invadopodia. Here, cortactin was shown to regulate cofilin and N-WASP activities and thus control the stages of invadopodia formation. Four stages were redefined here: Stage I – Precursor formation: Cortactin, N-WASP, cofilin, and Arp2/3 form a complex. Stage II – Activation of actin polymerization: Nck1 joins the precursor complex while phosphorylation of cortactin activates cofilin's severing activity, which in turn provides free barbed ends for Arp2/3 for new actin polymerization. Stage III– Stabilization: Cortactin is dephosphorylated, cofilin re-joins the complex, and invadopodia precursors are stabilized. Stage IV – ECM degradation: MT1-MMP is recruited to invadopodia and ECM is degraded. The model by Oser et al. was then refined in terms of involvement of Tks5 and SHIP2, which are shown to be required for invadopodia maturation but not initiation (Sharma et al., 2013). The integrated model we present here comprises 3 stages: initiation, stabilization, and maturation. Initiation here describes a combination of the previously described stages I and II and involves structural complex formation and actin polymerization. Stabilization includes MMP recruitment. At the maturation stage, MMPs are activated and matrix degradation takes place. To recapitulate, the first events in the signal transduction pathways that result in invadopodia formation are integrin and/or growth factor activation. Although the intermediates are not entirely known, activation of Src is the key event for invadopodia formation. Src in turn activates Arg, which phosphorylates cortactin. While unphosphorylated cortactin, unphosphrylated the maturation stage MT1-MMP is activated and matrix degradation takes place.

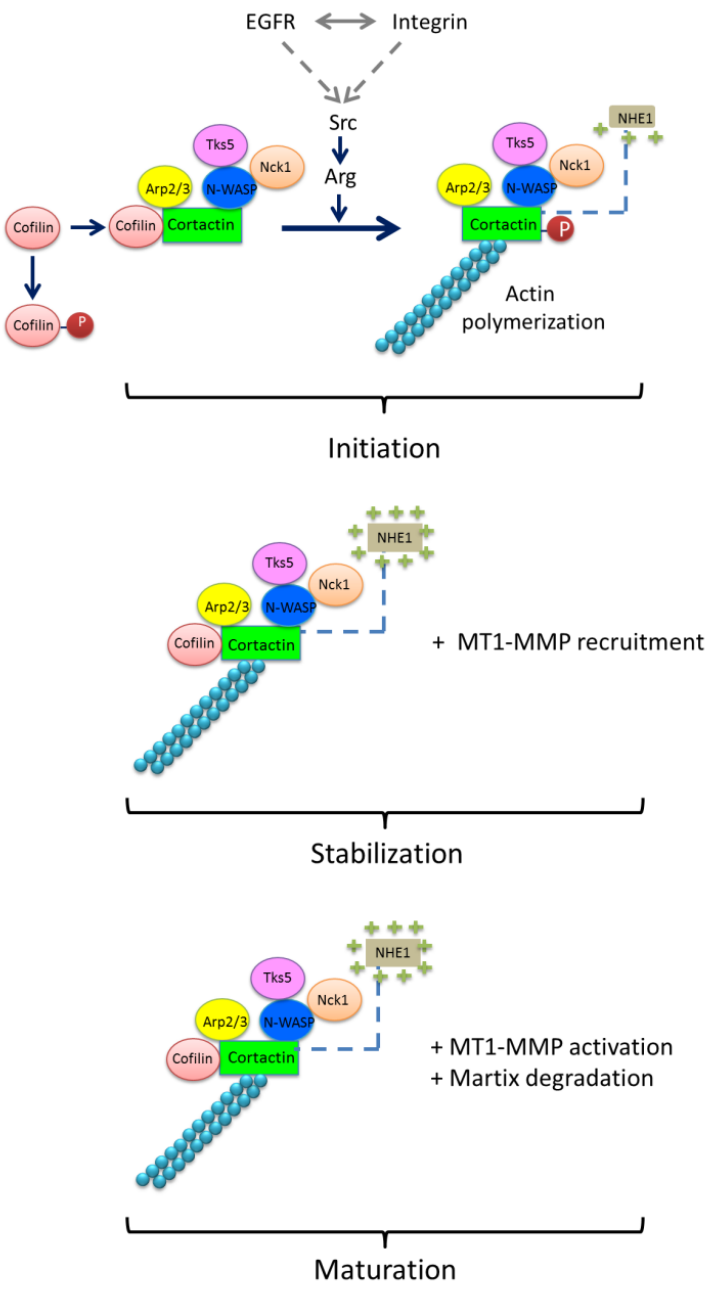

Figure 1.3. Integrated Model for The Initiation, Stabilization, and Maturation of Invadopodia. (Source: Batı and Pesen Okvur, 2014)

Presented is a combination of various models published in the literature through the years. Initiation: Growth factor and/or integrin initiated signaling cascades result in phosphorylation of cortactin by Arg, which in turn is activated by Src. Phosphorylation of cortactin releases cofilin from the invadopodial complex comprising Arp2/3, N-WASP, Nck1, and Tks5. Release of cofilin promotes actin polymerization. Stabilization: Cortactin is dephosphorylated and cofilin is rerecruitedto the complex.

NHE1 induces local decrease in pH and MT1-MMP is recruited. Maturation: MT1-MMP is activated and matrix degradation takes place.

1.5. Technical Bottlenecks for Research on Invadopodia

A technical limitation for research on invadopodia has been the limited number of assays for proteolytic activity. Fluorescently labeled gelatin or fibronectin is commonly used in addition to DQ-collagen, which becomes fluorescent upon degradation. In addition, Packard et al. (2009) have used a substrate that shows sites of degradation by MT1-MMP. Fluorogenic peptide substrates have alsobeen utilized to assay matrix degradation by MMPs (Leightet al., 2013). The field would greatly benefit from novel assays that allow the determination of matrix degradation, particularly for 3D culture and in vivo settings. Another bottleneck has been the difficulty in analyzing invadopodia in a quantitative manner. Counting invadopodia in a cell or in a field of view based on colabeling of actin and cortactin, for instance, requires either brute force of manual counting or elegant image processing approaches. An alternative approach has been to quantify the area of matrix degraded by invadopodia rather than counting individual structures (Li et al., 2010a). Well designed image processing approaches would be greatly beneficial for research on invadopodia.

1.6. Conclusions and Open Questions

In conclusion, while our understanding of invadopodia continues to improve despite confusion even at the definitions level, the field requires the incorporation of new technologies and there are many open questions waiting to be answered, such as: Do focal adhesions, podosomes, and invadopodia share a common precursor? Do invadopodia have an adhesive function? How is the cellular localization of invadopodia controlled? Is EGFR present at invadopodia and does it act directly or indirectly? How can we better assay the proteolytic activity of invadopodia? How can we improve the quantitative analysis of invadopodia? How can we better exploit upstream regulators and structural components of invadopodia for the diagnosis and therapy of cancer?

CHAPTER 2

MATERIALS AND METHODS

2.1. Cell Culture

MDA-MB-231 cell line was used in this project. DMEM (High glucose DMEM) that contains 10% serum was used to supply essential medium for MDA-MB-231 cells. During the preparation 450 ml of DMEM (Dulbecco's Modified Eagle's Medium-Biological Industries-01-055-1A), 50 ml fetal bovine serum (Biological Industries), 5 ml of Penisilin Streptomisin (Biological Industries-03-031-1B), 5 ml L-glutamin (Biological Industries-03-020-1B) are mixed and filtered. Finally, this mixture was used as a medium.

500 ml Leibovitz's (1X) (GIBCO by life technologies-21083-027-500 ml) and 1,725 gram albumin bovine serum (Sigma-A9418-5G) are mixed and used as a medium for the experiments were set at the basal conditions. It is abbreviated as L15-BSA. L15-BSA was used for cells during the starvation conditions.

Cell culture was done in the laminar flow cabinet (Thermo Scientific MSC1.2 and Nüve MN120). Cells were placed into incubator (Binder and ThernoScientific 3404) to provide the balance of CO_2 and temperature. Inverted phase-contrast microscope (Olympus CKX41) was used to observe during cell culture.

2.1.1. Cell Culture of MDA-MB-231 Breast Cancer Cells

MDA-MB-231 cells were used between 30 and 50 passage number.

2.1.1.1. Thawing of MDA-MB-231 Breast Cancer Cell line

Firstly, a certain amount of medium was put into the petri dish and placed into the incubator for the balance of temperature and CO_2. Cryo tube was taken from liquid nitrogen tank (Thermo Scientific Locator JR Plus) and holded in the water bath (Nüve bath nb2) whose temperature was arranged to 37°C. After the thawing of cell mix

solution, all solution was transfered into falcon tube and final volume completed to 10 ml with medium. Then 1000 rpm spin was applied for 5 minutes (Nüve bench top centrifuge NF 400R) so cells were precipitated to leave from DMSO. Cells were at the bottom of the falcon as a pellet at the end of the centrifuge and then solution was removed by vacuum. Cells were dissolved into fresh medium and added into petri dish that was placed into incubator previously. After the cell thawing process, cells were reached routine conditions in one and half week. Cells were passaged three times in a week periodically.

2.1.1.2. Passage Process for MDA-MB-231 Breast Cancer Cells

After seeding of cells, petri dishes were observed under the microscope every other day. Cells with 80% confluence in the petri dish were used for passage.

Firstly, a certain medium was added into petri dish (Treated CORNING) and placed into incubator to provide balance of CO_2 and temperature. All passage process was completed in the laminar flow cabinet. Medium in petri dish was aspirated and surface of petri dish rinsed with 2 ml Trypsin. Then 4 ml Trypsin was added to remove cells from the surface. This petri dish was holded into incubator for 3 minutes to action of enzyme efficiently. At the end of 3 minutes, cells were observed under the microscope and taken into laminar flow cabinet. 1 ml medium with serum was added into cells to stop the enzyme activation and the petri dish surface were washed with the solution 5-6 times in the petri dish. Same washing process was applied to cells with 5 ml medium to remove all cells from the petri dish surface to the falcon tube. 1000 rpm spin was applied to total of 10 ml solution for precipitation of cells. At the end of the centrifuge process, all solution was aspirated by vacuum and cells were dissolved in the fresh medium. Finally, cells were added into petri dish which was placed into incubator previously.

2.1.1.3. Freezing Process of MDA-MB-231 Breast Cancer Cells

After the cell passage process, cell precipitation was dissolved into 7% DMSO for freezing process and total solution was transferred into cryo tubes. These cryo tubes were placed into cell freezing tank which was filled with isopropanol at -80°C for a week and cells were transfered into liquid nitrogen tank.

2.2. Chip Preparation

Silicon (Universal wafer) was used in experiments.

2.2.1. APTES (3-aminopropyltriethoxysilane) Coating

It was supplied to clean any kind of molecules from surface by using UV/ozone cleaning device without dissolution of coating in 3% acetone APTES solution. Hydrophobic surfaces were qualitatively determined by water drop test.

2.2.2. K-casein Coating on Silicon Surface

Firstly, chalets were rinsed with acetonefor cleaning of chips. Then silicones were placed on plastic carriers. The isopropanol were cleaned with acetone and water repeatedly by ultrasonic bath. Then silicones were dried with gas nitrogen. Silicon chips were exposed to UV/ozone for 10 minutes to remove any organic molecule. Then, 3% APTES were prepared in acetone solution foractivation of surface and silicon chips were incubated in this solution for 30 minutes. The silicon chips were washed with acetone and water repeatedly after incubation. Then silicon chips were dried under gas nitrogen and they were incubated in previously adjusted to 110°C oven (Nüve Dryheat Sterilizer) for 3 hours to dry them completely. The oven was closed and silicon chips were kept in the oven that cools down until next day. On the following day, silicon chips were first tested for APTES coating welded hydrophobicity. Each silicon chips were tested about 10 μm ultra pure water dropwise and drops were not seen to spread on glass. Then 1% Gluteraldehyde solution (Gluteraldehyde 70% solution EM grade

distillation prufied- Electron Microscopy Sciences) were prepared in 1X PBS and silicon chips were coated in this solution for one hour.

Basement surface of the petri dish was covered with parafilm. Aliquots of K-casein (1 mg/ml) about half an hour prior to use, heat from -80°C to +4°C had been increased. Coated surfaces of silicon chips were immersed in protein solution and left at 24 hours for culturing.

After 24 hours, silicon chips were rinsed with 1X UB three times and ultra pure water 3 times and then were dried under gas nitrogen. They were then stored under the vacuum until experiment.

2.2.3. Fibronectin Coating on K- casein Coated Silicon Surface

Fibronectin (Sigma F2006) coating: Lower surface of the petri dish was covered with parafilm. K- casein aliquots (1 mg/ml) about half an hour prior to use, heat from -80°C to +4°C had been increased. Final volume of 1 ml aliquots were completed with 1X UBand left onto the parafilm without pipetting. Coated surfaces of silicon were immersed in protein solution and left at 1 hour of incubation. After 1 hour, silicon chips were rinsed with 1X UB three times, with ultra distilled water three times and then they were dried under gas nitrogen. They were then stored under the vacuum until experiment. They were used within 2 weeks.

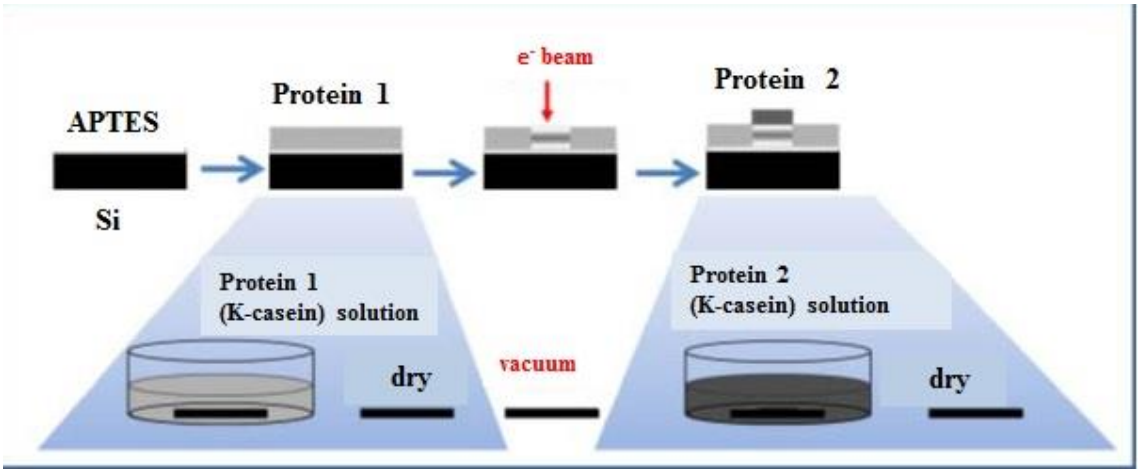

Figure 2.1. Creating Fibronectin Nanopatterns on K-casein Coated Surface.

The method in Firure 2.1 was used to form protein patterns on nanometer scale. Silicon (Si) surfaces were cleaned with oxygen plasma was used after drying the cleaning in ultrasonic bath of acetone and water respectively. In EBL method, firstly silicon surface was coated with APTES. Surface was left in 3% APTES in acetone followed by washing with acetone and water. APTES coating was completed by drying surface for three hours at 110°C. Then, K- casein solution was used to coat surface by keeping in this solution. K-casein, surfaces with 1 mg/ml K-casein (Global buffer solution: 150 mM NaCl, 5 mM TrisHCl, pH 7.6, 0.1% NaN_3) was incubated for three hours at ambient temperature or sixteen hours at +4°C. Surfaces were rinsed with global solution and dried with deionized water.

2.3. Test of Cells on Fibronectin and K-casein Surfaces

Cells were tested on K-casein and Fibronectin coated surfaces. CDB (cell dissociation buffer) was used instead of trypsin to observe the invadopodia formation via EGF (epidermal growth factor) stimulation on starved cells cultured for 24 hours. K-casein or fibronectin control surfaces were cleaned with 70% ethanol and rinsed with L-15 medium containing 0.35% BSA (bovine serum albumin). Certain volume of medium was added onto these clean control surfaces. Cells were waited in the starvation condition for one and half hour until EGF stimulation. Invadopodia formation was observed with MDA-MB-231 breast cancer cells cultured for 24 hours after EGF stimulation.

2.4. Cell Applications on Fibronectin Nanopatterns on K-casein Surfaces for Observation of Invadopodia Formation Experiments

Nanopatterns were created by electron beam lithography on K-casein surfaces and then these nanopatterns were coated with fibronectin under the optimized conditions. This surfaces were named “One Component”. Cell culture was applied onto one component surfaces. Then immunoflourescent staining was applied to detect invadopodia proteins (cortactin, actin) and pattern protein (fibronectin). For some samples, dylight marked fibronectin was used for coating of surfaces were created by EBL (Electron Beam Lithography). At this point, aim of used dylight fibronectin was

providing a facility for showing the locations where invadopodia was colocalized or not with focal adhesions thanks to immunoflourescent experiment to detect actin, vinculin and cortactin proteins together. In addition, detection of MT1-MMP, cortactin proteins in invadopodia was realized at the same time. Images were taken from fluorescent microscope and analyzed by using ImageJ programme.

2.5. DoubleActive Componenet on Silicon Surface

2.5.1. DoubleActive Componenet Patterning

Fibronectin was used as a first protein on silicon surface for double activecomponent patterning experiments. EBL was applied to laminin surface and then patterns were coated with fibronectin.

2.5.1.1. Pattern Coating with Laminin on Fibronectin Coated Silicon Surface

Fibronectin (F2006 Sigma) coating: Glass petri was coated with parafilm. Fibronectin aliquots (1 mg/ml) were taken from -80°C and holded at +4°C half hour ago before experiment. Aliquot final volume was completed to 1 ml with 1X UB by avoiding pipetting more than two times. Silicon surfaces were onto protein solution 1 h. At the end of the incubation silicon coated surface rinsed with 1X UB then rinsed with ultra pure water. Finally fibronectin coated sample was dried with gas nitrogen and protected under the vacuum until experiment for maximum 2 weeks.

Laminin (L2020 Sigma) coating: Glass petri was coated with parafilm. Laminin aliquots (1 mg/ml) were taken from -20°C and holded at +4°C half hour ago before experiment. Aliquot final volume was completed to 1 ml with 1X UB. Silicon surfaces were onto protein solution 1 h. At the end of the incubation silicon coated surface rinsed with 1X UB then rinsed with ultra pure water. Finally fibronectin coated sample was dried with gas nitrogen and protected under the vacuum until experiment for maximum 2 weeks.

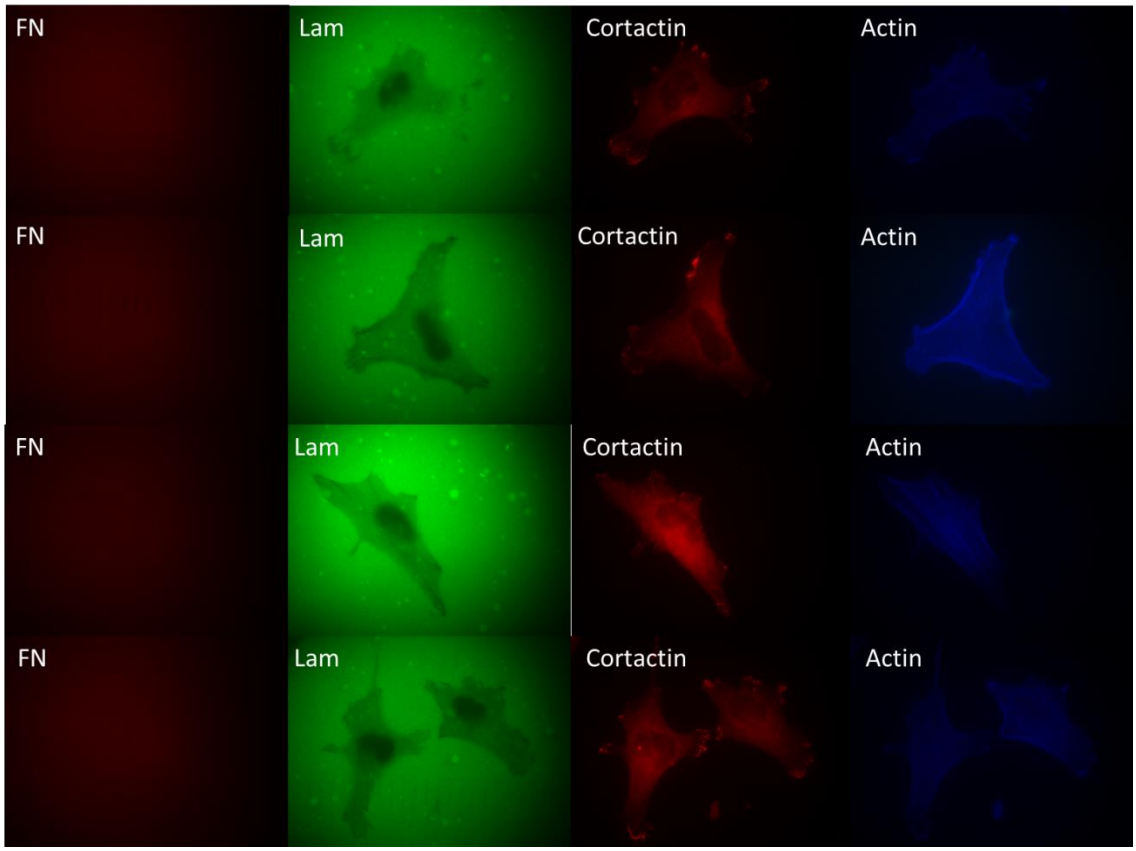

Figure 2.2. Cells on laminin coated patterns onto fibronectin coated silicon surfaces.

Silicon surface were coated with fibronectin. Then patterns were created onto fibronectin by EBL and patterns were coated with laminin. Fibronectin coating were performed well but laminin coating were failure so laminin coated patterns were not observed. Other option was pattern coating with fibronectin on laminin coated surface.

2.5.1.2. Pattern Coating with Fibronectin on Laminin Coated Silicon Surface

Laminin (L2020 Sigma) coating: Glass petri was coated with parafilm. Laminin aliquots (1 mg/ml) were taken from -20°C and holded at +4°C half hour ago before experiment. Aliquot final volume was completed to 1 ml with 1X UB. Silicon surfaces were onto protein solution 1 h. At the end of the incubation silicon coated surface rinsed with 1X UB then rinsed with ultra pure water. Finally fibronectin coated sample was dried with gas nitrogen and protected under the vacuum until experiment for maximum 2 weeks.

Fibronectin (F2006 Sigma) coating: Glass petri was coated with parafilm. Fibronectin aliquots (1 mg/ml) were taken from -80°C and holded at +4°C half hour ago before experiment. Aliquot final volume was completed to 1 ml with 1X UB by avoiding pipetting more than two times. Silicon surfaces were onto protein solution 1 h. At the end of the incubation silicon coated surface rinsed with 1X UB then rinsed with ultra pure water. Finally fibronectin coated sample was dried with gas nitrogen and protected under the vacuum until experiment for maximum 2 weeks.

Fibronectin was marked with dylight dye. Because fibronectin and laminin antibodies were produced same organism. Therefore there was not need immunoflourescent staining for fibronectin. This protein was labeled with dylight 650 and dylight 350. Dylight 350 is more useful so experiments were performed with this dylight protein.

2.6. Steps of Image Analyze for Invadopodia

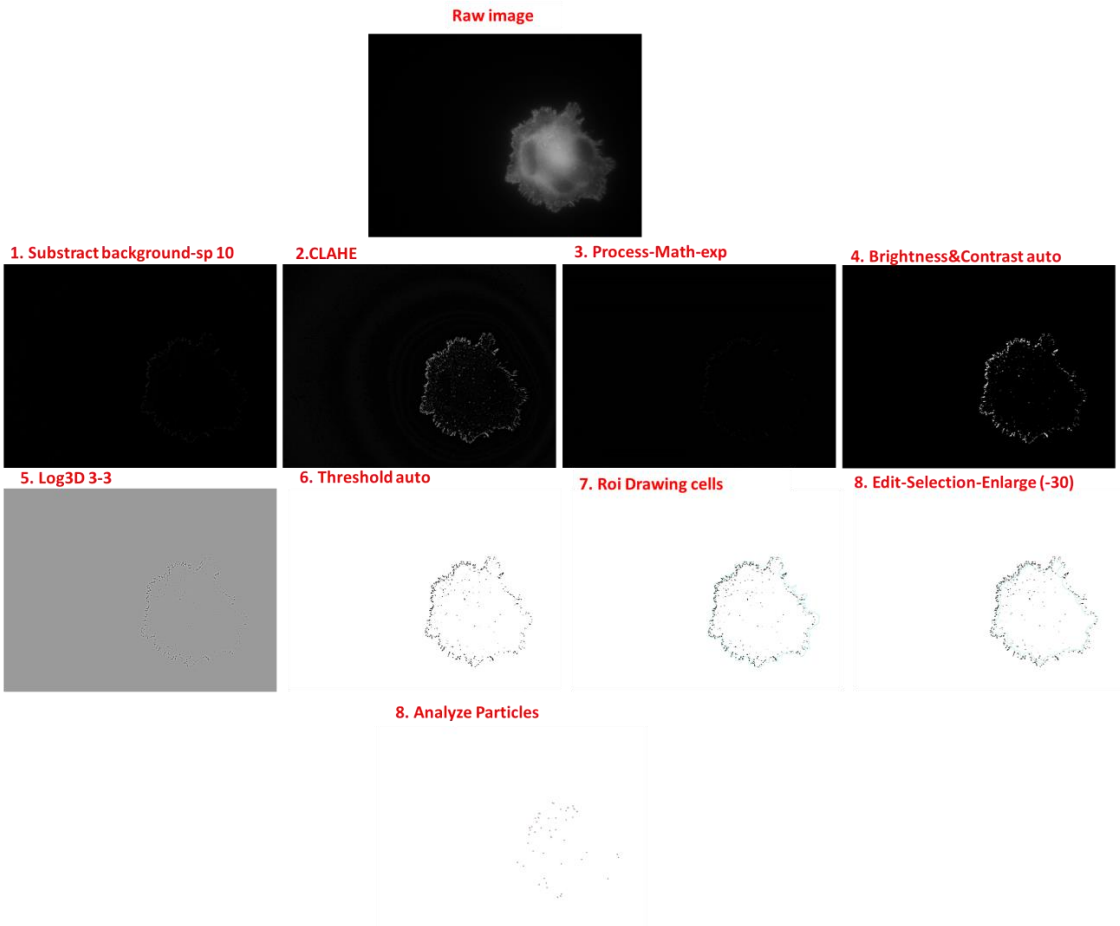

Figure 2.3. Steps of Image Analyze.

This figure shows raw image of a cell that was detected with cortactin protein by immunoflourescent experiment and steps of analyze were applied to the raw image by using ImageJ programme. RGB format images of fluorescent microscope were split into color channels. Images were taken 16-bit format from microscope but 8-bit format images were used for analyze process. Firstly, quantitative analyze of cortactin was completed and then invadopodia markers (cortactin, actin) were checked based on colocalization of them. Points where cortactin and actin colocalized together were detected as pre-invadopodia. Major steps and plugins: substract background-rolling ball radius>sliding paraboloid, Brightness&Contrast, math>exp, CLAHE, Log3D, analyze particles, adjust>threshold, selection>enlarge. After the detection of invadopodia, location of invadopodia was observed according to nanopatterns with pattern photos. Analyze values were adjusted based on exposure values for each photo set. These

values: 5-10-20 for sliding paraboloid, 3-5-10-20 for maximum slope in CLAHE. Sigma X and Y values 3-3 for Log3D, block size 9 – histogram bins 256 in CLAHE. Auto was applied for Brightness&Contrast and Threshold processes. In the last step – analyze particles, 30 pxl inner cell area was selected for analyze to prevent the deception about quantitative invadopodia data because of the membrane ruffling. Values were arranged for particle size between 30 and 400 pxl, circularity between 0.00 and 1.00.

2.7. Electron Beam Lithography

Electron Beam Lithography process was realized by using Raith E-line electron beam lithography machine (Raith GmbH, Dortmund, Germany) which was in the department of Physics. Vacuum was decreased so machine valve could open to load sample. “Unload” was selected from the “Navigator” tab. Gas nitrogen was opened two minutes later. Therefore decreasing of vacuum and opening of the valve were provided. Sample is placed into the stage and then the stage was placed into the machine and the valve was closed. “Load” was selected from “Navigator” tab and gase nitrogen flow was closed to do vacuum that was applied to close the valve. Coordinate of loaded sample was entered into machine. Values of “stigmation” and “aperture” was corrected to the sensitivity of writing process. The center location of electron gun was ensured the arrangement of “writefield alignment”. Working distance was measured from three different location that was on the sample. Current was measured at the “Faraday Cup” location at the average working distance. “Dwell time” was calculated based on desired step space. After that patterns were placed onto sample and writing process was started. 5-100μC cm^{-2} for area and 2-3200 pAs cm^{-1} for dot dose were tried. 5 kV voltage was applied.

2.7.1. Dose Determination of Silicon Surfaces in Electron Beam Lithography Application

EBL dose (D), waiting time (t) and step size (s),dose tests were performedto determine. These three factors are associated with each other depending on strength of current.

For area writting: D= (I *t) / (s * s). For line writting: D= (I * t) / (s). For point writting: D= (I * t).

Current magnitude increases with acceleration voltage and aperture width. Current in 10kV is higher than current in 5kV which reduces the waiting time, but it is more advantageous to process a low voltage protein coating due to protein patterns was made with backscattered electrons. 5 kV was used in EBL .

Patterns occured can be greater when aperture increases, but in this case the writing time for a given dose is reduced with respect to increase in current. 30 μm aperture was used in the experiments. Lines are created from dots, but if step size is large, points may occur instead of line. If we use writting option with dot, electron beam stops at every point and this increases the time to write. Here EBL presents option to write with line were tested by using large step size and thus to create nanodots by reducing writing time. We have incubated Si surface and 0.1 mg/ml of fibronectin solutions about three hour in room temperature and sixteen hours in +4°C. As a result, an hour at room temperature is sufficient to see fluorescence signal of fibronectin was determined. Fibronectin was stuck to areea of surface exposed to electron beam. Surfaces were dried after global bufer and then surfaces were rinsed with deionized water. In this way, to determine the results of experiments which resulted in patterning, recognizes the fibronectin antibody produced in rabbit and immunofluorescent staining that recognizes antibody produced in rabbit (Alexa 555) antibodies staining was performed. Both antibody 1: 200 in 1X PBS and used for one hour by waiting periods. Samples were examined in a fluorescent microscope. Images were taken with a digital camera connected to the microscope. All analysis was performed with ImageJ software. ImageJ "subtract background - rolling ball - sliding paraboloid" option was used to get rid of background signal.

Craeting fibronectin nanodots was performed by the method described above primarly (Figure 2.4, Figure 2.5).

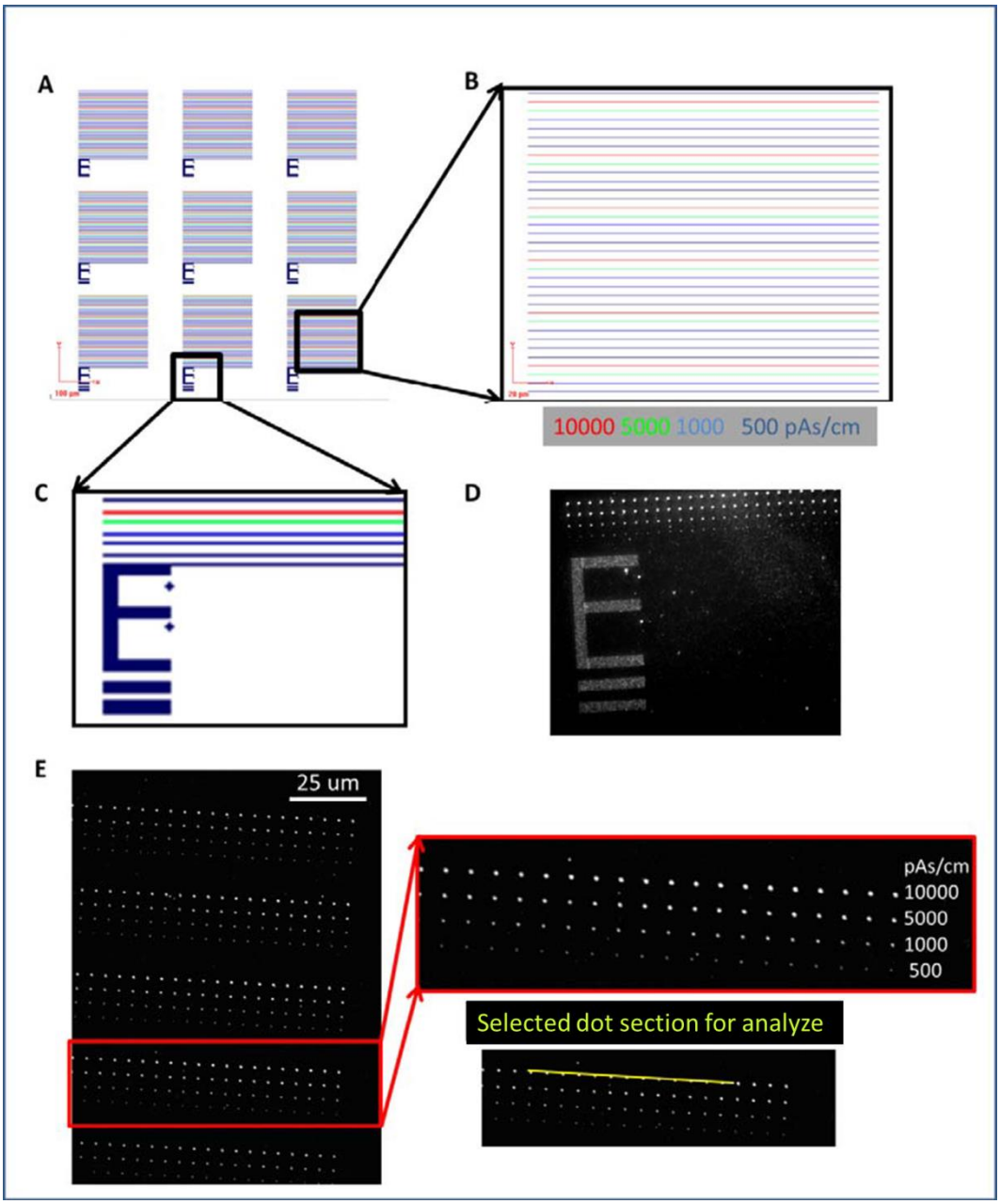

Figure 2.4. Silicon -K- casein - EBL - In Patterns of Fibronectin Nanodots - Fluorescence Imaging.

(A), (B), (C) EBL pattern designs. Lines in the pattern help to find patterns,Signs (E) designed with space are available. (D) in the pattern (C) where in the fluorescence of the portion picture. (E) Fluorescence microscopy images and dose-dependent fluorescence signal change.

When the lines were written by increments of 5 microns in the pattern, nanodots are 5 microns spacing was created. It was determined that the fluorescence was low while dose was decreasing. In fibronectin patterns, for line writing, threshold dose value

was determined 500 pAs/cm based on quality of fluorescent images. Fluorescent images were analyzed quantitatively by sections (Figure 2.4).

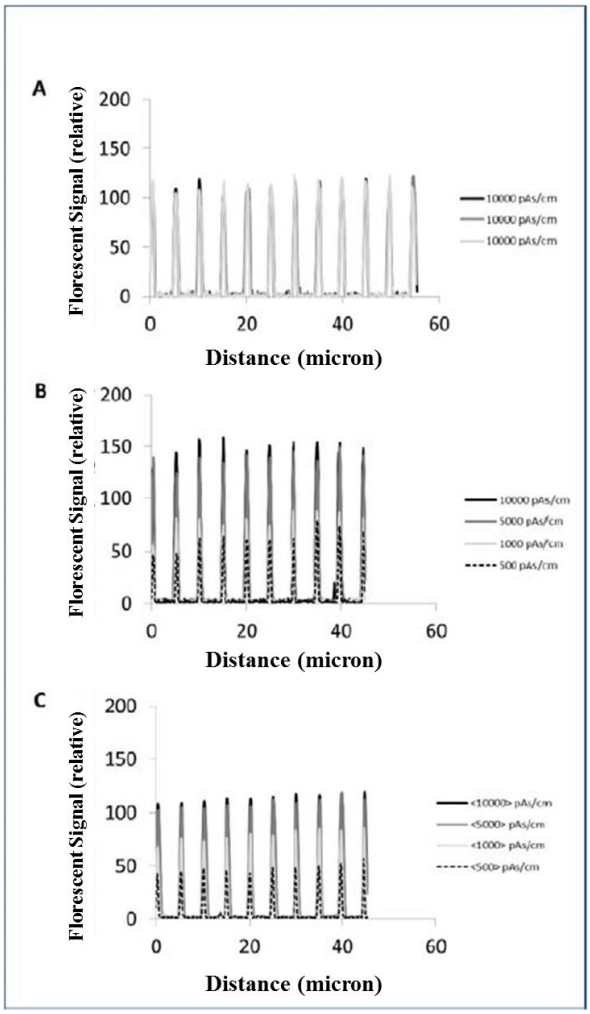

Figure 2.5. Silicon – K - casein - EBL - In Patterns of Fibronectin Nanodots - Analysis of Fluorescent Images.

Quantitative analysis of the pattern image in Figure 2.5. At least 10 nanodots for each dose in each 10 section were examined. (A) 10000 pAs/cm for three sections Graphs coincide as expected. (B) For 10000, 5000, 1000 and 500 pAs/cm one section for each. As expected, the fluorescence signal is reduced by lowering the dose. (C) For 10000, 5000, 1000 and 500 pass/cm for the average of 10 sections. 10000 pAs/cm at doses far higher than we see the formation of the ring dose (106 pAs/cm) were tested and realized the nanoring formation. 105 pAs/cm started to form on the nanoring and 106 pAs/cm line dose was determined can create nanoring (Figure 2.5, Figure 2.6)

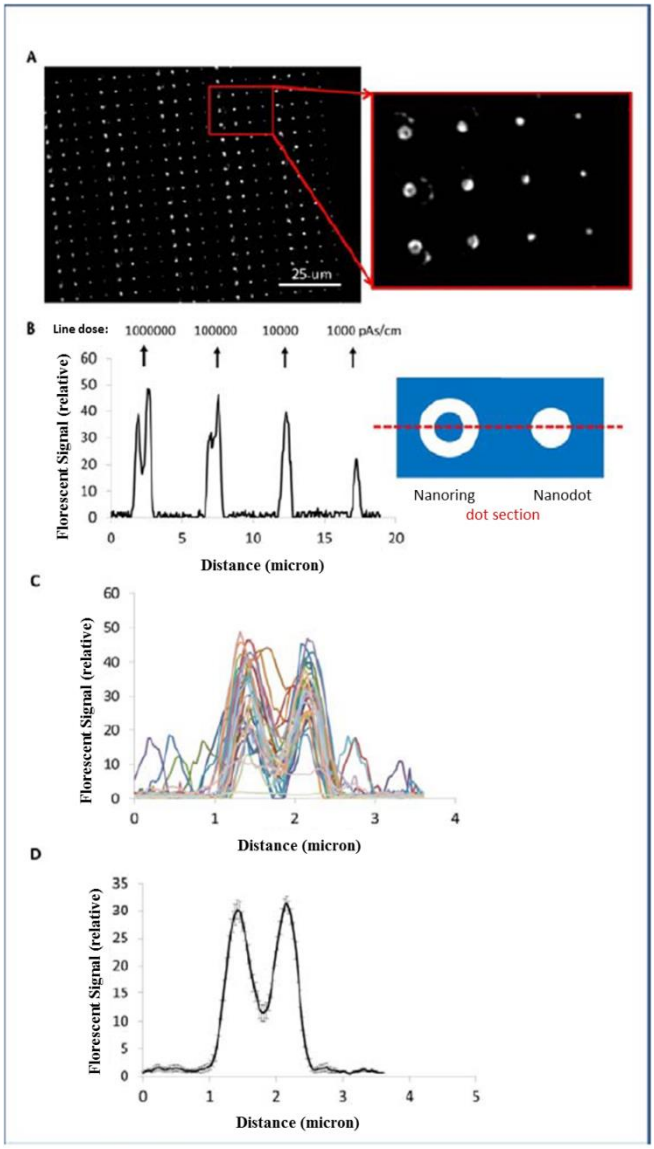

Figure 2.6. Silicon -K- casein - EBL - Fibronectin Nanoring the Patterns - Fluorescent Images and Quantitative Analysis.

(A) Fluorescence microscopy images and dose-dependent fluorescence signal change. When EBL pattern lines are written in increments of 5 microns by 5 microns spaacing nanodots (103, 104, 105 pAs/cm) and nanodots (106 pAs/cm) was created. (B) It was determined that the higher dose increased fluorescent signal. Over 105 pAs/cm it was started to form the nanoring and by 106 pAs/cmline dose was determined to be formed nanoring. (C) Lines section obtained from the fluorescent images of 30 different nanoring is written in 106 pAs/cm dose line. (D) Average lines section obtained from the fluorescent images of 30 different nanoring is written in 106 pAs/cm dose line (standard error lines are indicated in gray). Nanoring was determined that in the same way they could be created.

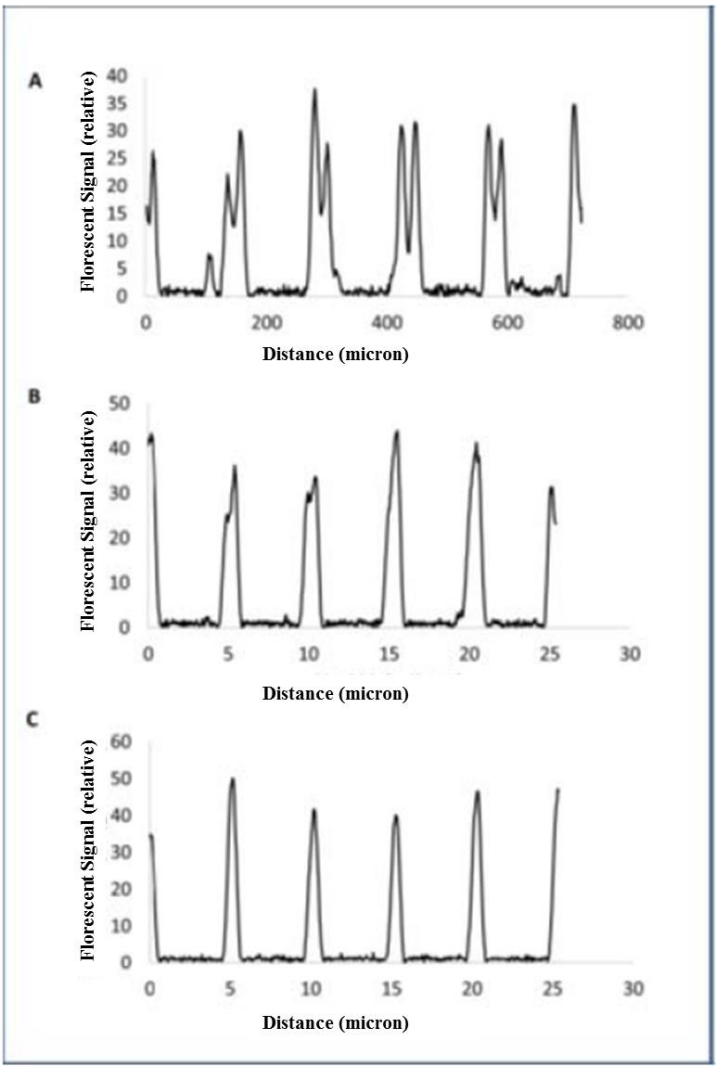

Figure 2.7. Silicon - K-casein - EBL – Comparison Between Patterning Fibronectin Nanodots and Nanorings-Quantitative Analysis of Fluorescent Images.

(A) Average of 4 sections, each of them contains at least 4 nanopatterns for nanopatterns written in 106 pAs/cm line dose. (B) Average of 4 sections, each contains at least 4 nanopatterns for nanopatterns written in 105 pAs/cm line dose. (C) Average of 4 sections, each of themcontains at least 4 nanopatterns for nanopatterns written in 104 pAs/cm line dose. Over 105 pAs/cm it was started to form the nanoring and by 106 pAs/cm line dose was determined to be formed nanoring. Silicon - K-casein - EBL – Size of nanodots were determined depends on electron dose by imaging samples of fibronectin in scanning electron microscope which is more practical than the suggested atomic force microscope (Figure 2.7). According to these results, to create 400 mm

diameter nanopoint, 1800 pAs/cm should be used. In order to create nanoring, at least 7x105 pAs/cm line dose should be used.

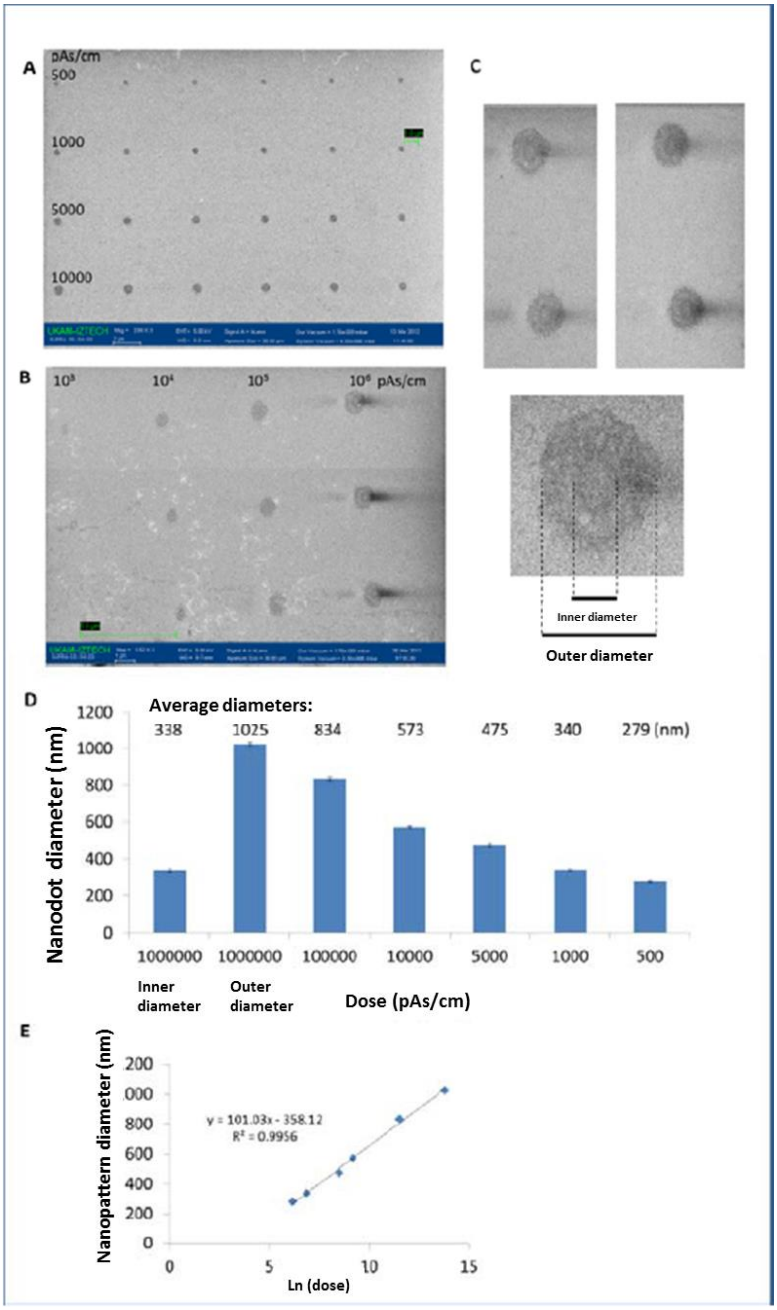

Figure 2.8. Silicon -K- casein - EBL - The Patterns of Fibronectin Nanoring.

Scanning electron microscopy images and quantitative analysis. (A) Nanodots. (B) Nanodots and nanorings. (C) Example nanoring images and descriptions of inner and outer diameter. (D) It was measured by diameter of the nanopatterns for each dose (n = 27-62). Mean values and standard deviation values are shown. T-tests of all doses create different diameters of nanopatterns from each other were determined. ($p<0.0001$).

(E) Change of nanopattern diameter depends on logarithm of dose was determined to be linear. As a result, appropriate parameters to fibronectin nanodot and nanoring patterns on K-casein were determined by EBL.

CHAPTER 3

RESULTS & DISCUSSIONS

3.1. Number of Invadopodia in 0 min, 10 min and 4 hours on Fibronectin Control Surfaces

Invadopodia formation is not evident after 10 min of stimulation with EGF, it was planned not to use this time point in future experiments. Quantitative analysis of this experiment (Total positive, cortactin and actin positive number of invadopodia per cell, number of containing cells) have been completed (Figure 3.1).

According to the results that are compatible with Models in the literature (Artym et al., Cancer Res 2006). Firstly cortactin secondly actin is recruited in associated points. The percentage of the positive cells containing cortactin positive invadopodia in 0 min, 10 min and 4 hours increase 31%, 60%, 75% respectively. On the other hand,the average number of invadopodia per cell (determined by staining cortactin) For 0 minutes,10 minutes and 4 hours are 0.30 ± 0.13 for 1.9 ± 0.70, 7.63 ± 2.82. Both cortactin and actin positive invadopodia numbers for points at the same time periods are 0.15 ± 0.10, 0.7 ± 0.33 and 4.25 ± 1.78. The average number of invadoppodia per microscopic area (determined by staining cortactin) 0 min , 1 min and 10 ± 0.40 for 4 hours, 9 ± 2.48 and 10.34 ± 36.75. (Table 3.3) Average of both cortactin and actin positive number of invadopodia for points at the same time periods are 0.5 ± 0.29, 1.75 ± 0.85 and 20.75 ± 6.80. Numbers of microscopic areas are higher than the numbers per cell, because all the cells in which only the image while counting invadopodia per cell was examined. Invadopodia investigations can be expected to be examined for 4 hours or even long-term based on these quantitative results.

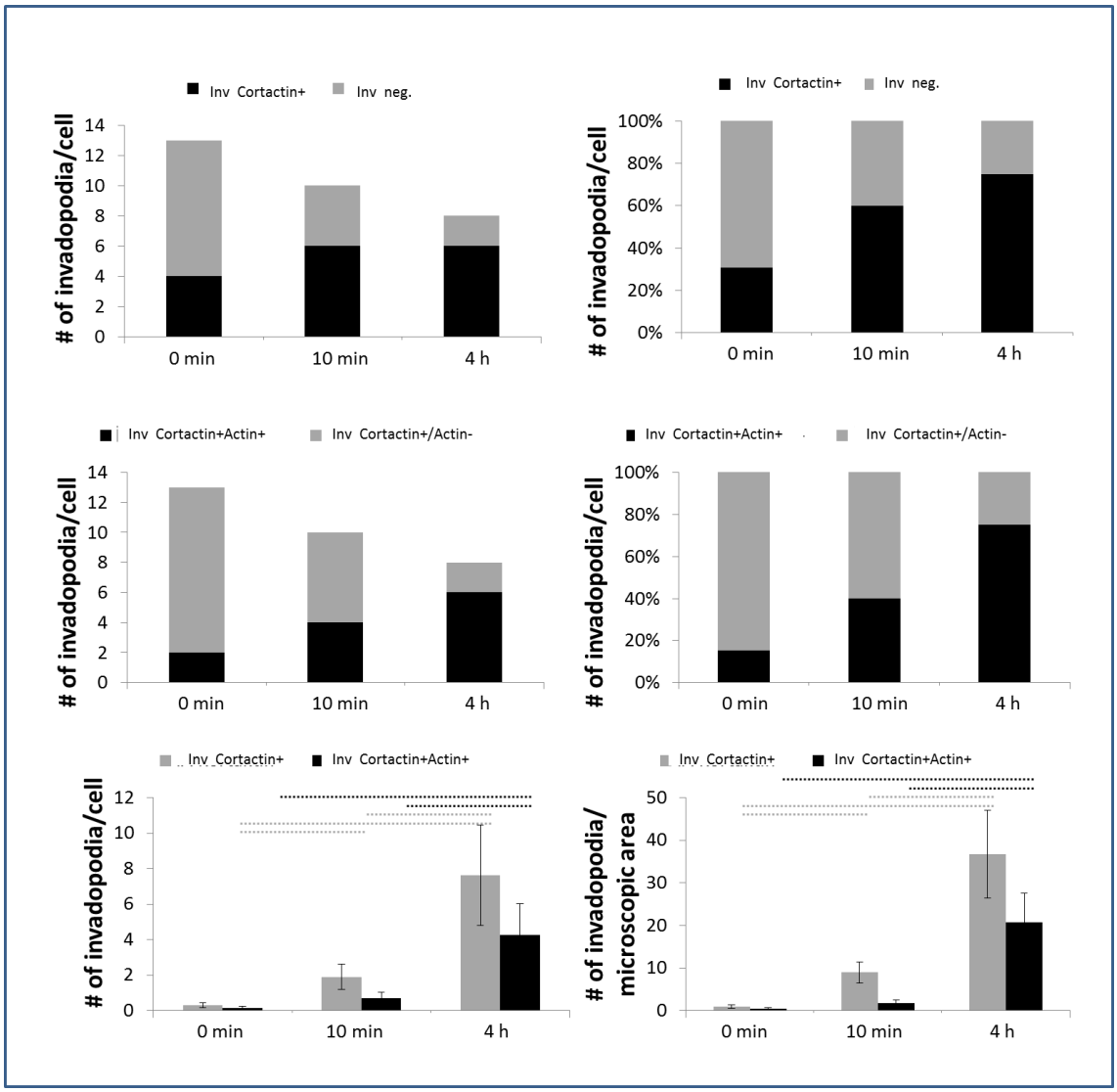

Figure 3.1. Quantitative Analysis of Invadopodia on The Fibronectin Control Surfaces.

Dotted lines on the invadopodia charts per cell and per microscopic area are pairing groups different from each other at the level of $p<0.005$.

Table 3.1. The Number of Cells Containing Cortactin+ and Cortactin+ Actin+ Invadopodia on Fibronectin Surfaces for 0 min, 10 min and 4 hours.

Number of invadopodia	0 min (n=13)	10 min (n=10)	4 hour (n=8)
Cortactin+	4 (31%)	6 (60%)	6 (75%)
Cortactin+ Actin+	2 (15%)	4 (40%)	6 (75%)

Table 3.2. The Average Number of Invadopodia per Cell Containing Cortactin+ and Cortactin+ Actin+ on Fibronectin Surfaces for 0 min, 10 min and 4 hours.

Average Number of invadopodia/cell	0 min (n=13)	10 min (n=10)	4 hour (n=8)
Cortactin+	0.30 ± 0.13	1.9 ± 0.7	7.63 ± 2.82
Cortactin+ Actin+	0.15 ± 0.10	0.7 ± 0.33	4.2 5± 1.78

Table 3.3. The Average Number of Invadopodia per Microscopic Area Containing Cortactin+ and Cortactin+ Actin+ on Fibronectin Surfaces for 0 min, 10 min and 4 hours.

Number of invadopodia/microscopic area	0 min (n=13)	10 min (n=10)	4 hour (n=8)
Cortactin+	1 ± 0.40	9 ± 2.48	36.75 ± 10.34
Cortactin+ Actin+	0.5 ± 0.29	1.75 ± 0.85	20.75 ± 6.80

3.1.1. Experiments for Optimization of Cortactin and Fibronectin Antibodies

Experiments were performed for different antibody dilution and incubation temperature to eleminate nonspecific signals. 1:400 dilution rate is determined for both primary and secondary antibodies of fibronectin and cortactin at room temperature.

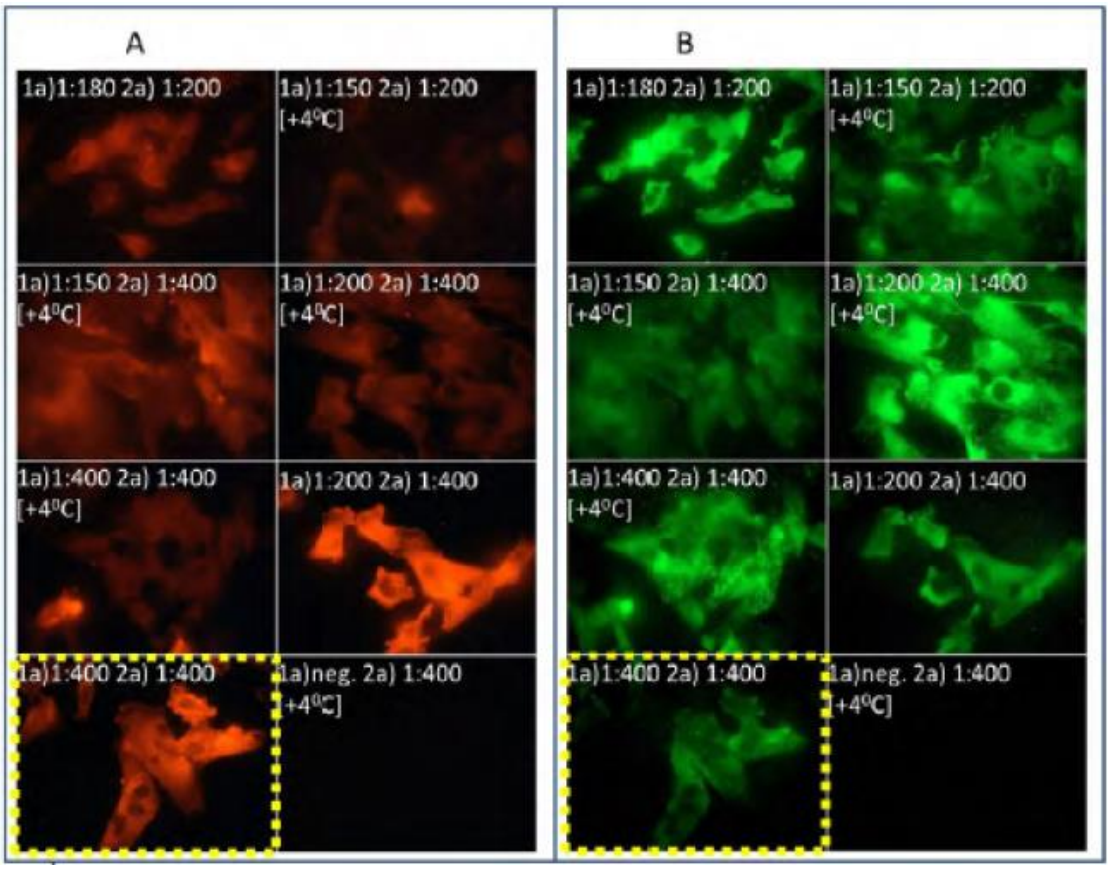

Figure 3.2. Images of Dilution Rates for Optimization of Cortactin and Actin Antibodies.

Immunoflourescent staining color is red for cortactin and green for fibronectin. 1a): Primary antibody dilution, 2a): Secondary antibody dilution. Neg: No primary antibody. [+4°C]: Primary antibody was used at +4°C instead of room temperature. Best results were obtained with 1:400 dilution rate at room temperature.

3.1.2. Experiments for Observation of Matrix Degradation with MMP Activation in Invadopodia

Durations of starvation were decreased to block saturation of matrix degradation. For that reason experiments on fibronectin control surfaces were done again. Cells were removed from petri dish surface by nonenzymatic buffer solution, CDB (Cell Dissociation Buffer), and resuspended in L15-BSA. Cells in L15-BSA in the presence of EGF cultured on test surfaces. Process between removing from petri dish and seeding onto test surfaces took for about 1.5 hours. Subsequently, culture of cells were performed for 1.5 hours instead of 4 hours. Cells did not adhere to surface at this situation. Then cells cultured in the presence of EGF directly for 16 hours. At these conditions, cells adhered to surfaces and spread in Figure 3.3. Invadopodia formation was detected by immunoflourescent staining for cortactin and actin. Definite degradations were not observed on fibronectin surface in Figure 3.3. In addition, long-term observation was determined to matrix degradation for invadopodia. Because degradation by MT1-MMP and invadopodia activation occurs at the last stages.

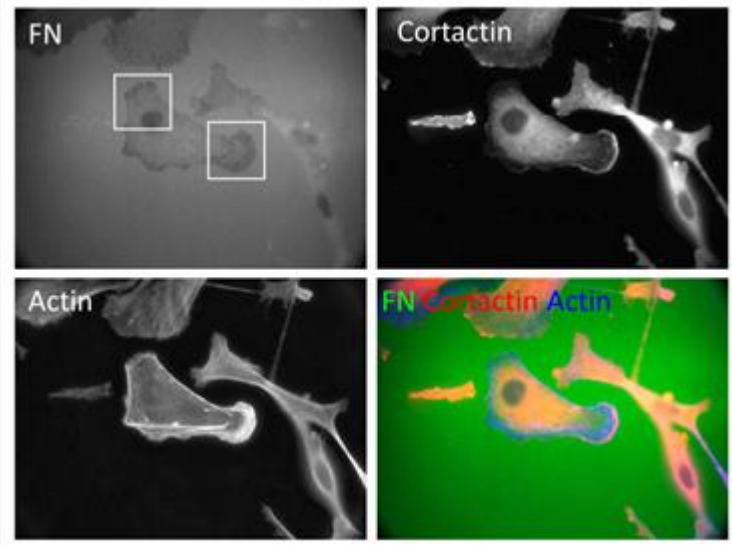

Figure 3.3. Invadopodia In a Cancer Cell Cultured In The Presence of EGF for 16 hours on Fibronectin Control Surface.

This figure shows a representative cell cultured in the presence of EGF for 16 hours on fibronectin surface. Fibronectin, cortactin, actin and merge images are represented in panels. Boxes in Figure 3.3 is magnified in Figure 3.4.

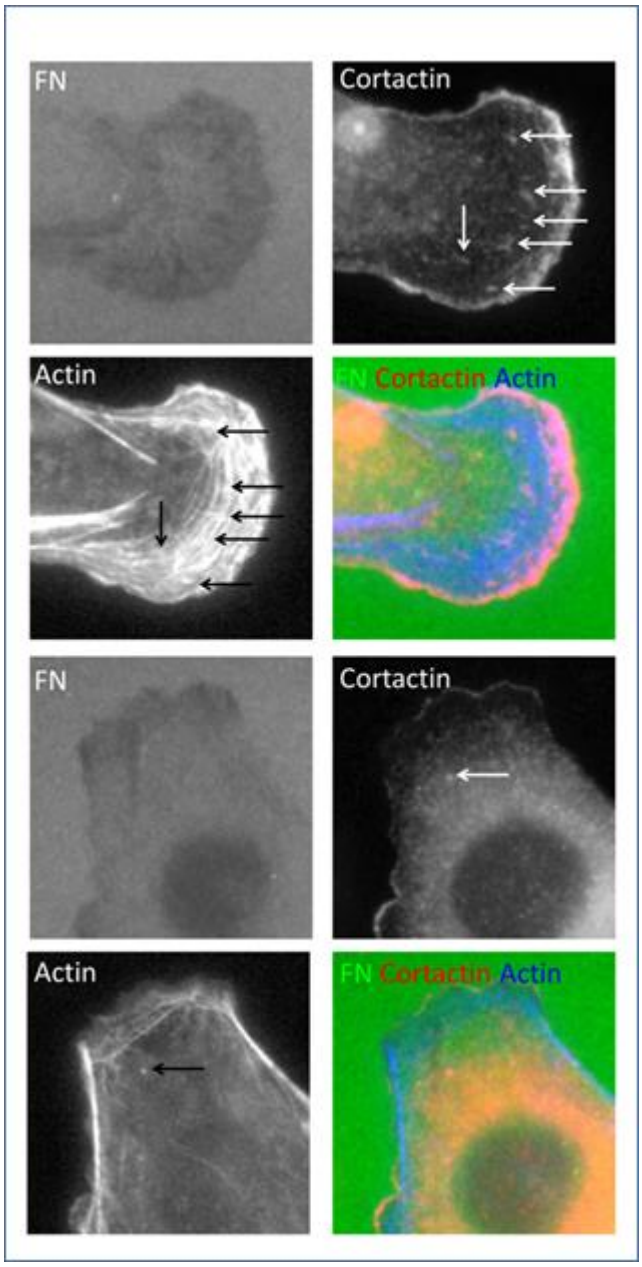

Figure 3.4. Magnification of invadopodia associated areas of Figure 3.3.

This figure shows at high magnification the lower right area and the upper area of Figure 3.3. White and black arrows show invadopodia positive for cortactin and actin.

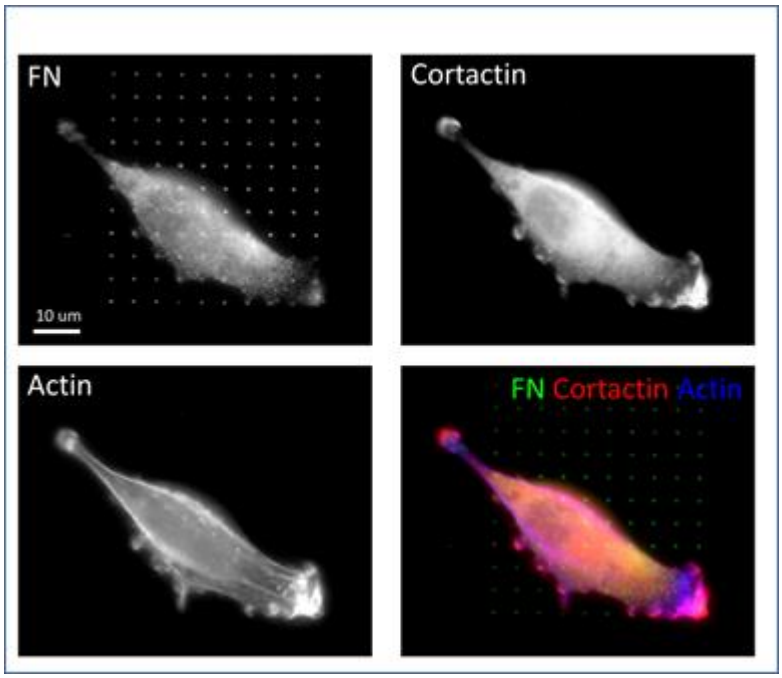

Figure 3.5. Invadopodia in a cancer cell cultured in the presence of EGF for 16 hours on fibronectin nanopatterns on K-casein coated surface.

This figure shows a representative cell cultured in the presence of EGF for 16 hours on fibronectin surface. Associated area is magnified in Figure 3.6.

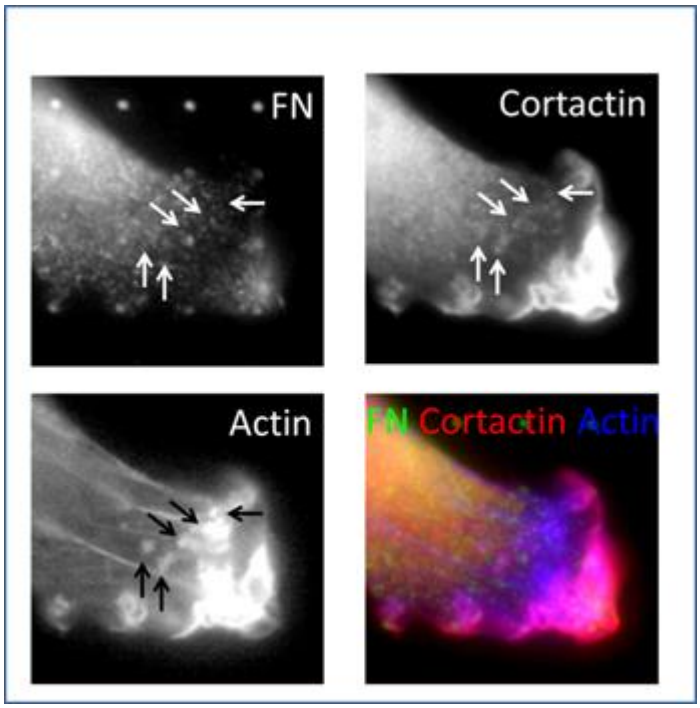

Figure 31.6. Magnification of Invadopodia Associated Area of Figure 3.5.

This figure shows at high magnification the lower right cell area of Figure 3.5. White and black arrows show invadopodia positive for cortactin and actin. Represented points are not colocalized with fibronectin nanodots. These results show localized cell adhesion is not required for invadopodia formation.

3.1.3. Experiments for Selection of Appropiate Environment for Long-term Observation of Invadopodia Formation

Number of invadopodia reaches to highest level in 5-10 minutes by adding EGF after starvation for example MTLn3 cells in standart invadopodia experiments are performed using adhered cells. EGF stimulation after starvation was prefered because of providing of increment of invadopodia, but in these experiments special surfaces were used. In the duration of the work flow culture of cells-starvation-EGF stimulation respectively, nanopatterns could be deleted. Because serum contains fibronectin. Other method is culture of cells in normal environment conditions without starvation for 16 or 24 hours and analyze of invadopodia in steady-state cells. Serum contained medium should be used for steady-state cell method.

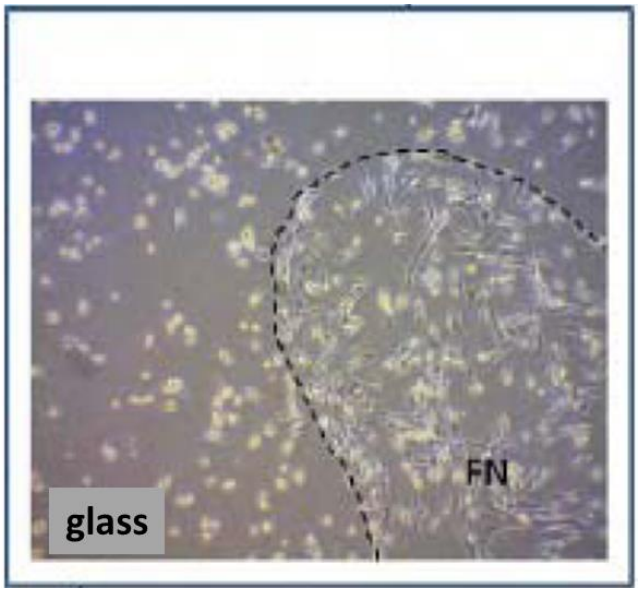

Figure 3.7. Phase-contrast Images of Cultured MDA-MB-231 Cancer Cells for 51 hours on Fibronectin Coated and Fibronectin Noncoated Surfaces.

Duration of cell viability was tested in the presence of L-15 BSA and EGF. Fibronectin coated area was created by fibronectin drop on glass lamel surface. Cells were removed from petri dish surfaces by CDB and seeded on fibronectin coated surface. Flourescent images were taken after 51 hours culture of cells in Figure 3.7. Cells adhered to fibronectin coated surface and spread, cells in noncoated surface looked like spherical. This control experiment shows using of L15 BSA in the presence of EGF is suitable for long-term observation of invadopodia formation on test surfaces. Collagen was observed as an inappropiate protein to create nanopattern. Collagen can dissolve in acidic solution and this is a technical obstacle. Furthermore immobilization of collagen to surface by poly-lysine and APTES were failure. For these reasons laminin were used instead of collagen.

3.2. Pre-Invadopodia Formation in a Cancer Cell Cultured in The Presence of EGF for 24 hours on Single Active Component Nanodot Patterns

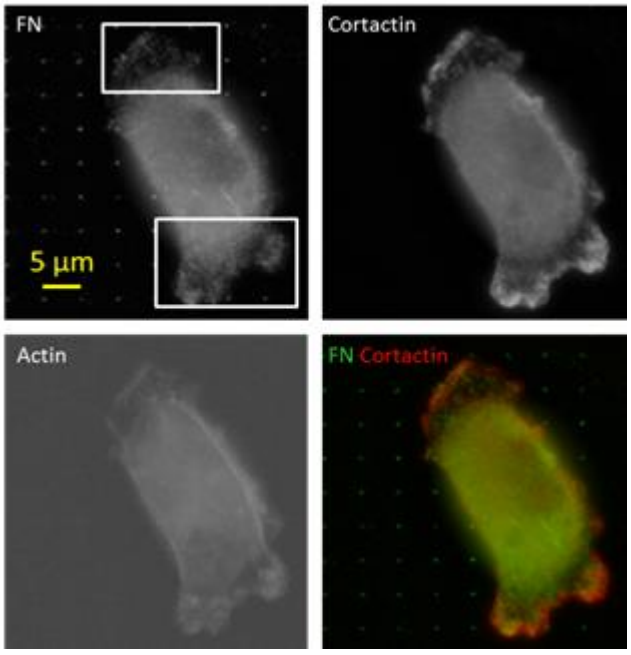

Figure 3.8. Pre-invadopodia in a cancer cell cultured in the presence of EGF for 24 hours on K-casein-fibronectin surface.

This figure shows a representative cell cultured in the presence of EGF for 24 hours on single active component surface. Fibronectin, cortactin, actin and merge images are represented in panels. Boxes in Figure 3.8 is magnified in Figure 3.9.

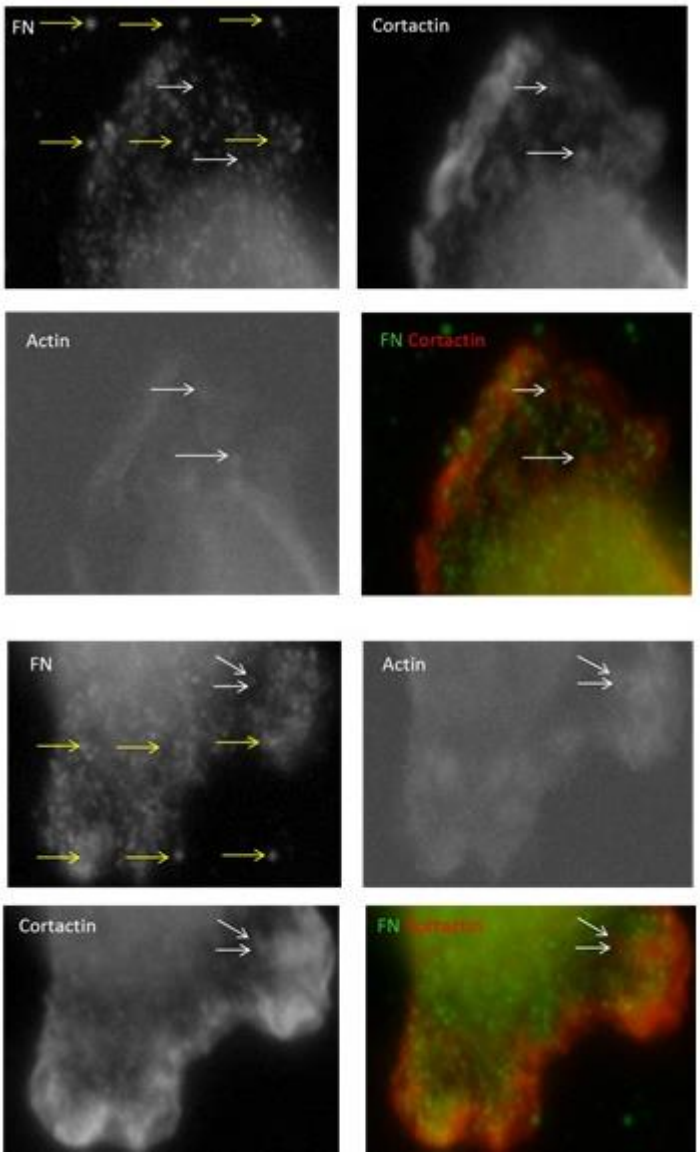

Figure 32.9. Magnification of Invadopodia Associated Areas of Figure 3.8.

This figure shows at high magnification the upper cell area and the lower cell area of Figure 3.9. White arrows show invadopodia positive for cortactin, actin and yellow arrows show fibronectin nanodots. Invadopodia formation was observed between fibronectin nanodots. These results indicate that breast cancer cells prefer to form invadopodia

3.2.1. Pre-invadopodia Formation in Cancer Cells Cultured in The Presence of EGF for 24 hours on Fibronectin Control Surfaces

Culture of cancer cells were performed for 24 hours in the presence of EGF. Because activation of MMPs and matrix degradation are performed at the last stages in invadopodia.

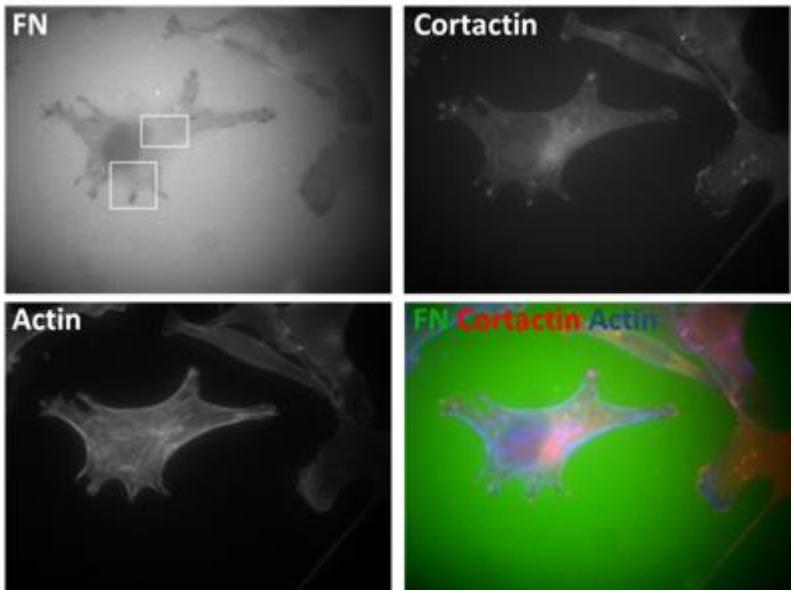

Figure 3.10. Pre-invadopodia in a cancer cell cultured in the presence of EGF for 24 hours on fibronectin control surface.

This figure shows a representative cell cultured in the presence of EGF for 24 hours on fibronectin control surface. Fibronectin, cortactin, actin and merge images are represented in panels. Boxes in Figure 3.10 is magnified in Figure 3.11.

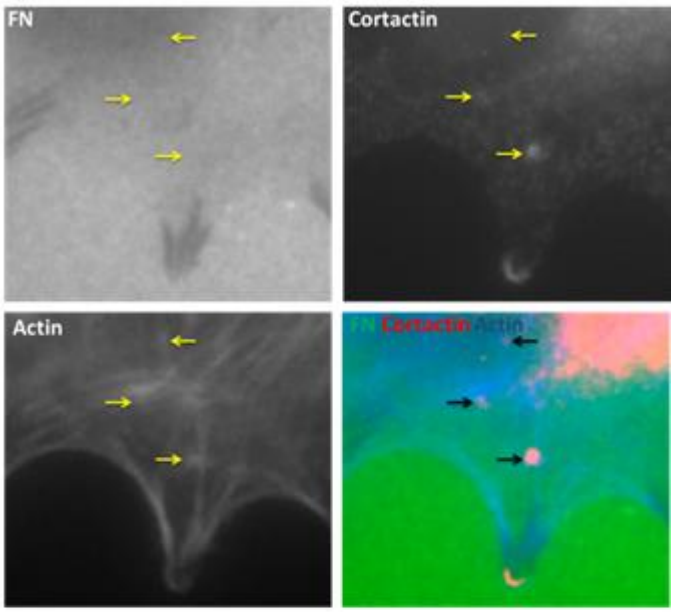

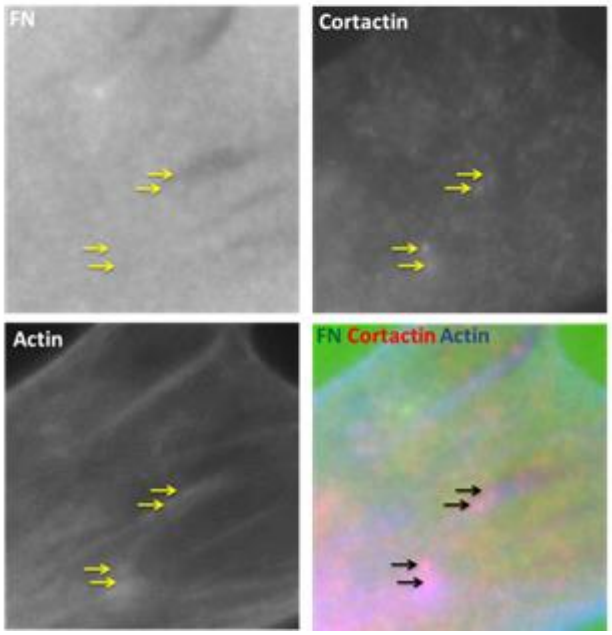

Figure 3.11. Magnification of invadopodia associated areas of Figure 3.10.

This figure shows at high magnificationthe lower right cell area and the upper right area of Figure 3.10. Yellow and black arrows show invadopodia positive for cortactin and actin. There are degradations on fibronectin surface. We can say that some invadopodia transfor into mature invadopodia so they can realize matrix degradation.

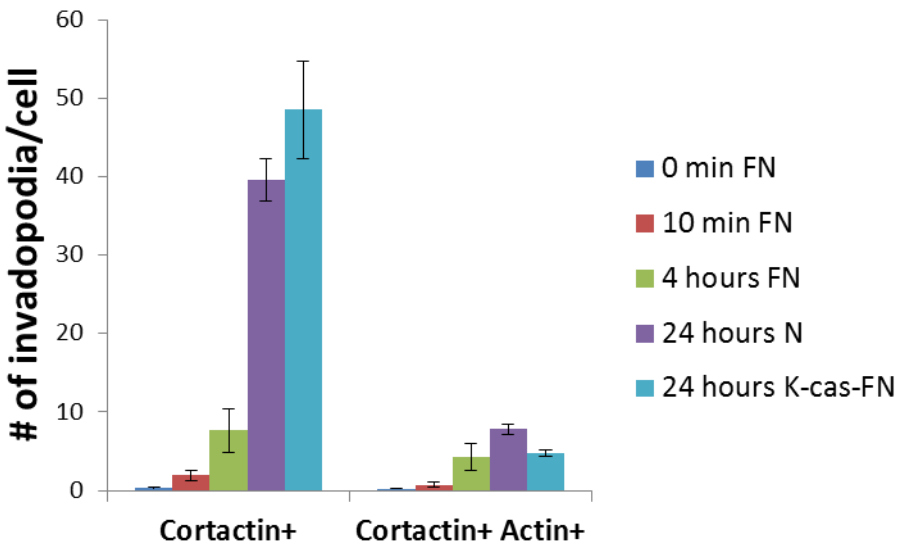

Figure 3.12. The distribution of invadopodia formation according to duration of cell culture and different surfaces.

This figure shows the distribution of invadopodia in cels cultured in the presence of EGF on fibronectin control surfaces for 0 min, 10 min, 4 hours, 24 hours on fibronectin surfaces and 24 hours for K-casein-fibronectin surface. The increment for number of pre-invadopodia (cortactin+ actin+) was observed on fibronectin surfaces based on culture duration in the presence of EGF.

3.3. Detection of Invadopodia Formation by Using Alternative Tks5 Marker on Fibronectin Control Surfaces

In the presence of Tks5 protein is known both podosome and invadopodia. Tks5 protein as an alternative marker was used for the examination of invadopodia formation by immunoflourescent staining.

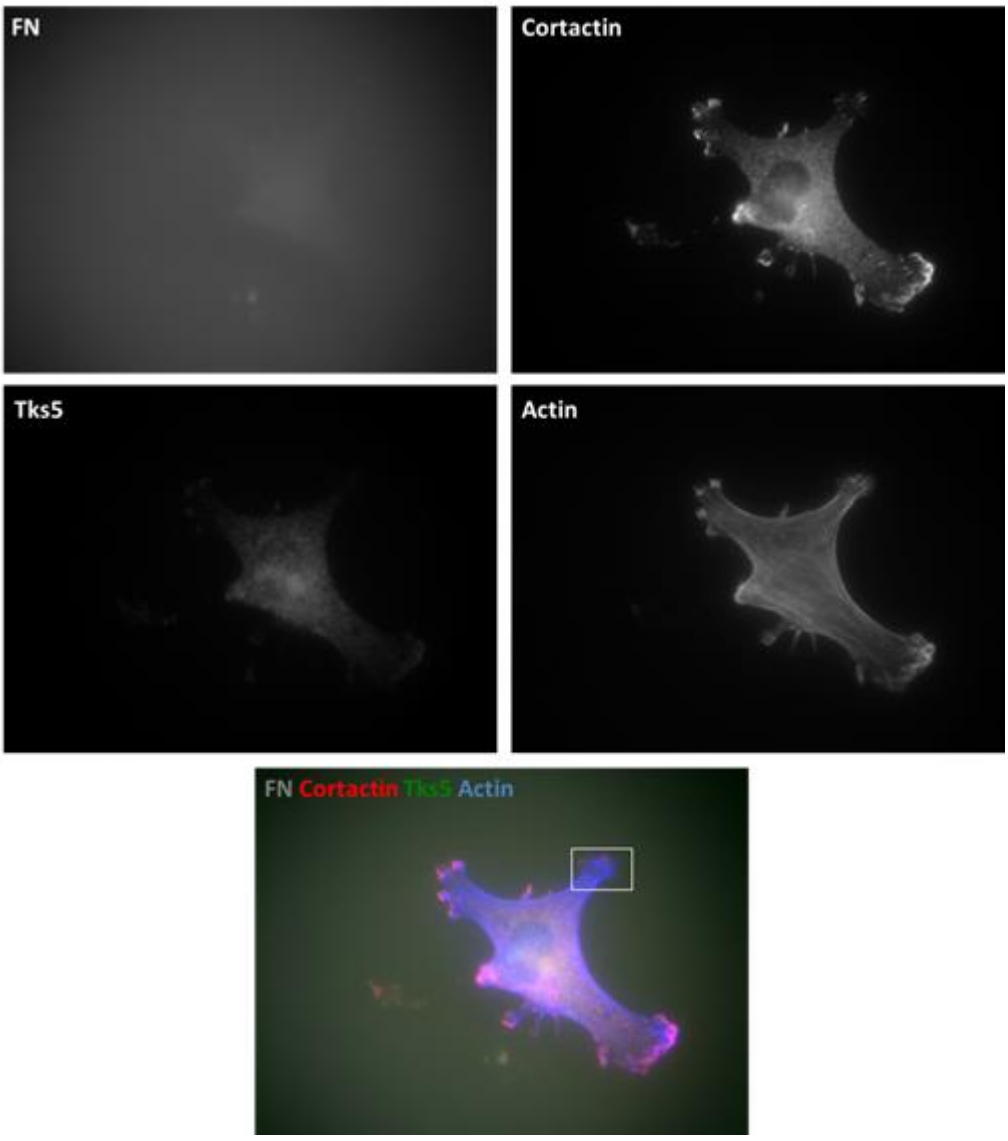

Figure 3.13. Invadopodia in a cancer cell cultured in the presence of EGF for 24 hours on fibronectin control surface.

This figureshows a representative cancer cell cultured in the presence of EGF on fibronectin control surface. Box in Figure 3.13 is magnified in Figure 3.14. Fibronectin, actin, cortactin, tks5 and merge images are represented in panels.

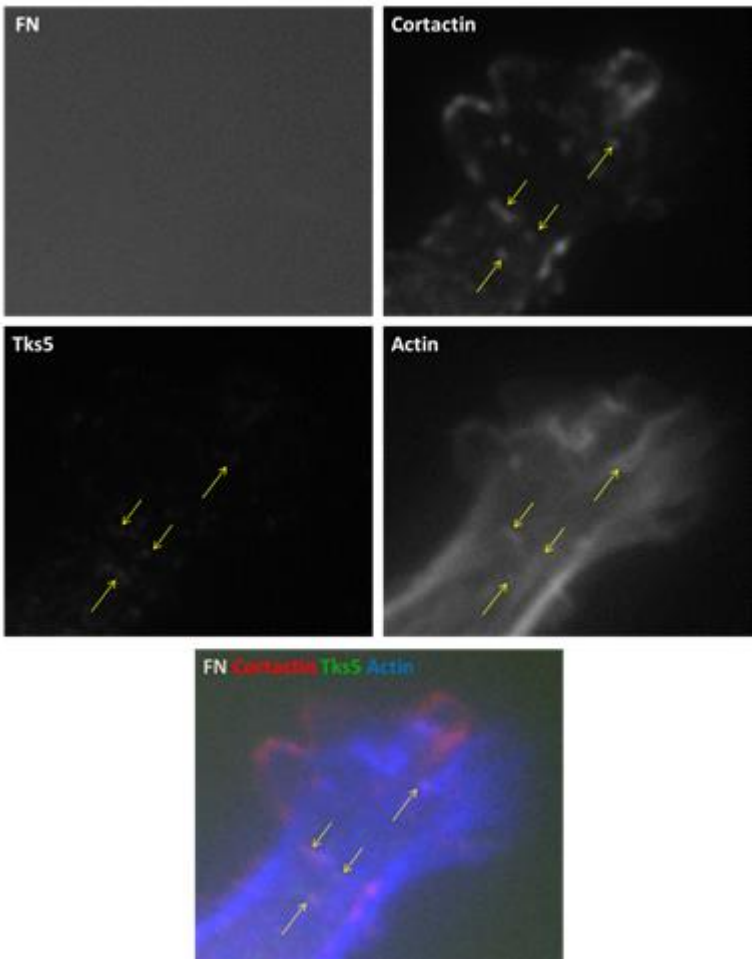

Figure 3.14. Magnification of Invadopodia Associated Area of Figure 3.13.

This figure shows at high magnification the upper rightcell area of Figure 3.14. Yellow arrows show pre-invadopodia positive for cortactin, tks5 and actin.

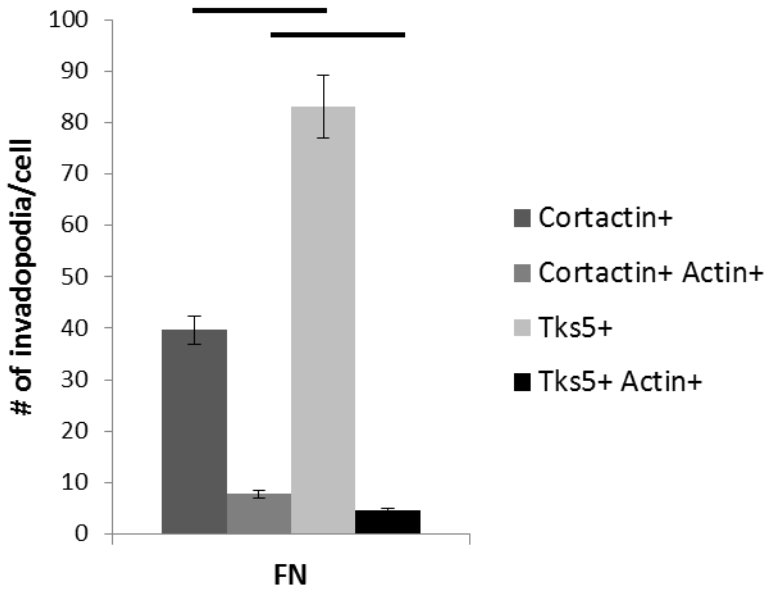

Figure 3.15. Number of Invadopodia per Cell were Examined with Tks5, Cortactin, Actin.

Cortactin+ Actin+ and Tks5+ Actin+ show pre-invadopodia. Horizontal straight lines show the statistical difference is $p<0.05$ at one tail level while horizantal dotted lines show the statistical difference is $p<0.05$ at two tail level. Number of tks5 per cell is more than cortactin but number of pre-invadopodia positive for cortactin-actin and tks5-actin are similar. Therefore similar results were obtained with tks5 protein for detection of invadopodia.

Vinculin exists in both podosomes and focal adhesions so this protein was examined in cancer cells by immunoflourescent experiment to observe the differences of focal adhesions, podosomes and invadopodia.

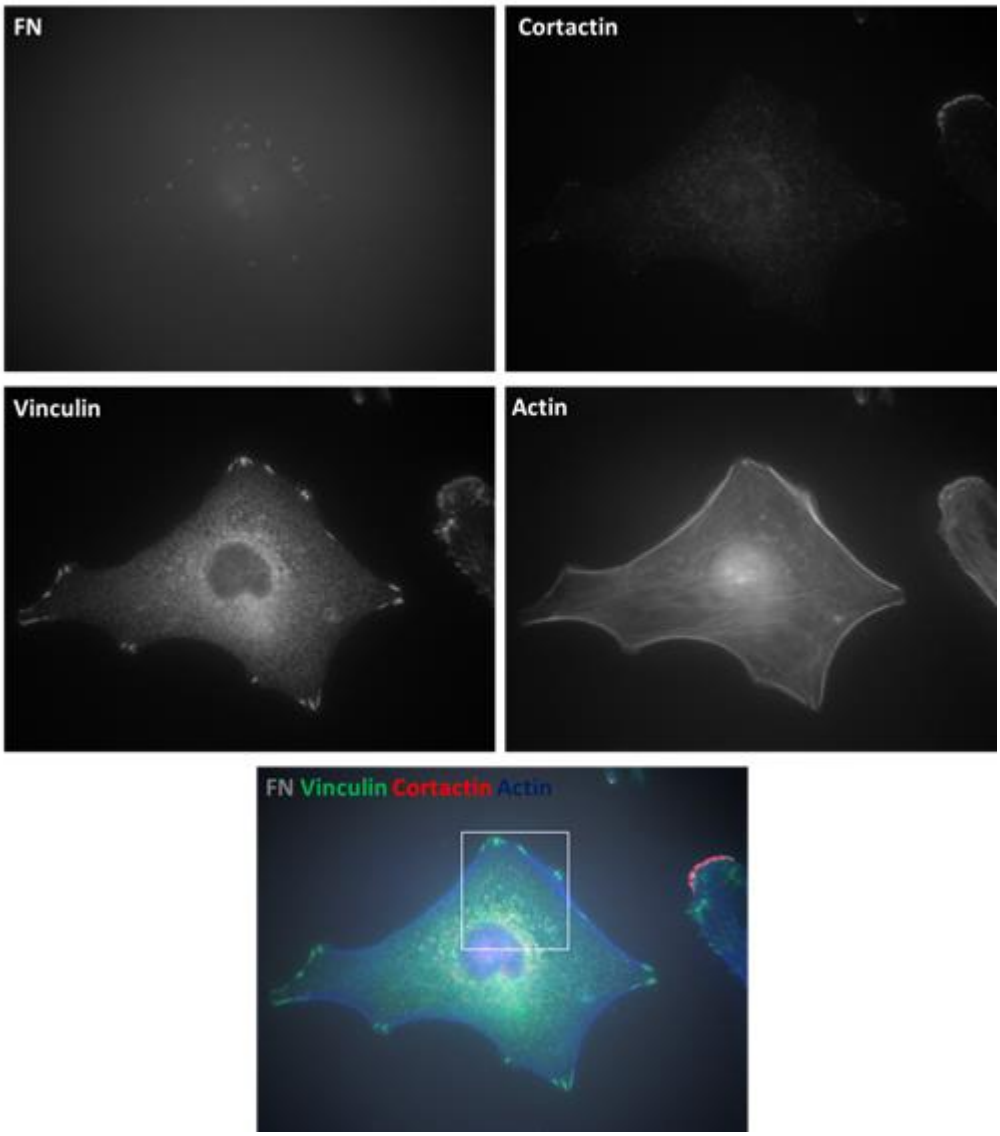

Figure 3.16. Invadopodia and Focal Adhesions in A Cancer Cell Cultured in The Presence of EGF for 24 hours on Fibronectin Control Surface.

This figure shows a representative cancer cell cultured in the presence of EGF for 24 hours on fibronectin control surface. Fibronectin, actin, tks5, vinculin and merge images are represented in panels. Box in Figure 3.16 is magnified in Figure 3.17.

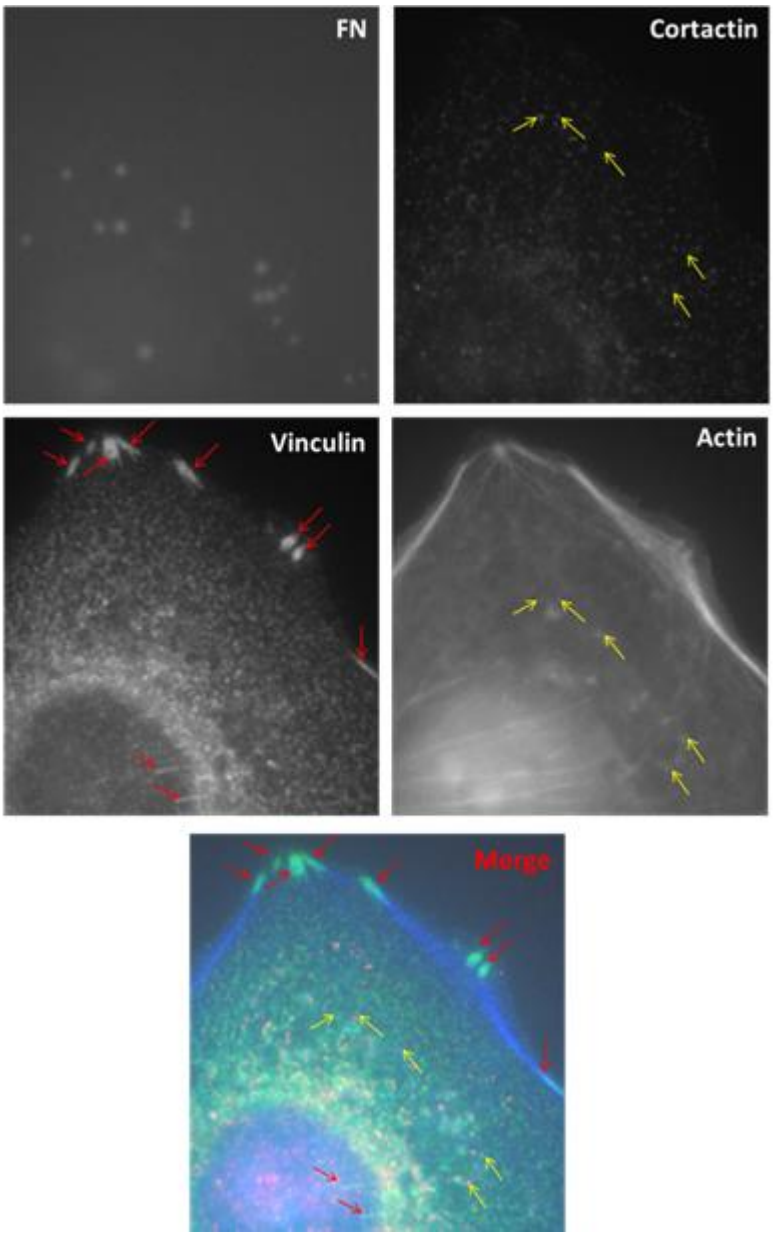

Figure 3.17. Magnification of Invadopodia Associated Area of Figure 3.18.

This figure shows at high magnification the upper cell area of Figure 3.17. Yellow arrows show pre-invadopodia positive for cortactin, actin and red arrows show focal adhesions.

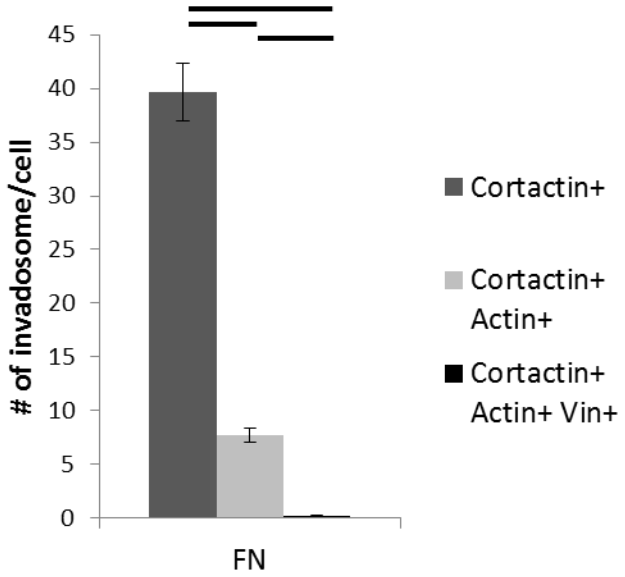

Figure 3.18. Number of Invadopodia and Locations Positive for Cortactin, Actin and Vinculin per Cell on Fibronectin Control Surface.

Cortactin+ Actin+ shows all pre-invadopodia and Cortactin+ Actin+ Vinculin+ shows the locations where invadopodia and focal adhesions colocalize. Pre-invadopodia formation and focal adhesions were observed in cancer cells cultured in the presence of EGF on Fibronectin control surface. Horizontal straight lines show the statistical difference is $p<0.05$ at one tail level while horizantal dotted lines show the statistical difference is $p<0.05$ at two tail level. Focal adhesions and invadopodia were not observed at the same location. This situation shows cancer cells do not need focal adhesions during the formation of invadopodia. In addition, this observed structures are invadopodia not podosomes.

3.4. Formation of Invadopodia and Podosome on Fibronectin Control Surfaces

Existence of Tks5 in both podosomes and invadopodia is known. Cells cultured in the presence of EGF for 24 hours on fibronectin control surface and observed by immunoflourescent experiment.

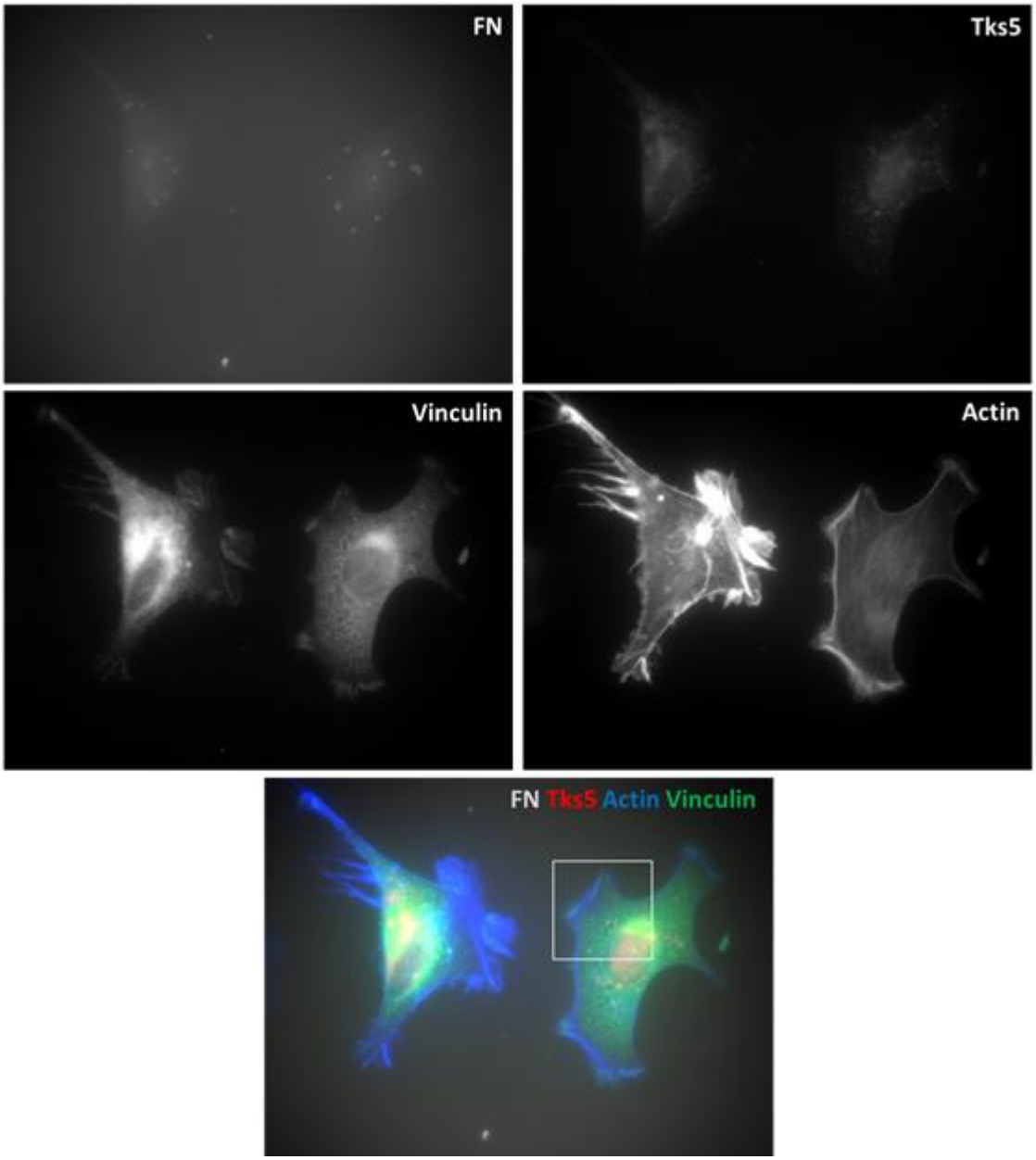

Figure 3.19. Pre-Invadopodia Positive for Tks5-actin and Focal Adhesions in a Cell Cultured in The Presence of EGF for 24 hours on Laminin Control Surface.

This figuration shows a representative cancer cell cultured in the presence of EGF for 24 hours on laminin control surface. Fibronectin, tks5, actin, vinculin and merge images were represented in panels. Box in Figure 3.19 is magnified in Figure 3.20.

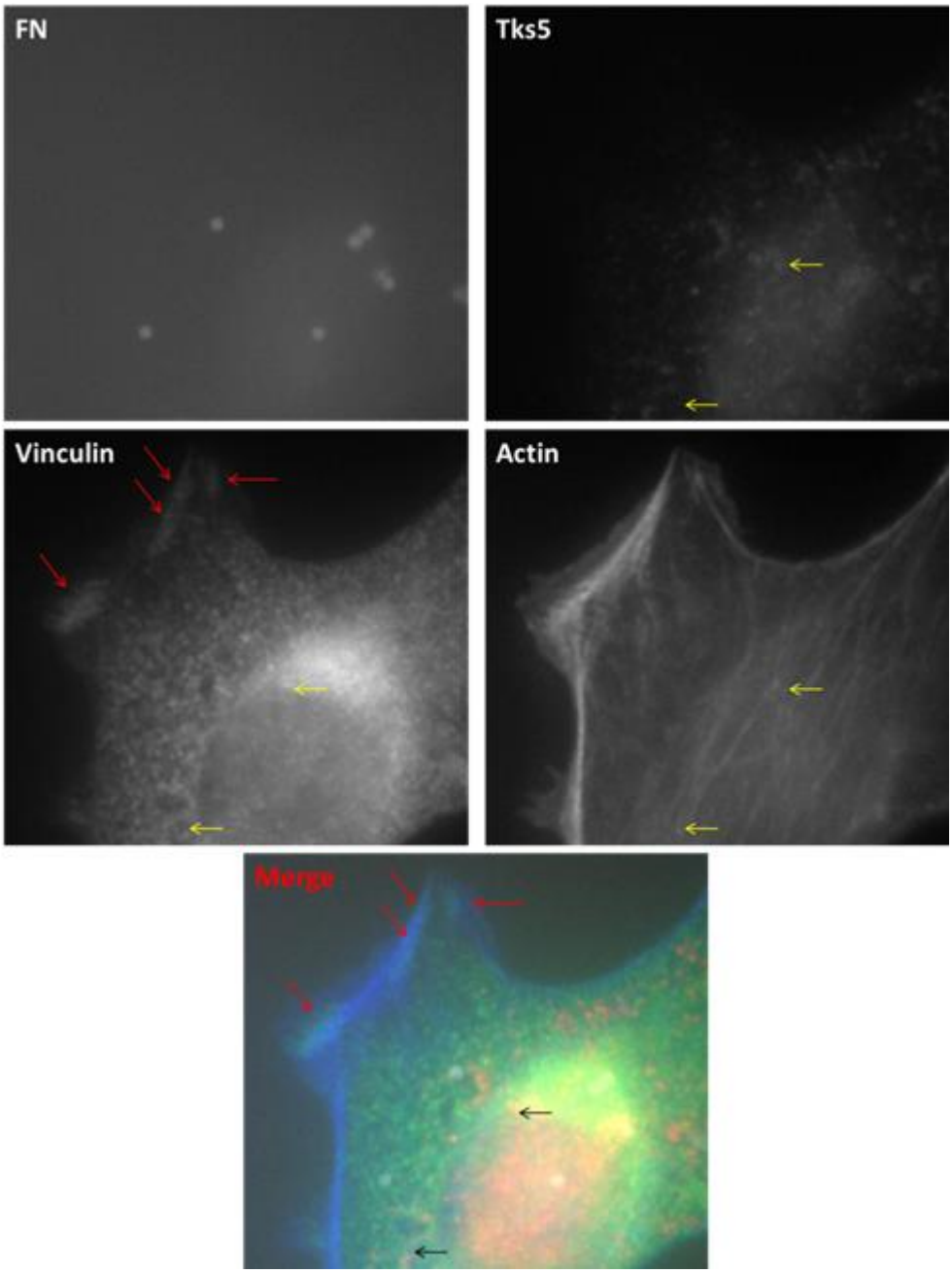

Figure 3.20. Magnification of Invadopodia Associated Area of Figure 3.19.

This figure shows at high magnification the upper right cell area of Figure 3.19. Yellow arrows show pre-invadopodia positive for cortactin and actin, red arrows show focal adhesions. Invadopodia are not formed at the same locations with focal adhesions.

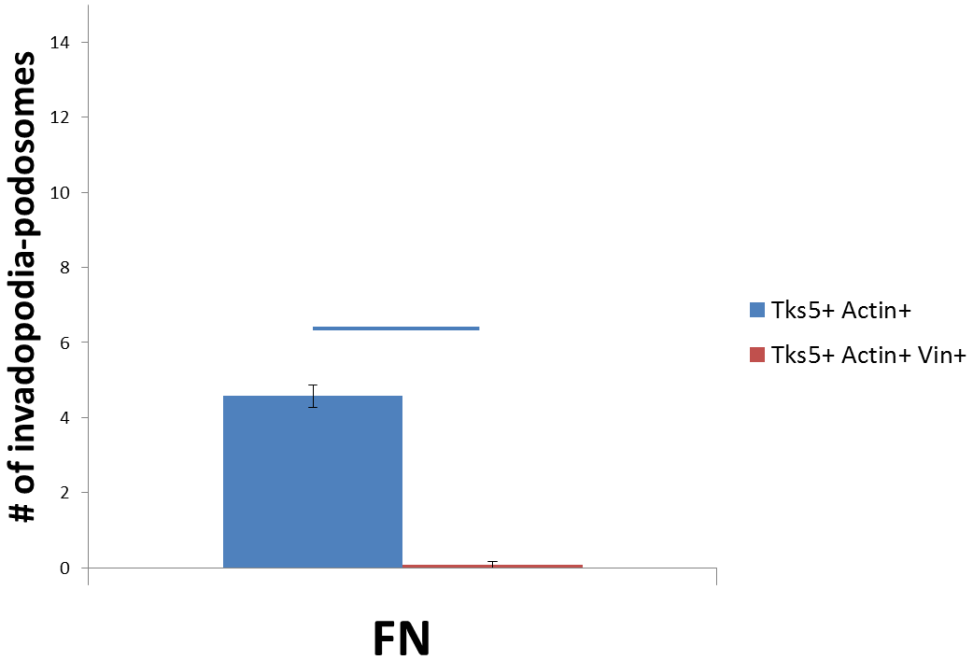

Figure 3.21. Number of Podosomes and Pre-invadopodia on Fibronectin Control Surface.

Tks5+ Actin+ shows pre-invadopodia and Tks5+ Vin+ Actin+ shows podosomes. Number of tks5 protein per cell was examined in the point of colocalization with actin and actin-vinculin. Horizontal straight lines show the statistical difference is $p<0.05$ at one tail level while horizantal dotted lines show the statistical difference is $p<0.05$ at two tail level. Invadopodia do not need vinculin. There is a difference between number of invadopodia positive for tks5-actin and number of podosomes positive for tks5-actin-vinculin.

3.4.1. Pre-invadopodia Formation in Cancer Cells Cultured in The Presence of EGF for 24 hours on Laminin Control Surface

MDA-MB-231 breast cancer cells cultured in the presence of EGF for 24 hours on laminin as one of the extracellular protein coated surfaces. Number of pre-invadopodia per cell was examined according to fibronectin and laminin surfaces.

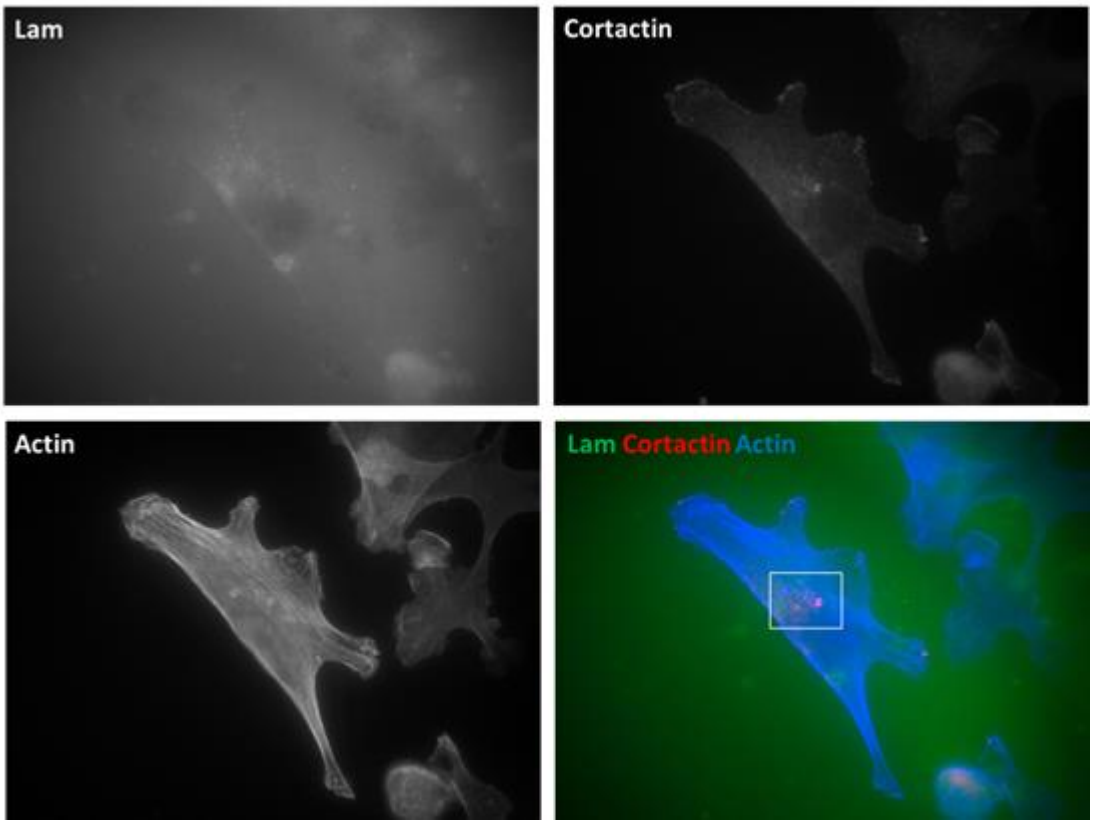

Figure 3.22. Pre-invadopodia in a Cancer Cell Cultured in The Presence of EGF for 24 hours on Laminin Control Surface.

This figure shows a representative cell cultured in the presence of EGF for 24 hours on laminin control surface. Laminin, cortactin, actin and merge images are represented in panels. Box in Figure 3.22 is magnified in Figure 3.23.

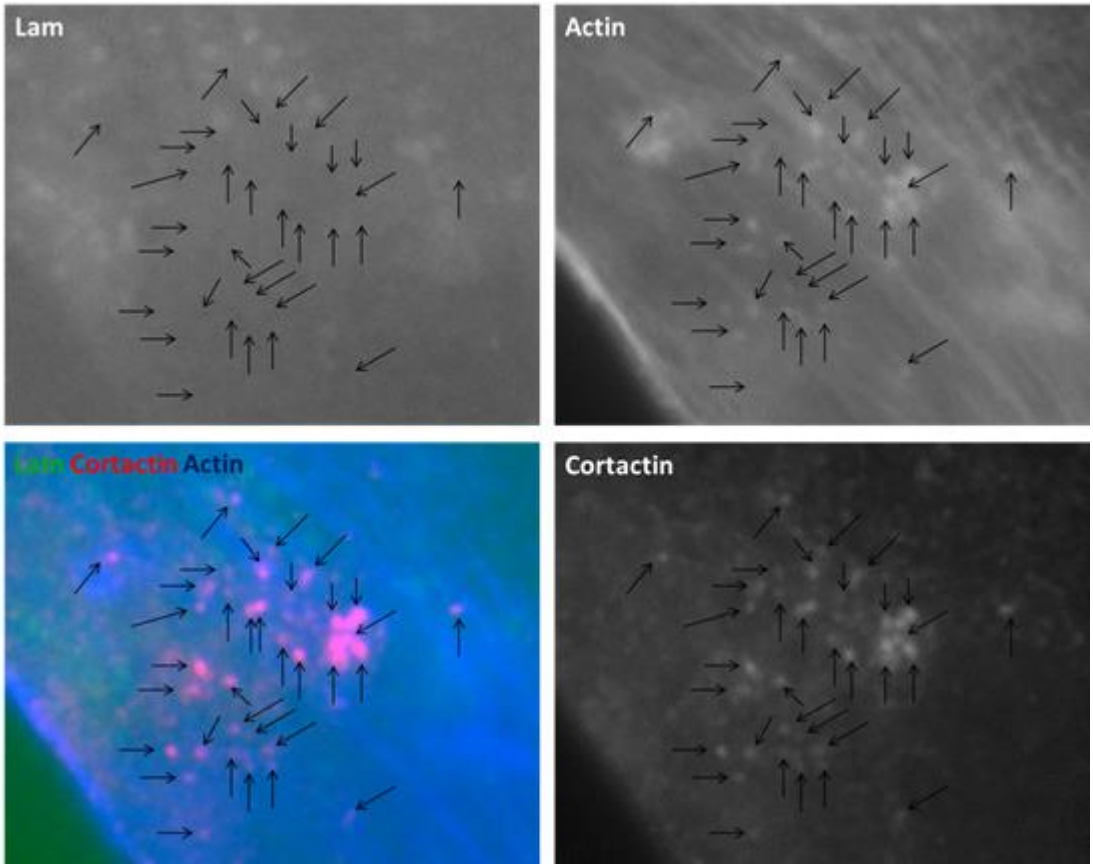

Figure 3.23. Magnification of Invadopodia Associated Area of Figure 3.22.

This figure shows at high magnification the middle cell area of Figure 3.22. Black arrows show pre-invadopodia positive for cortactin and actin.

3.4.2. Pre-invadopodia Formation in Cancer Cells Cultured in The Presence of EGF for 24 hours on K-casein-FN Nanoring Patterns

After the examination of cancer cells cultured in the presence of EGF for 24 hours on K-casein-FN nanodot patterns, invadopodia formation was analyzed in cells were cultured in the presence of EGF for 24 hours on K-casein-FN nanoring patterns. Cells were analyzed for number of invadopodia according to nanodot/nanoring patters.

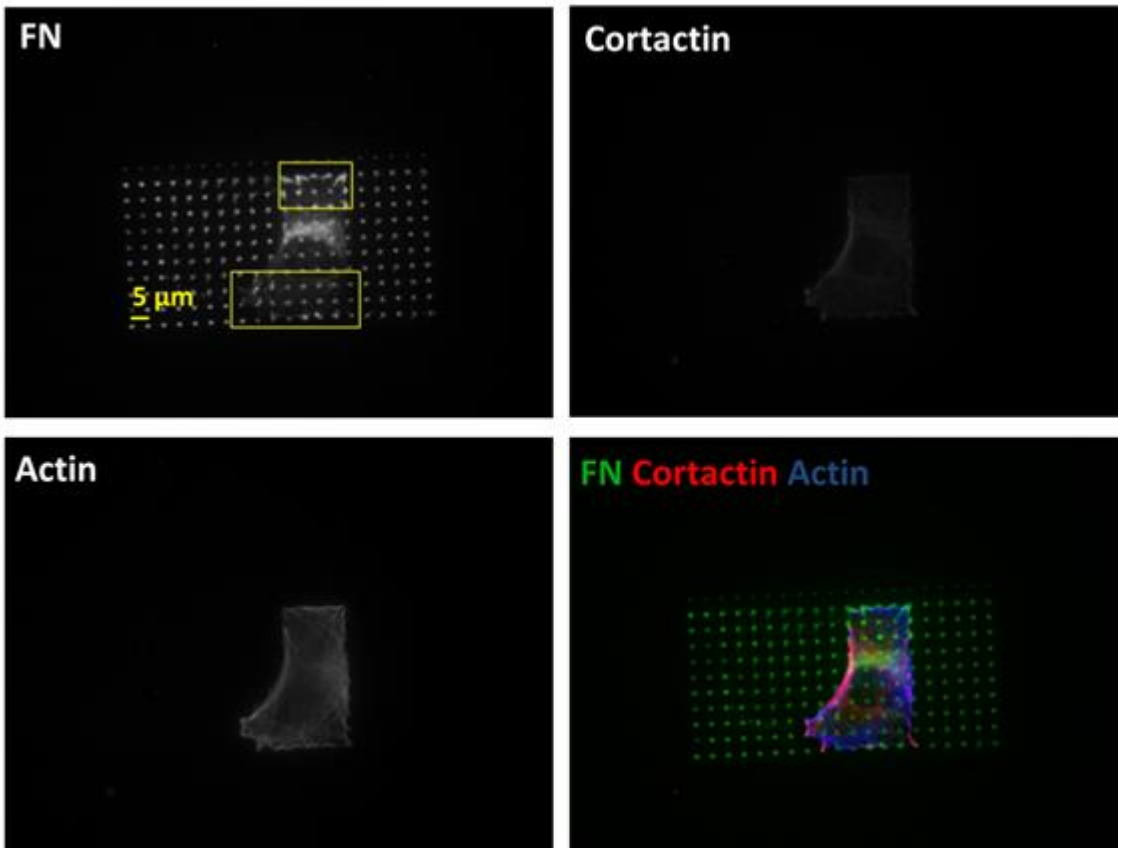

Figure 3.24. Pre-invadopodia in a Cell Cultured in the Presence of EGF for 24 hours on K-casein-FN Nanoring Patterns.

This figure shows a representative cell cultured in the presence of EGF for 24 hours on K-casein-FN nanoring patterns. Fibronectin, cortactin, actin and merge images are represented in panels. Boxes in Figure 3.24 are magnified in Figure 3.25.

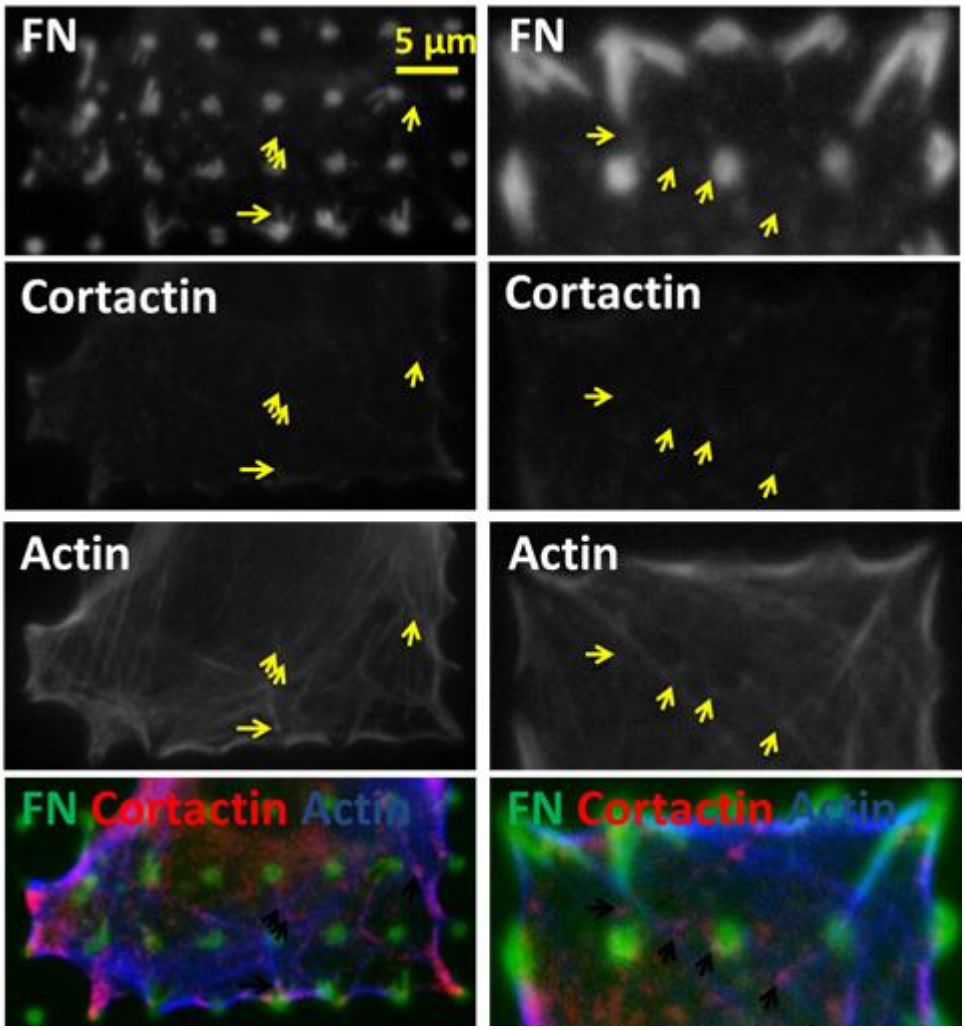

Figure 3.25. Magnification of invadopodia associated areas of Figure 3.24.

Left column shows at high magnification the lower cell area and right column shows at high magnification the upper cell area of Figure 3.24. Yellow and black arrows show pre-invadopodia positive for cortactin and actin.

3.4.3. Invadopodia Formation in Cancer Cells Cultured in The Presence of EGF for 24 hours on Dylight K-casein-FN Nanodot Patterns

To test and observe the stage of invadopodia (preinvadopodia or mature invadopodia) depends on degradations on K-casein coated surface, K-casein protein was tagged with dylight 555.

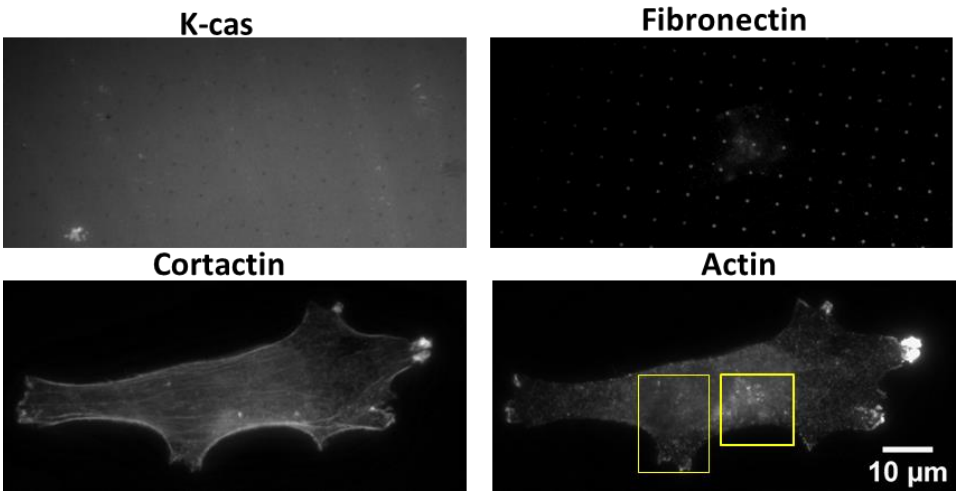

Figure 3.26. Invadopodia in a Cell Cultured in the Presence of EGF for 24 hours on Dylight K-casein-FN Nanodot Patterns.

This figure shows a representative cell cultured in the presence of EGF for 24 hours on Dylight K-casein-FN nanodot patterns. Fibronectin, cortactin, actin and merge images are represented in panels. Boxes in Figure 3.26 are magnified in Figure 3.27.

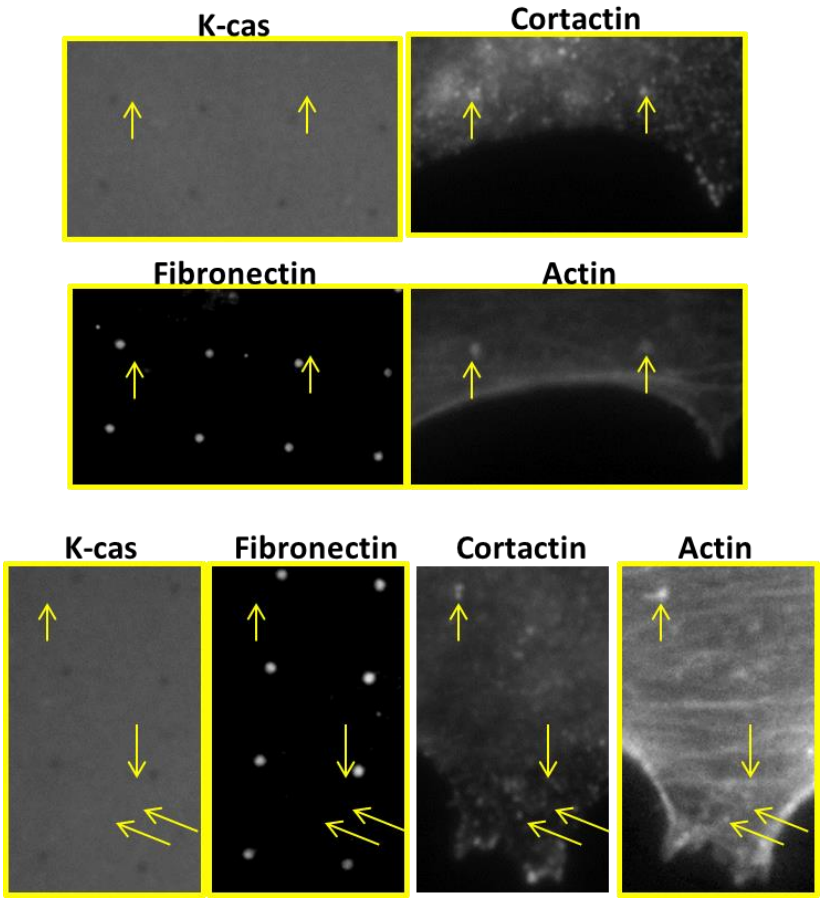

Figure 3.27. Magnification of invadopodia associated areas of Figure 3.26.

First set of four images shows at high magnification the middle cell area and second set of four images shows at high magnification another cell area of Figure 3.26. Yellow and black arrows show transported mmps on actin. There are not degradations on dylight K-casein coated surface. We can say that invadopodia are not at the mature stage and also there is not any transformation from pre-invadopodia to mature invadopodia.

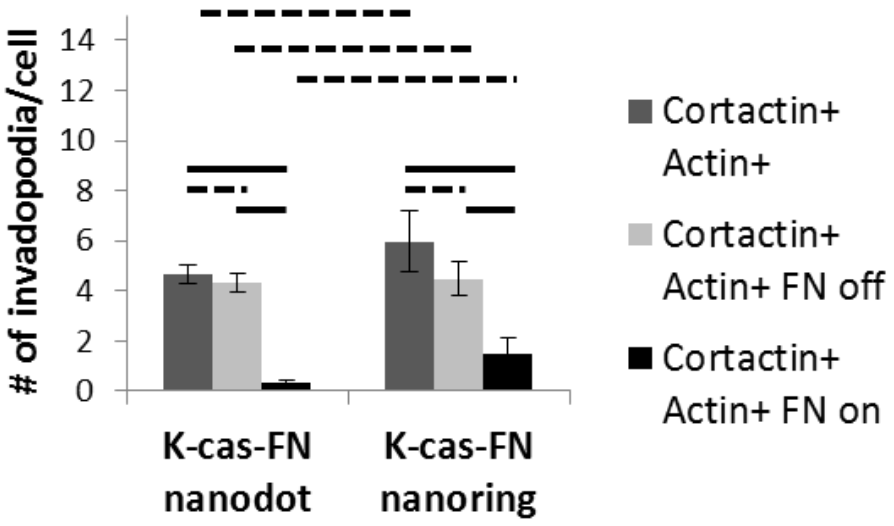

Figure 3.28. Number of Pre-invadopodia on K-casein-FN Nanoring and Nanodot Patterns.

Cortactin+ Actin+ shows all pre-invadopodia, Cortactin+ Actin+ FN on shows pre-invadopodia formed on nanopatterns, Cortactin+ Actin+ FN off shows pre-invadopodia formed between nanopatterns. Horizontal straight lines show the statistical difference is $p<0.05$ at one tail level while horizantal dotted lines show the statistical difference is $p<0.05$ at two tail level. Number of formed invadopodia per cell on FN patterns and between FN patterns are similar. Cells prefer to form invadopodia between nanopatterns for both nanoring and nanodot patterns.

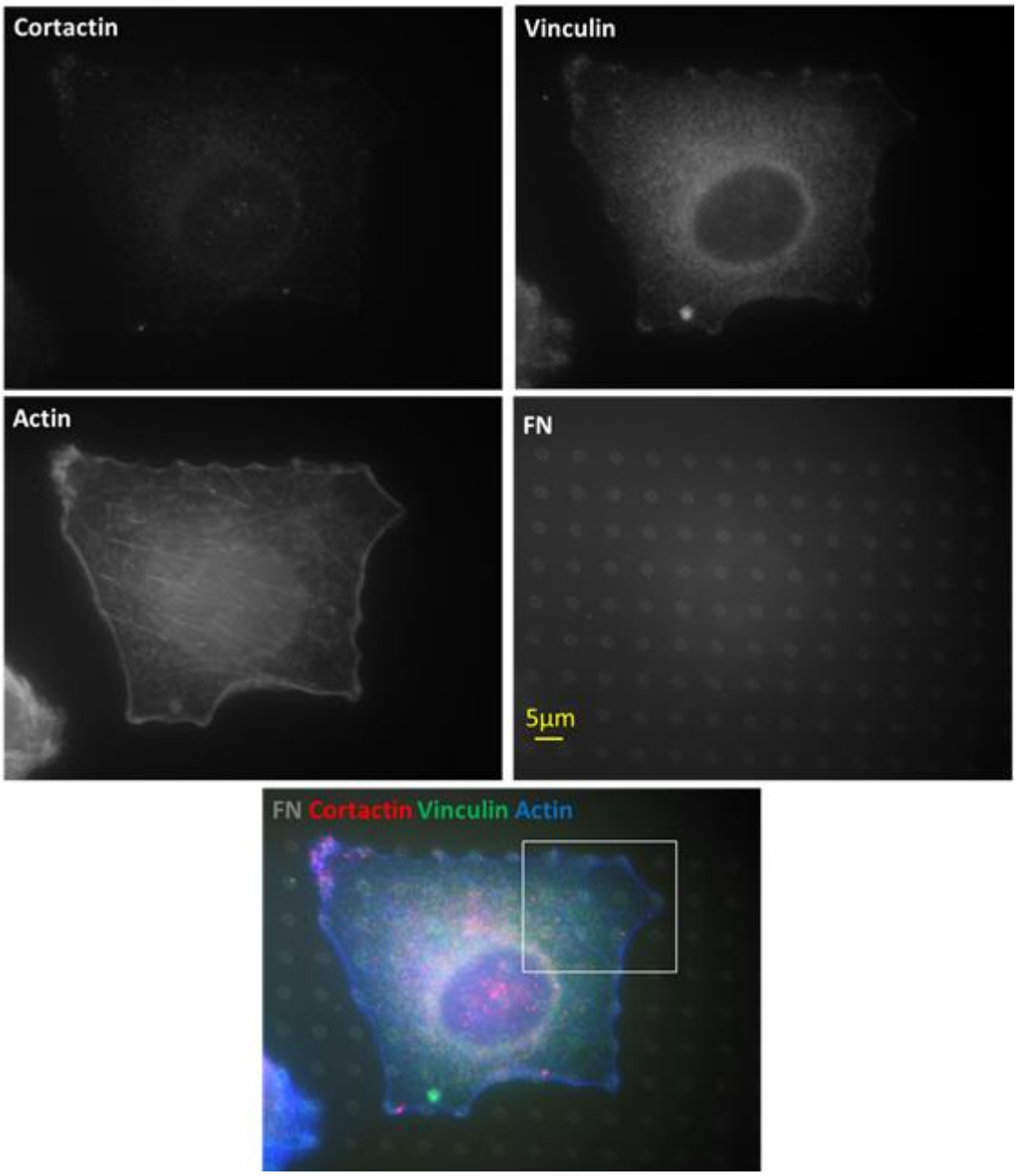

Figure 3.29. Pre-invadopodia and Focal Adhesions in Cell Cultured in the Presence of EGF for 24 hours on K-casein-FN Nanoring Patterns.

This figure shows a representative cell cultured in the presence of EGF for 24 hours on K-casein-FN nanoring patterns. Fibronectin, cortactin, actin, vinculin and merge images are represented in panels. Box in Figure 3.29 is magnified in Figure 3.30.

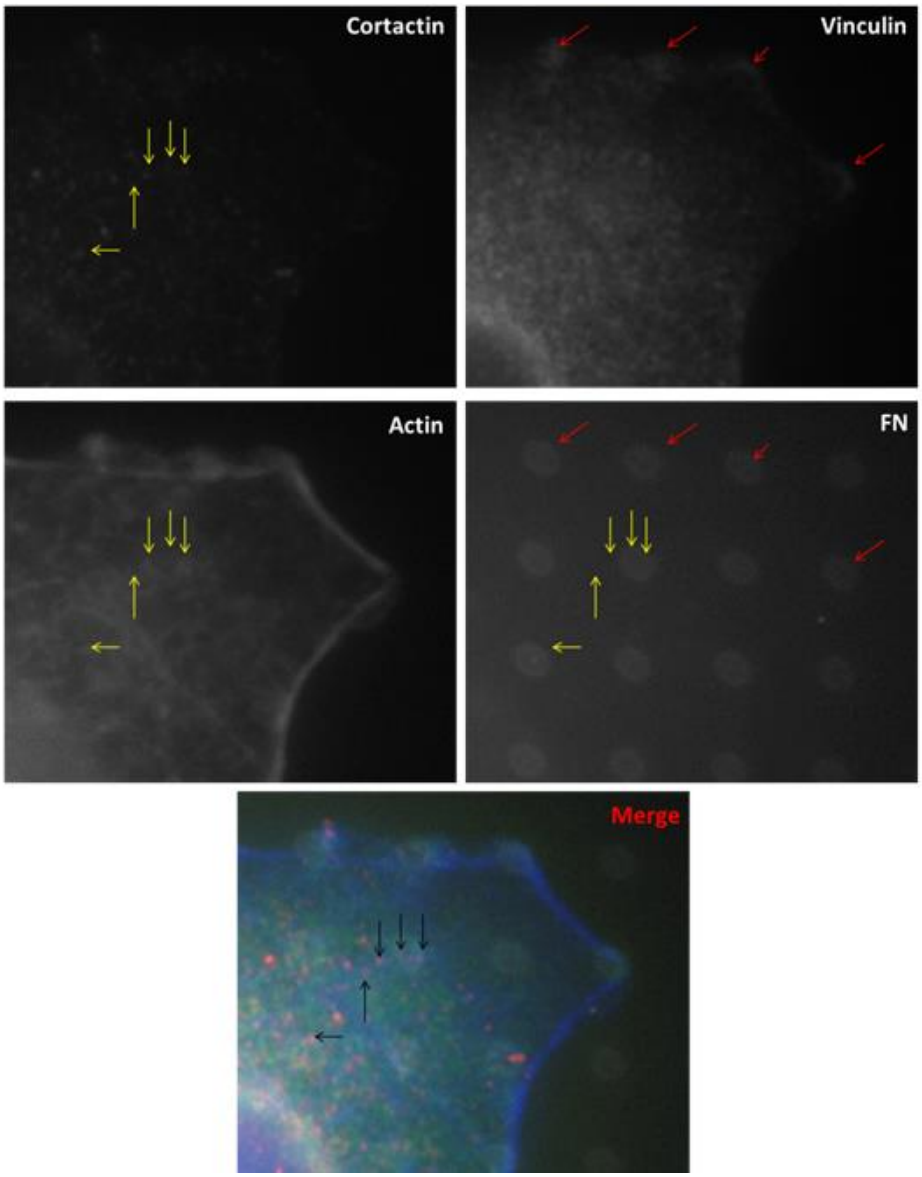

Figure 3.30. Magnification of Invadopodia Associated Area of Figure 3.29.

This figure shows at high magnification the upper cell area of Figure 3.29. Yellow arrows show pre-invadopodia positive for cortactin and actin, red arrows show focal adhesions. Invadopodia and focal adhesions were not observed at the same locations. We showed that there is not difference between localization of vinculin and actin proteins indicate that structure is podosome or focal adhesion. This means formation of podosomes can not be induced by ring shaped protein nanopatterns. There can be another genetic factors not depending on surface patterns cause the formation of podosome structure.

3.5. Invadopodia Formation in Cancer Cells Cultured in The Presence of EGF for 24 hours on Control and Single Active Component Surfaces

3.5.1. Invadopodia Formation on Fibronectin Control Surface

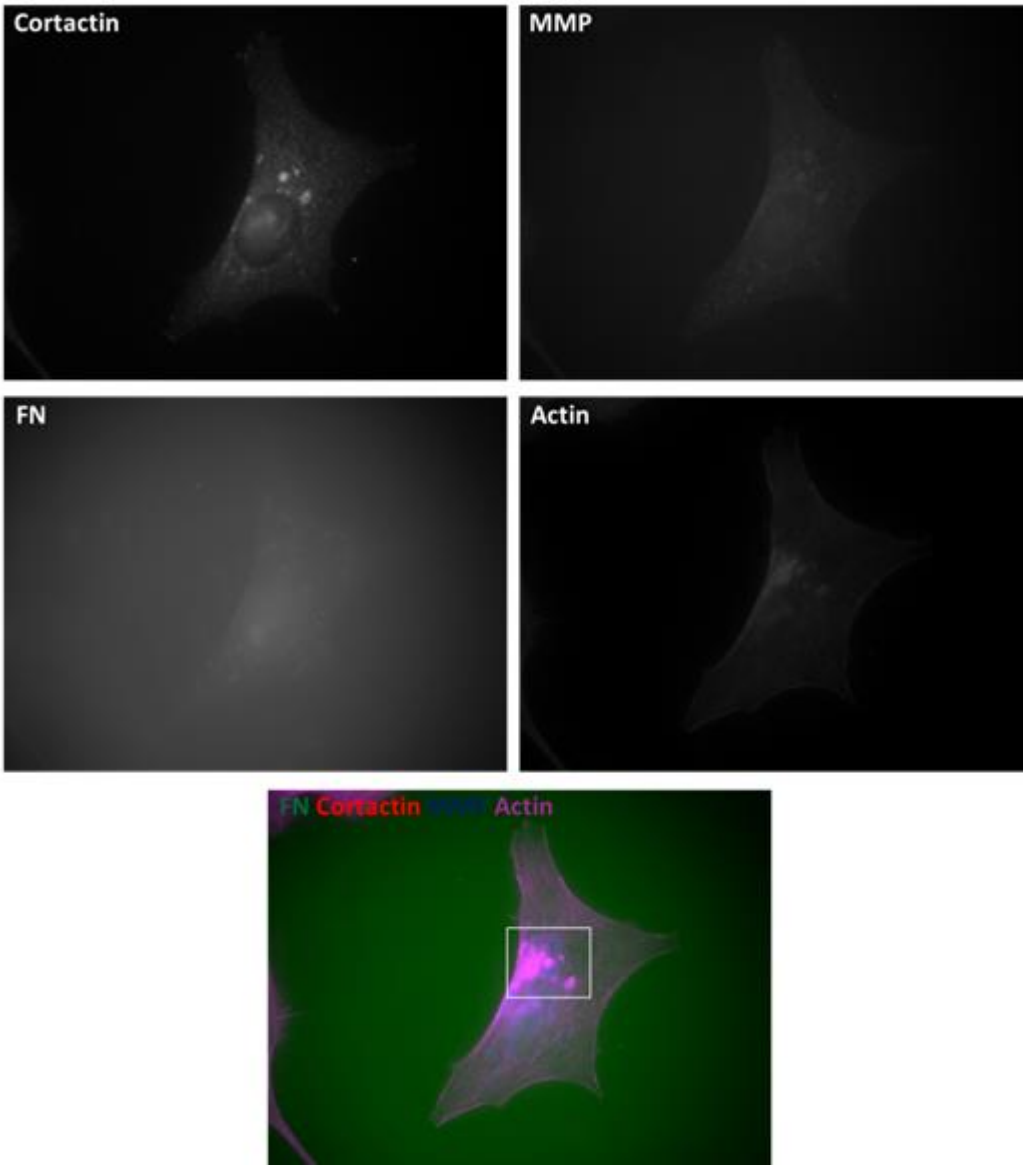

Figure 3.31. Invadopodia and MMP Transportation on Actin in a Cancer Cell Cultured in the Presence of EGF for 24 hours on Fibronectin Surface.

This figure shows a representative cell cultured in the presence of EGF for 24 hours on fibronectin surface. Fibronectin, cortactin, actin, MMP and merge images are represented in panels. Box in Figure 3.31 is magnified in Figure 3.32.

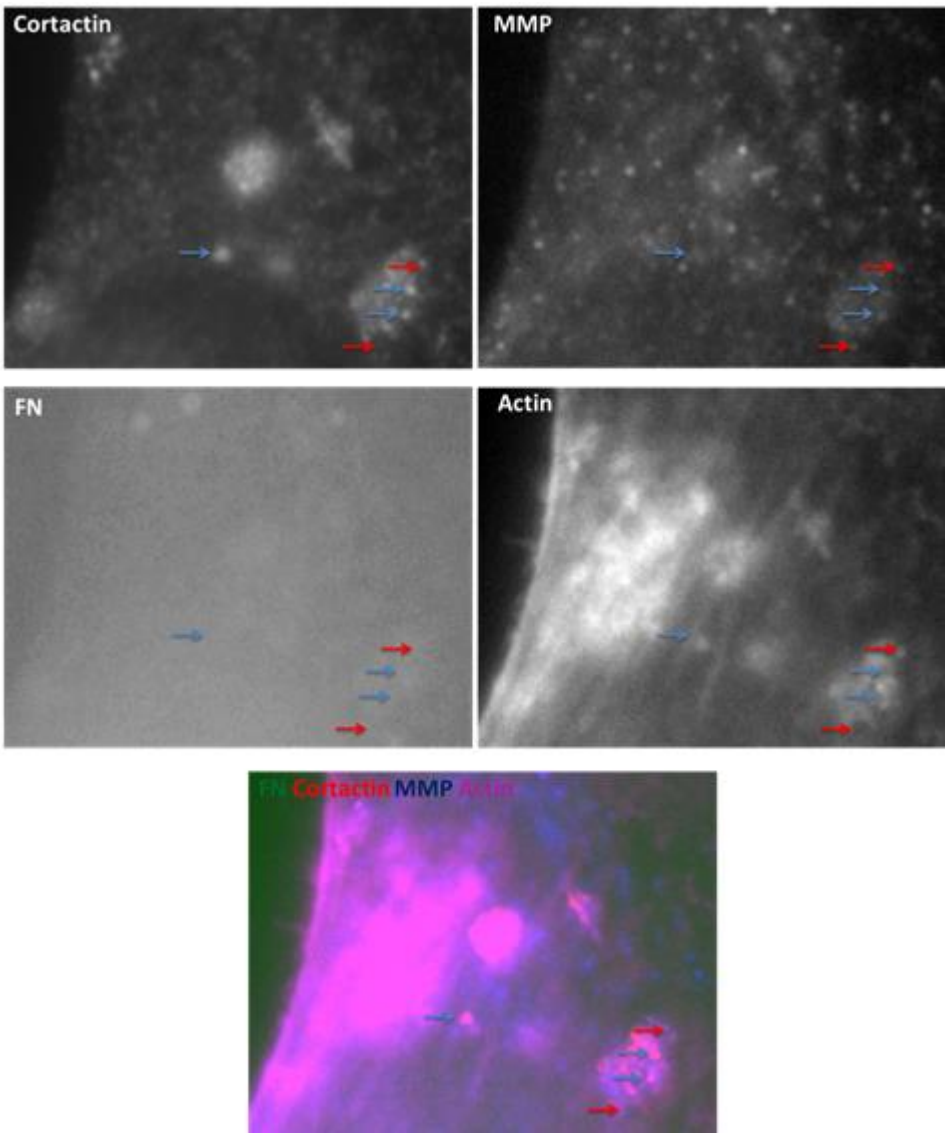

Figure 3.32. Magnification of Invadopodia Associated Area of Figure 3.31.

This figure shows at high magnification the middle cell area of Figure 3.31. Red arrows show transported MMPs on actin and blue arrows show invadopodia positive for MMP, cortactin and actin.

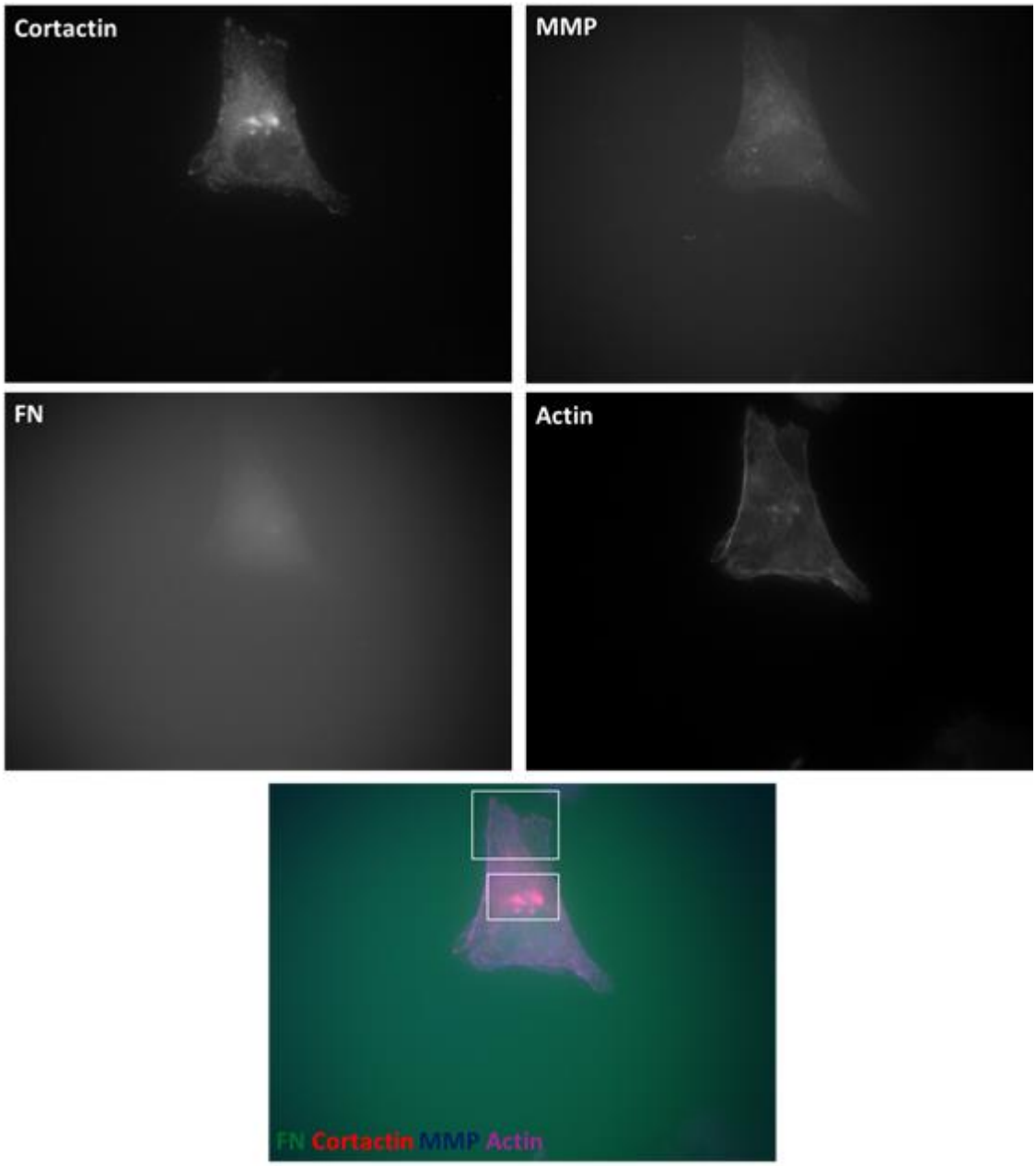

Figure 3.33. Invadopodia in a Cell Cultured in the Presence of EGF for 24 hours on Fibronectin Surface.

This figure shows a representative cell cultured in the presence of EGF for 24 hours on fibronectin surface. Fibronectin, cortactin, actin, MMP and merge images are represented in panels. Box in Figure 3.34 is magnified in Figure 3.35 and Figure 3.36.

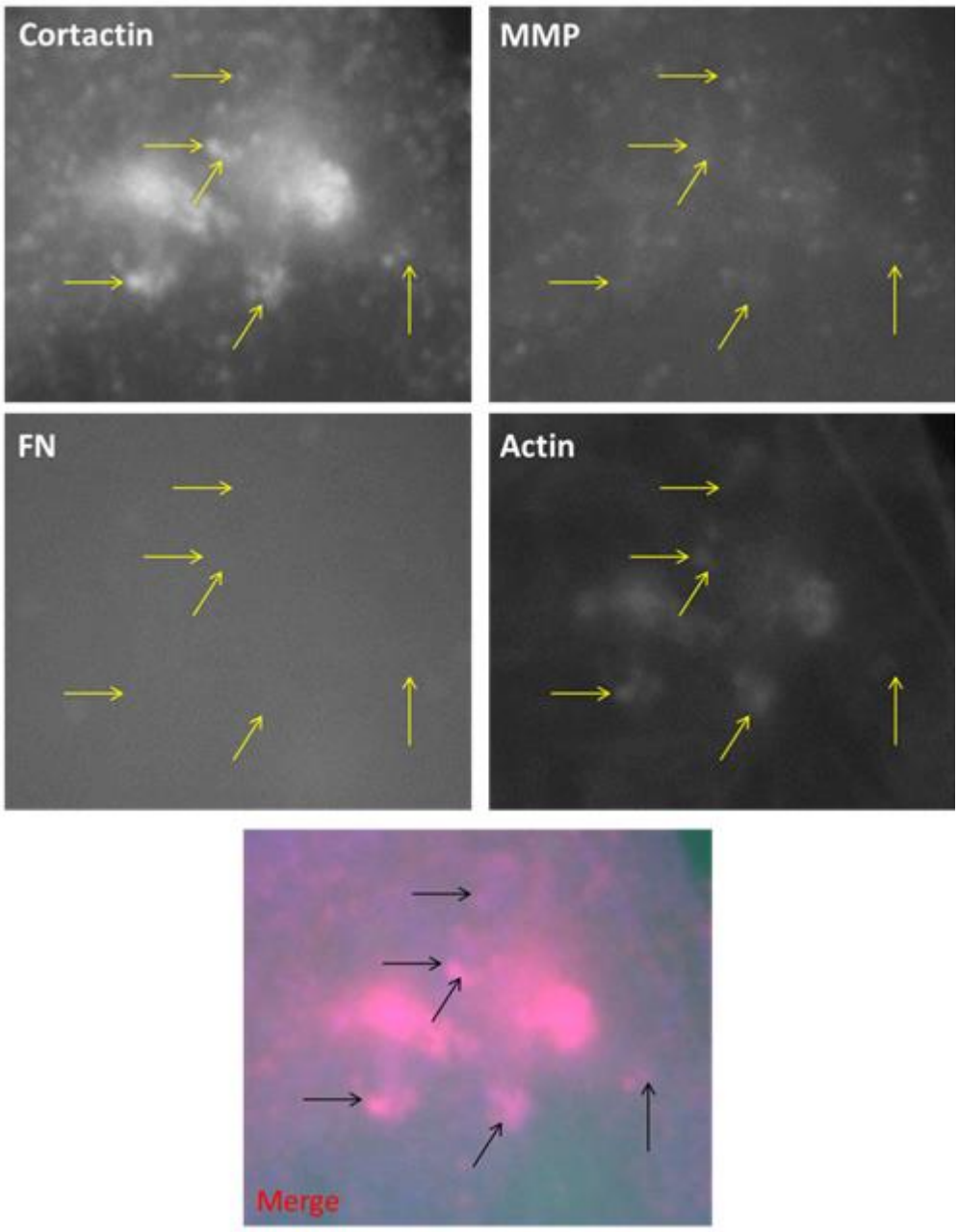

Figure 3.34. Magnification of Invadopodia Associated Area of Figure 3.33.

This figure shows at high magnification the middle cell area of Figure 3.33. Yellow and black arrows show invadopodia positive for MMP, actin, cortactin.

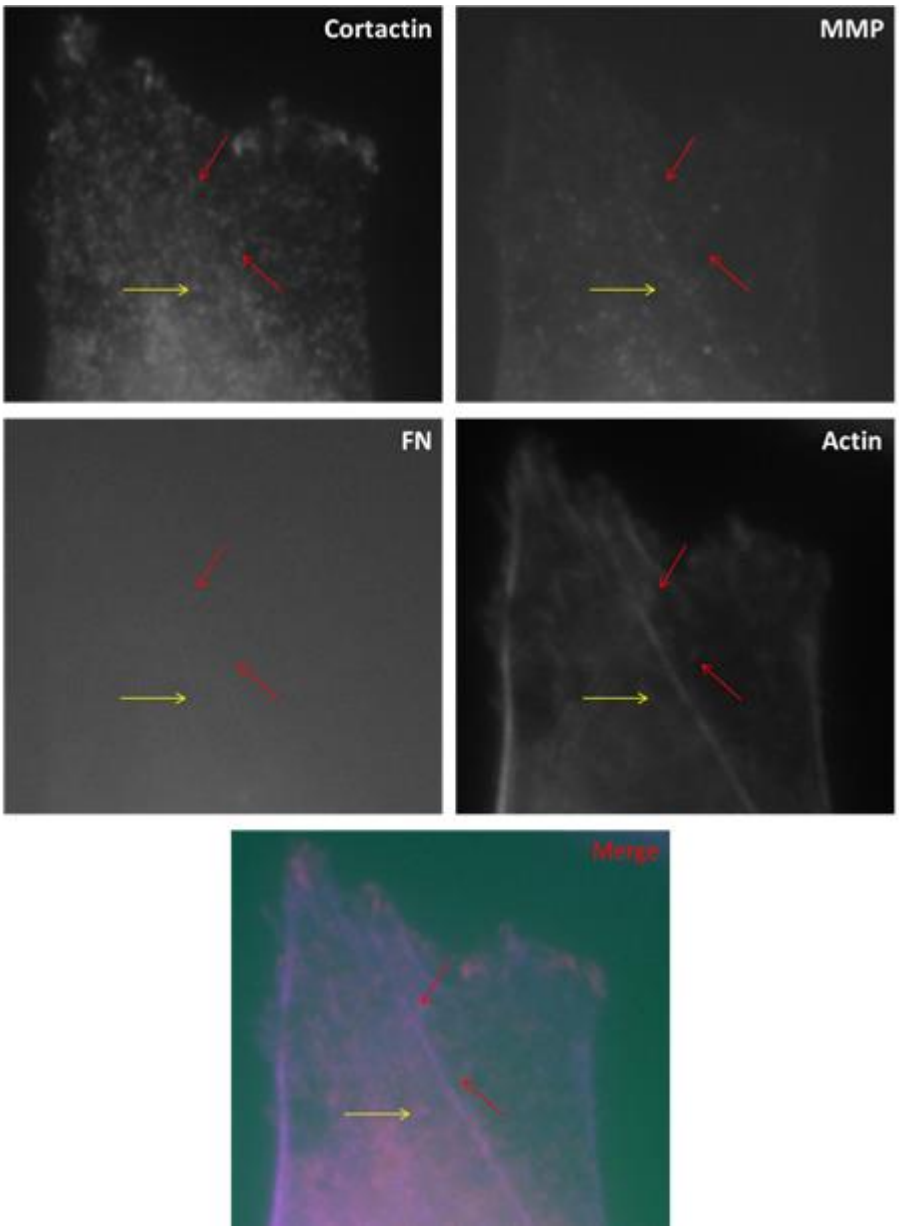

Figure 3.35. Magnification of Invadopodia Associated Area of Figure 3.33.

This figure shows at high magnification the upper cell area of Figure 3.33. Red arrows show pre-invadopodia positive for cortactin and actin.

3.5.2. Invadopodia Formation on Laminin Surface

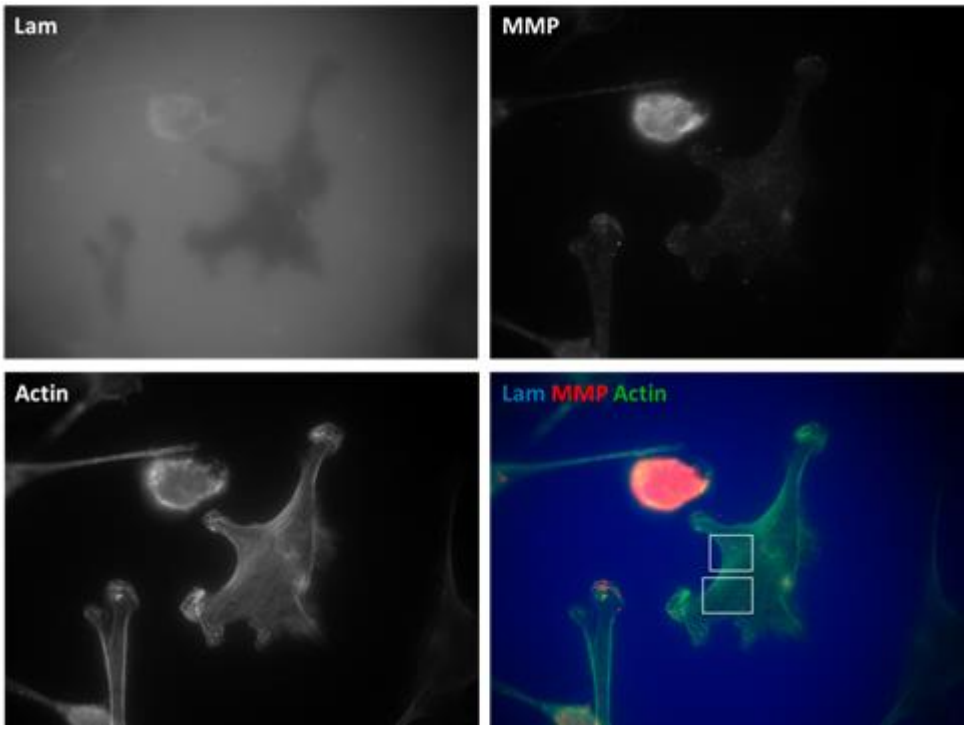

Figure 3.36. Invadopodia in a cancer cell cultured in the presence of EGF for 24 hours on laminin surface.

This figure shows a representative cell cultured in the presence of EGF for 24 hours on laminin surface. Laminin, actin, MMP and merge images are represented in panels. Boxes in Figure 3.36 is magnified in Figure 3.37 and Figure 3.38.

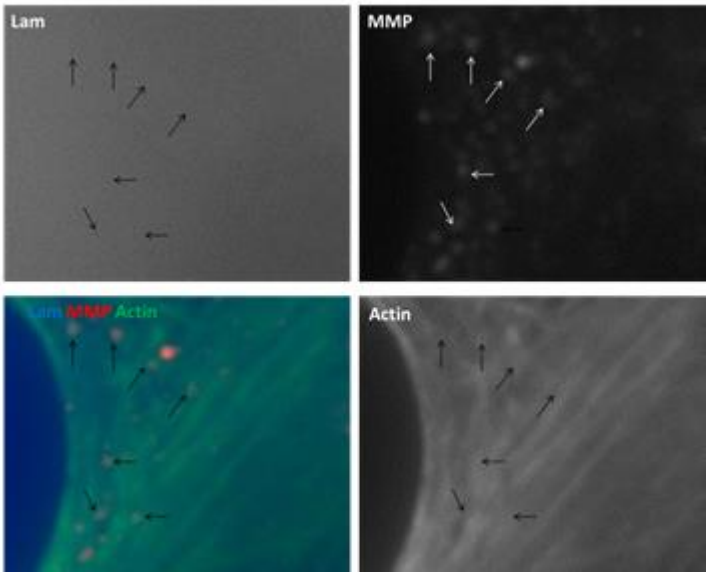

Figure 3.37. Magnification of invadopodia associated area of Figure 3.36.

This figure shows at high magnification the middle cell area of Figure 3.36. Black and white arrows show transportation of MMPs on actin. There are degradations on laminin surface. We can say that some invadopodia transform into mature invadopodia so they can realize matrix degradation.

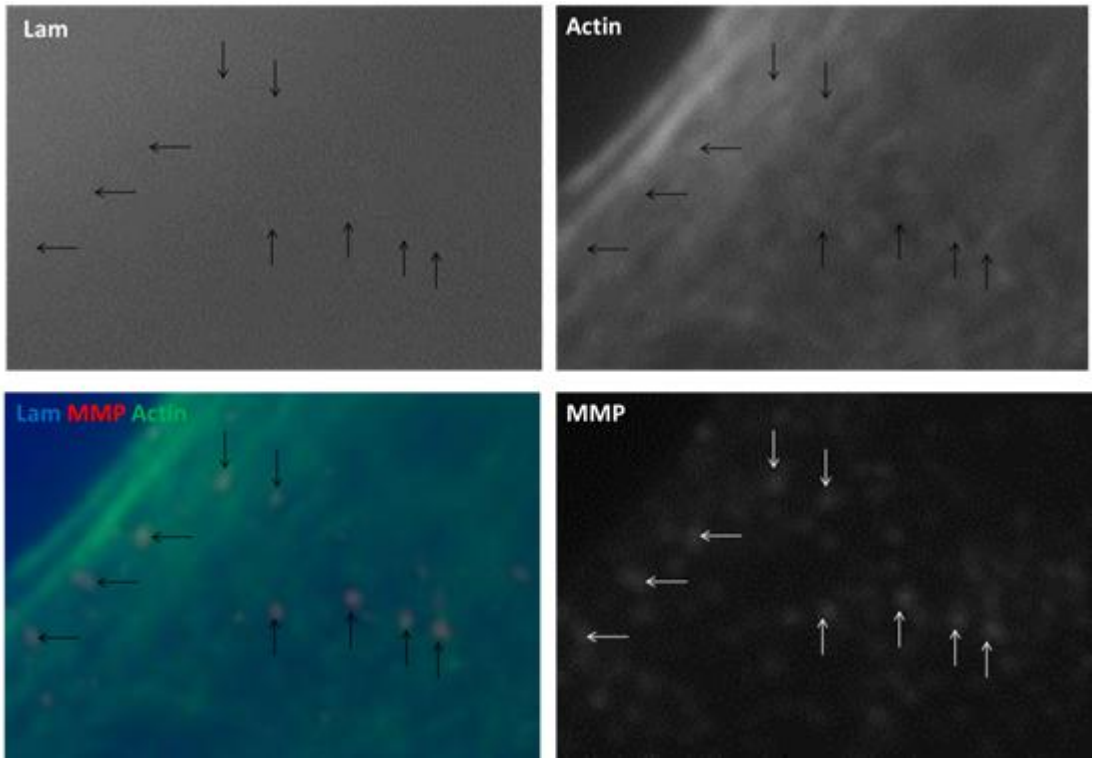

Figure 3.38. Magnification of invadopodia associated area of Figure 3.36.

This figure shows at high magnification the lower left cell area of Figure 3.36. Black and white arrows show transportation of MMPs on actin. There are degradations on laminin surface. We can say that some invadopodia transform into mature invadopodia so they can realize matrix degradation.

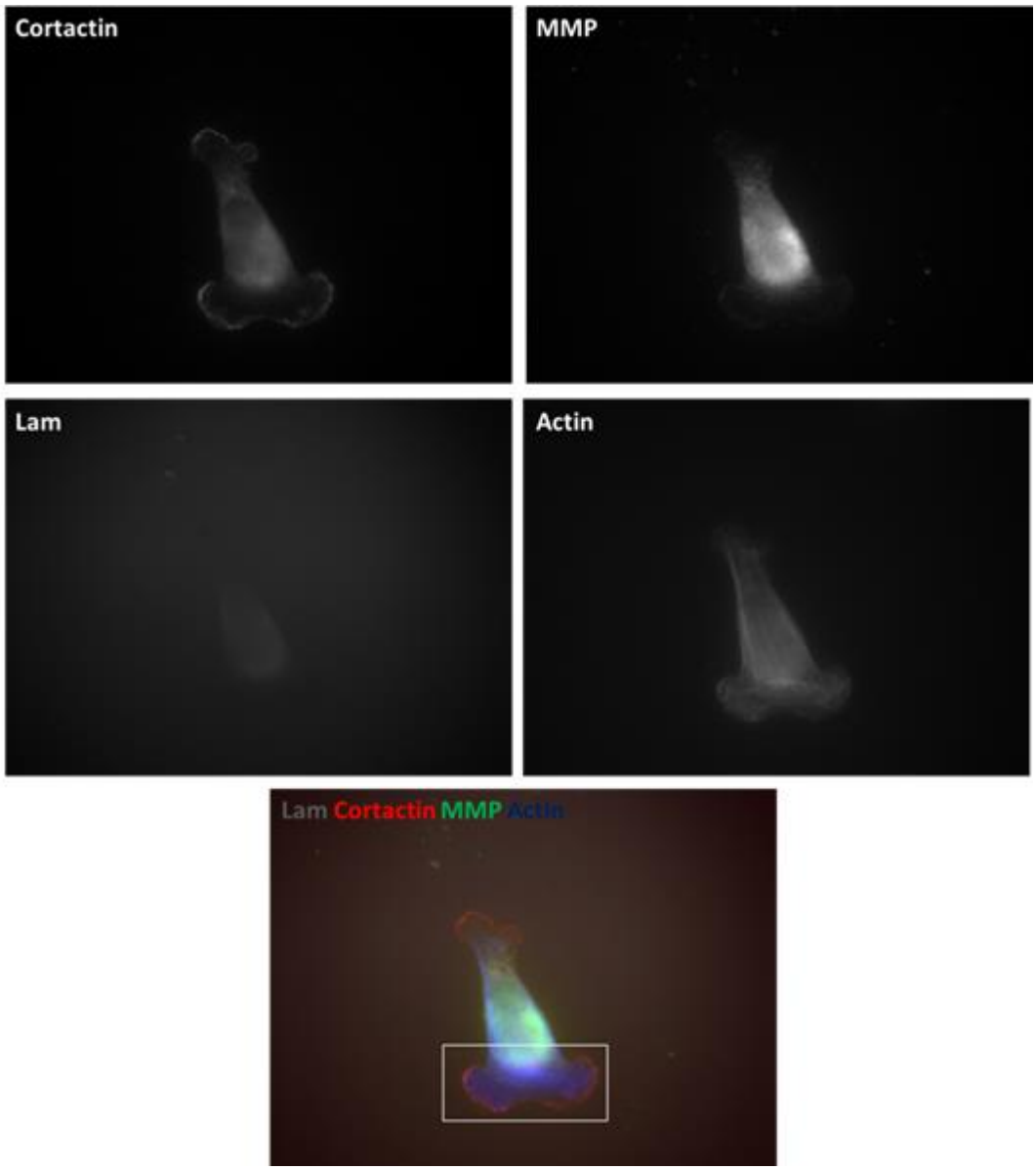

Figure 3.39. Invadopodia in a cell cultured in the presence of EGF for 24 hours on laminin surface.

This figure shows a representative cell cultured in the presence of EGF for 24 hours on laminin surface. Laminin, cortactin, actin, MMP and merge images are represented in panels. Box in Figure 3.39 is magnified in Figure 3.40.

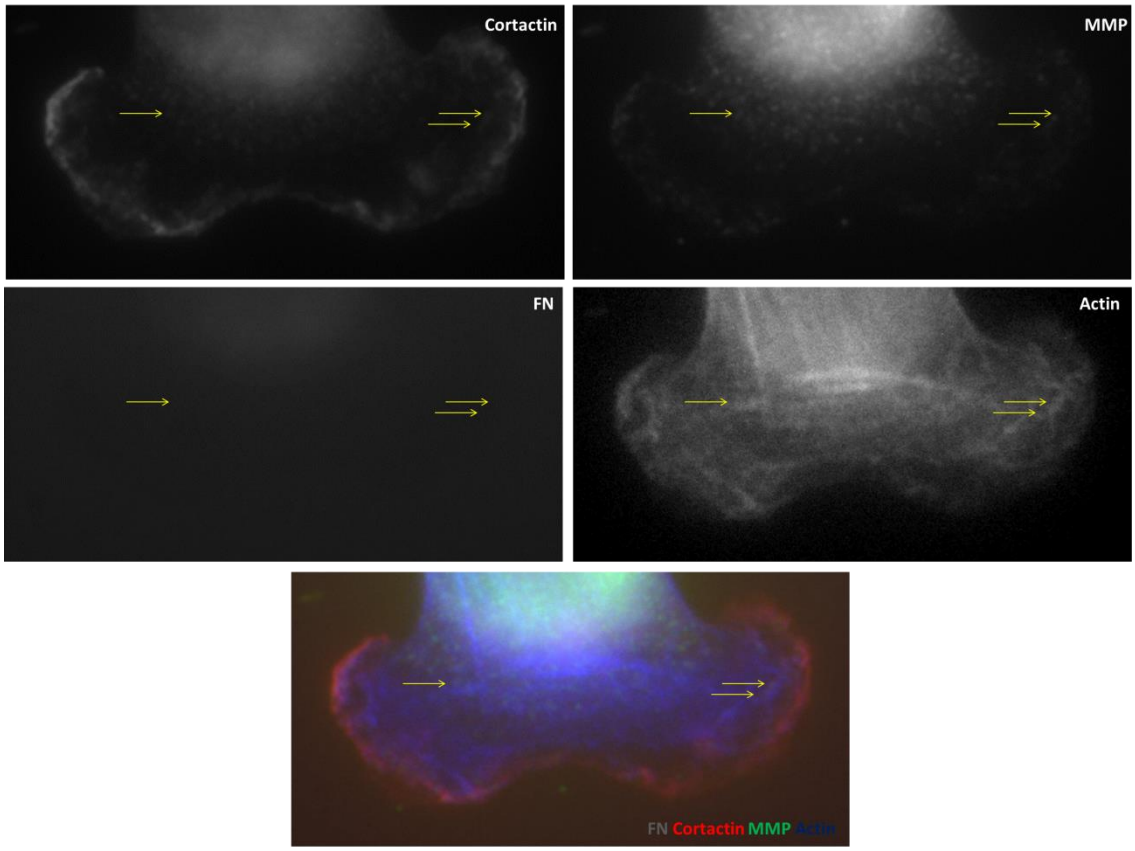

Figure 3.40.Magnification of invadopodia associated area of Figure 3.39.

This figure shows at high magnification the lower cell area of Figure 3.39. Yellow arrows show invadopodia positive for MMP, cortactin, actin.

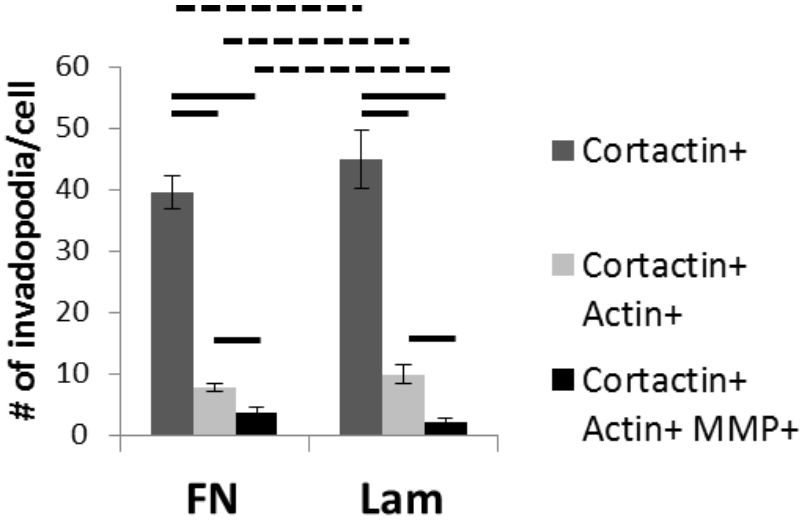

Figure 3.41. Number of invadopodia per cell in MDA-MB-231 breast cancer cells cultured in the presence of EGF for 24 hours on fibronectin and laminin surfaces.

Cortactin+ Actin+ shows all pre-invadopodia, Cortactin+ Actin+ MMP+ shows invadopodia. Horizontal straight lines show the statistical difference is $p<0.05$ at one tail level while horizantal dotted lines show the statistical difference is $p<0.05$ at two tail level. Number of invadopodia per cell on laminin surface is more than fibronectin surface but numbers are close to each other. Direct connection between FN and integrin is stronger compare to laminin at the focal adhesions. It means cells form higher number of focal adhesions on FN surface. So cells prefer weak adhesion areas as laminin which they can form invadopodia freely. That's why cells prefer to form invadopodia on laminin rather than fibronectin surfaces.

3.6. Invadopodia Formation on Double Active Componenet Laminin-Fibronectin

Silicon surfaces were coated with laminin after EBL patterning on fibronectin coated surfaces. Cells culturedin the presence of EGF for 24 hours on double active component surface. Invadopodia formation was analyzed in comparison with fibronectin and laminin control surfaces, single active component surface.

3.6.1. Pre-invadopodia Formation on Double Active Component Laminin-Fibronectin Nanodot Patterns

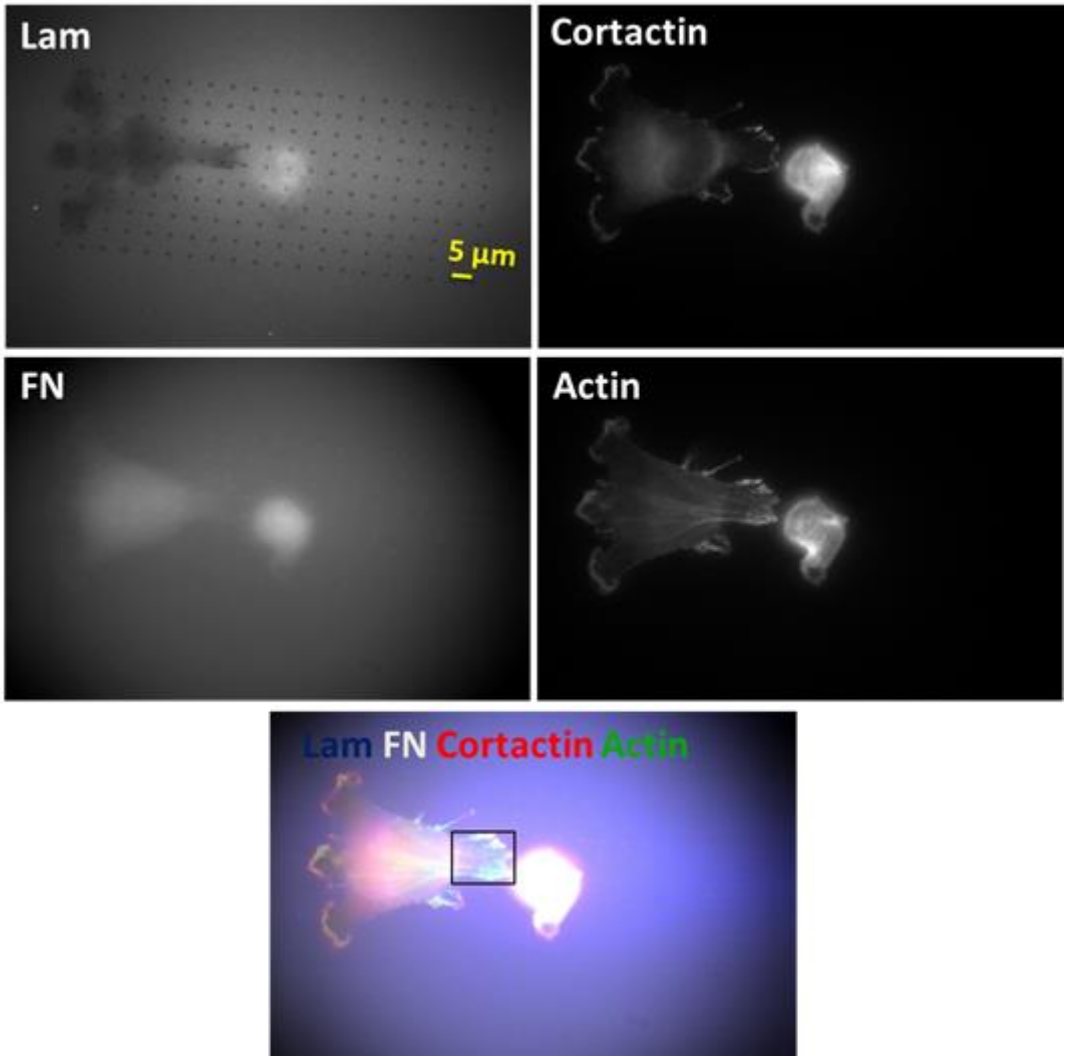

Figure 3.42. Pre-invadopodia in a cell cultured in the presence of EGF for 24 hours on double active component nanodot patterns.

This figure shows a representative cell cultured in the presence of EGF for 24 hours on double active component nanodot patterns. Laminin, fibronectin, cortactin, actin and merge images are represented in panels. Box in Figure 3.42 is magnified in Figure 3.43.

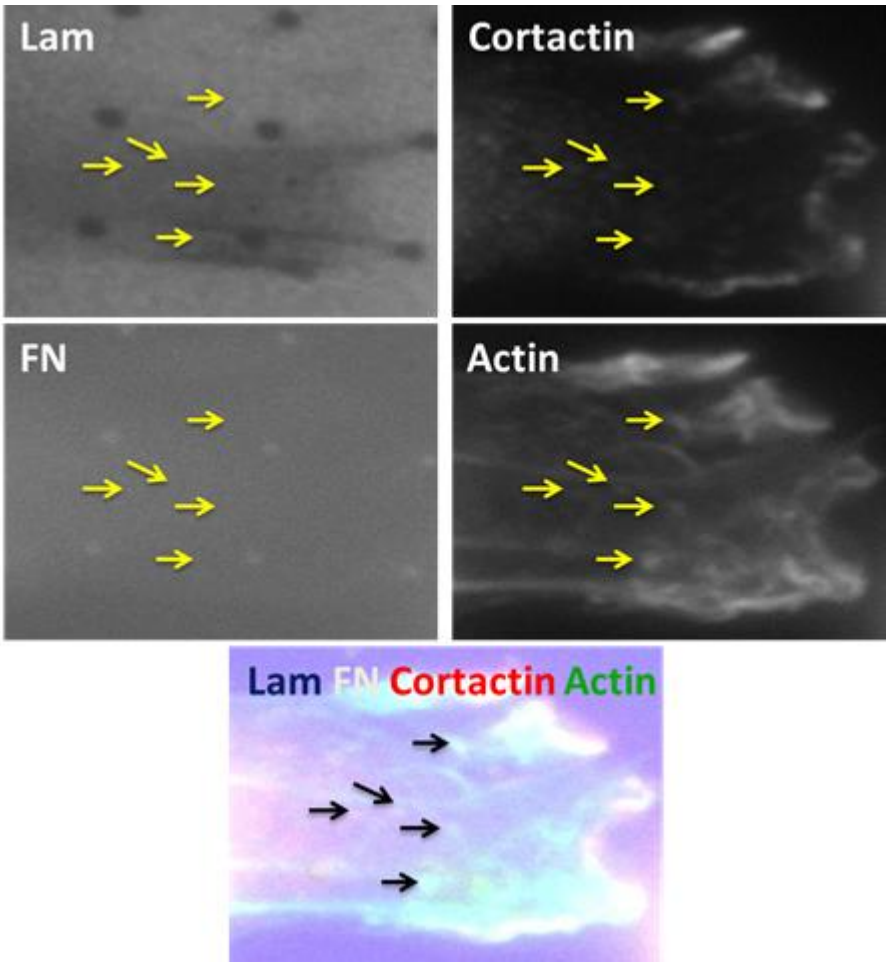

Figure 3.43. Magnification of invadopodia associated area of Figure 3.42.

This figure shows at high magnification the right cell corner of Figure 3.42. Yellow and black arrows show pre-invadopodia positive for cortactin and actin. Cells prefer to form invadopodia between fibronectin nanodot patterns. There are degradations on laminin surface. We can say that some invadopodia transform into mature invadopodia so they can realize matrix degradation.

3.6.2. Pre-invadopodia Formation on Double Active Component Laminin-Fibronectin Nanoring Patterns

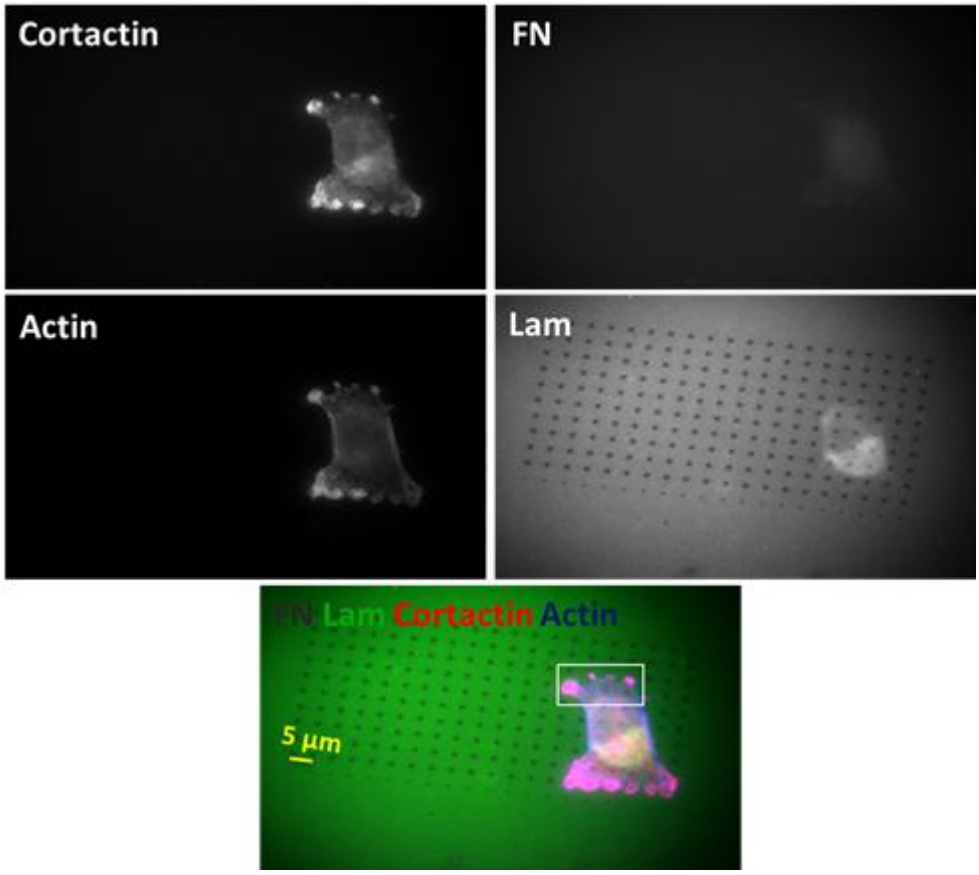

Figure 3.44. Pre-invadopodia in a cancer cell cultured in the presence of EGF for 24 hours on double active component nanoring patterns.

This figure shows a representative cell cultured in the presence of EGF for 24 hours on double active component nanoring patterns. Laminin, fibronectin, cortactin, actin and merge images are represented in panels. Box in Figure 3.45 is magnified in Figure 3.47.

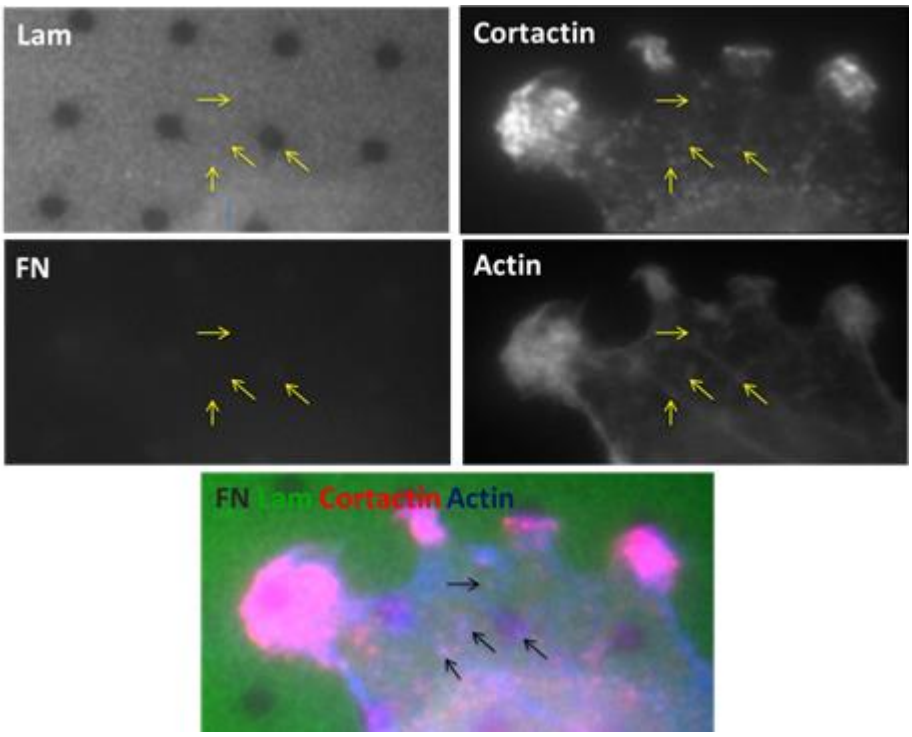

Figure 3.45. Magnification of invadopodia associated area of Figure 3.44.

This figure shows at high magnification the upper cell area of Figure 3.44. Yellow and black arrows show pre-invadopodia positive for cortactin and actin. Cells prefer to form invadopodia between fibronectin nanoring patterns.

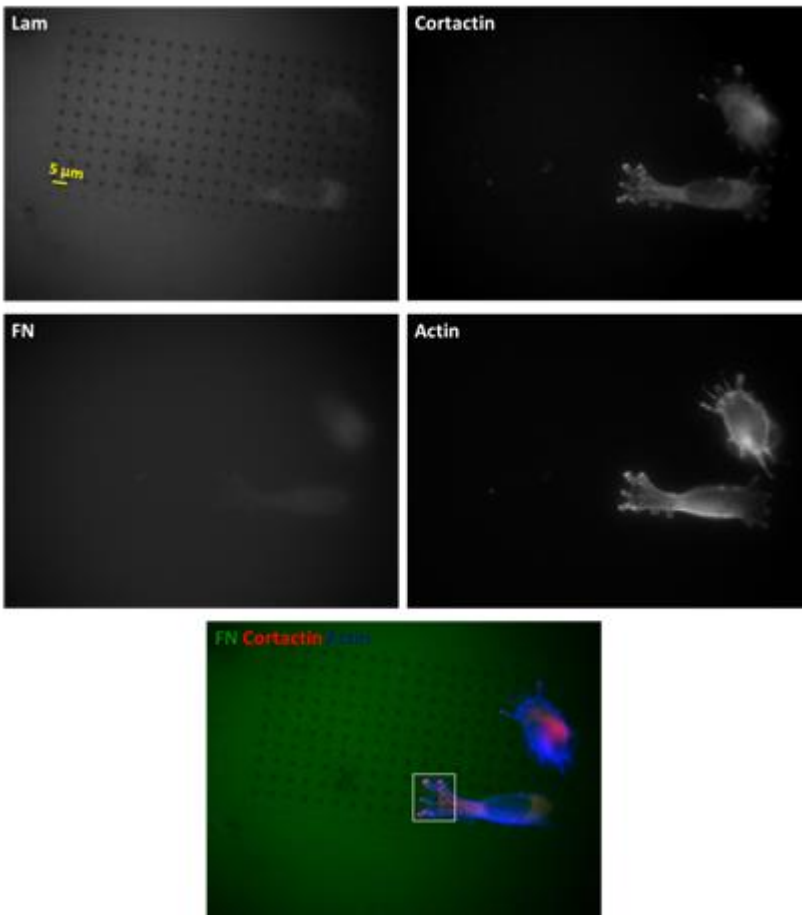

Figure 3.46. Pre-invadopodia in a cancer cell cultured in the presence of EGF for 24 hours on double active component nanoring patterns.

This figure shows a representative cell cultured in the presence of EGF for 24 hours on double active component nanoring patterns. Laminin, fibronectin, cortactin, actin and merge images are represented in panels. Box in Figure 3.46 is magnified in Figure 3.47.

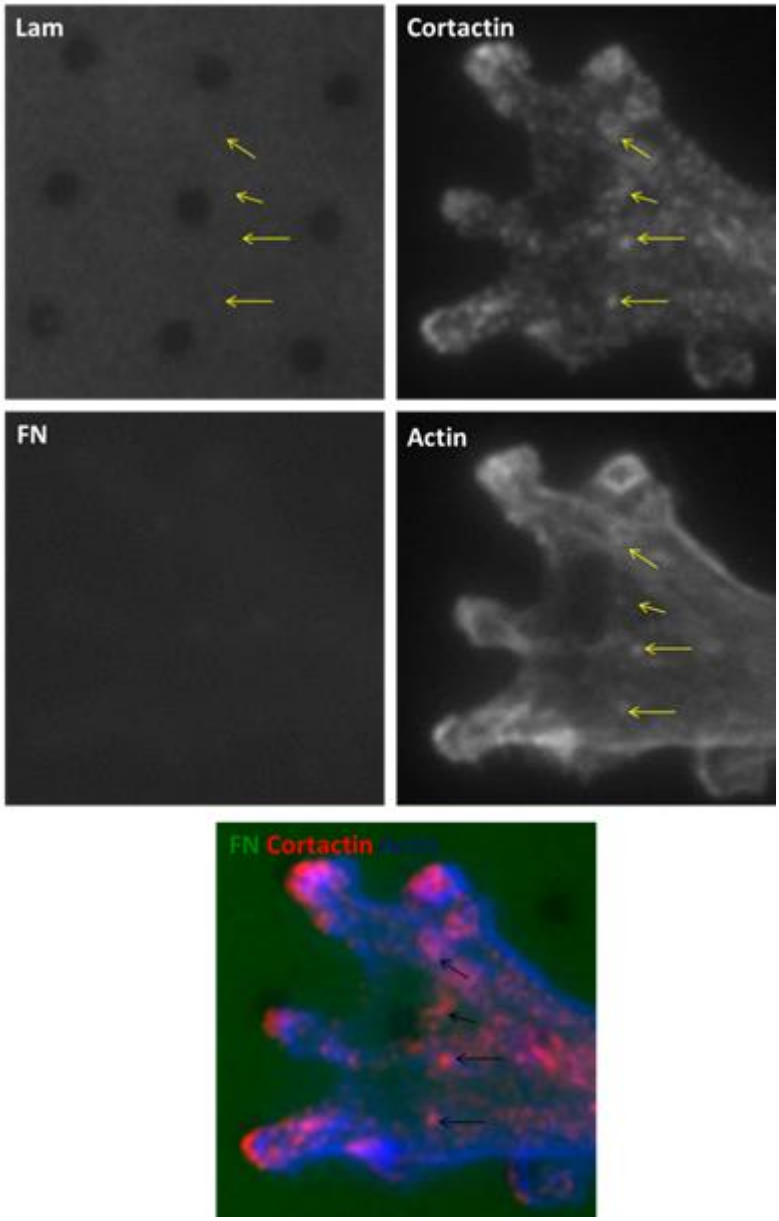

Figure 3.47. Magnification of invadopodia associated area of Figure 3.46.

This figure shows at high magnification the left cell corner of Figure 3.46. Yellow and black arrows show pre-invadopodia positive for cortactin and actin. Cells prefer to form invadopodia between fibronectin nanoring patterns.

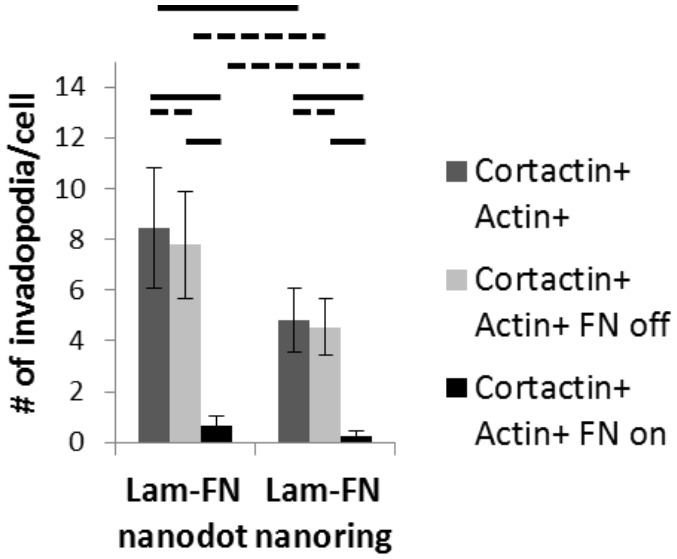

Figure 3.48. Quantitative distribution of invadopodia on Laminin-Fibronectin nanodot and Laminin-Fibronectin nanoring patterns.

Cortactin+ Actin+ shows all pre-invadopodia in MDA-MB-231 breast cancer cells, Cortactin+ Actin+ FN on shows pre-invadopodia formed on nanopatterns, Cortactin+ Actin+ FN off shows pre-invadopodia formed between nanopatterns. Horizontal straight lines show the statistical difference is $p<0.05$ at one tail level while horizantal dotted lines show the statistical difference is $p<0.05$ at two tail level. Number of formed pre-invadopodia per cell on nanodot patterns is more than nanoring patterns. Cells prefer to form invadopodia between fibronectin nanopatterns for each nanopatterns (nanodot/nanoring). There is a difference between formed invadopodia on fibronectin nanopatterns and beetween fibronectin nanopatterns.

3.7. Invadopodia Formation in Cancer Cells Cultured in The Presence of EGF for 24 hours on Single and Double Active Component Surfaces

3.7.1. Invadopodia Formation in Cancer Cells Cultured in The Presence of EGF for 24 hours on Single Active Component Nanodot Patterns

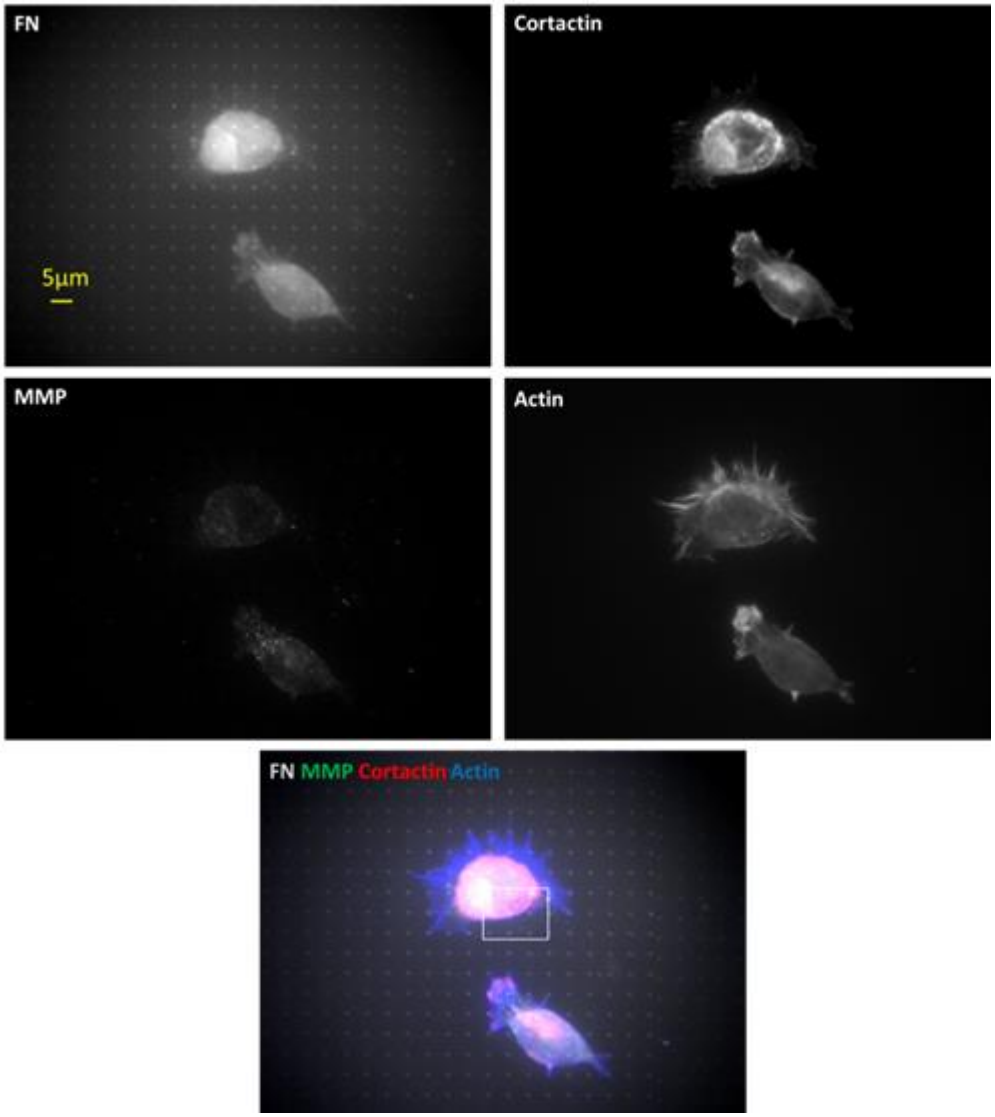

Figure 3.49. Invadopodia in a cell was incubated in the presence of EGF for 24 hours on single active component nanodot patterns.

This figure shows a representative cell was incubated in the presence of EGF for 24 hours on single active component nanodot patterns. Fibronectin, cortactin, actin, mmp and merge images are represented in panels. Box in Figure 3.49 is magnified in Figure 3.50.

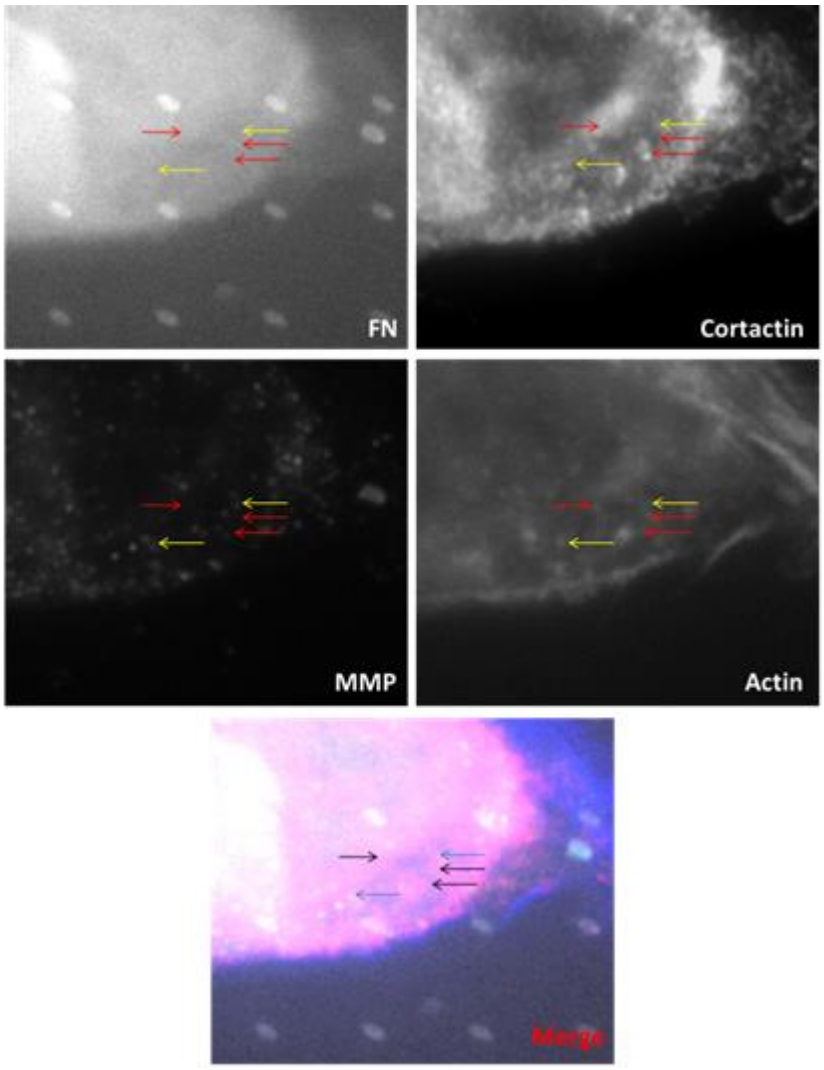

Figure 3.50. Magnification of invadopodia associated area of Figure 3.49.

This figure shows at high magnification the lower cell area of Figure 3.49. Yellow arrows show invadopodia positive for mmp, cortactin and actin, red arrows show pre-invadopodia positive for cortactin and actin. In merge image black arrows pre-invadopodia positive for cortactin and actin, blue arrows show invadopodia positive for mmp, cortactin and actin.

3.7.2. Invadopodia Formation in Cancer Cells Cultured in The Presence of EGF for 24 hours on Single Active Component Nanoring Patterns

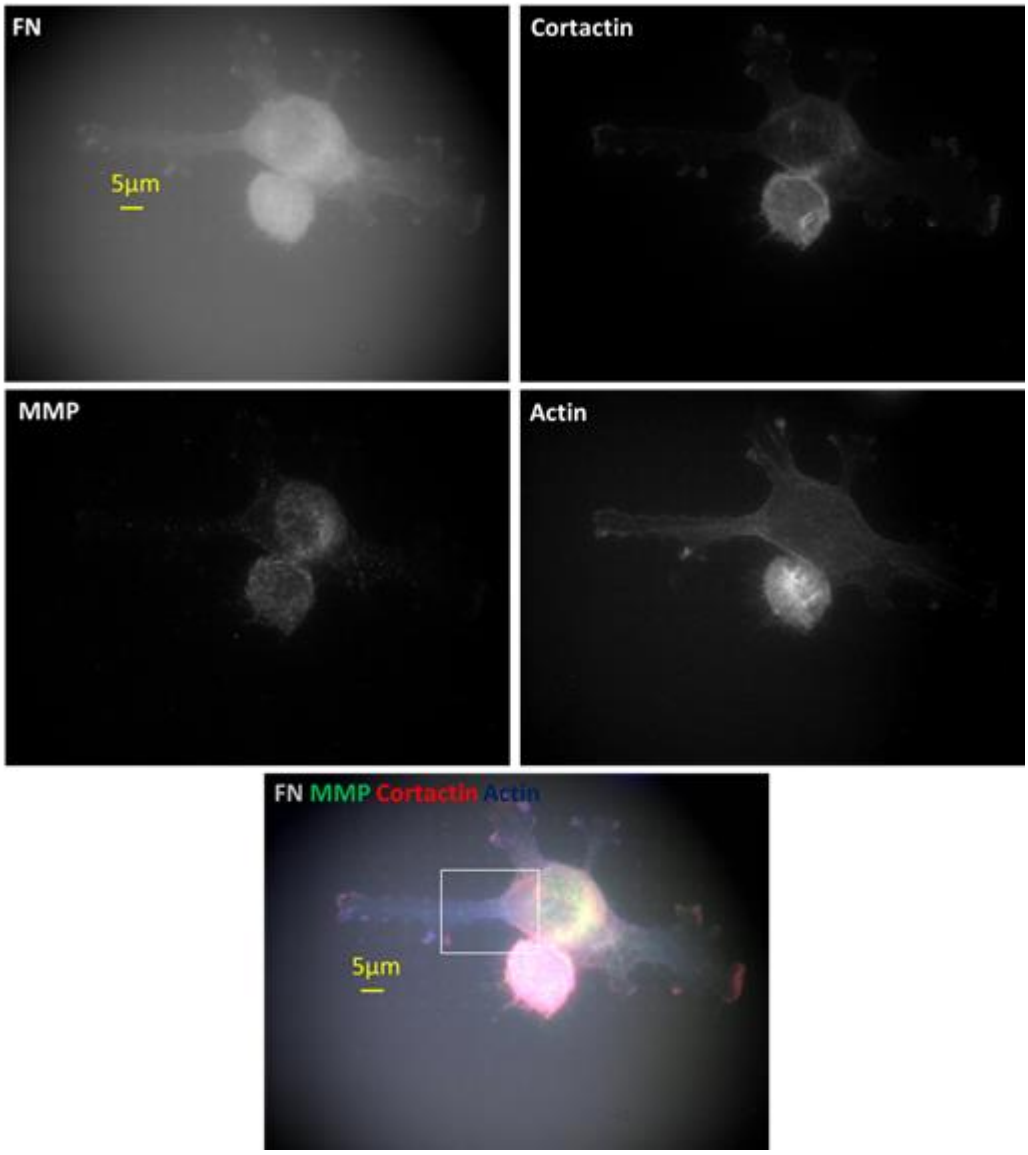

Figure 3.51. Invadopodia in a cell cultured in the presence of EGF for 24 hours on single active component nanoring patterns.

This figure shows a representative cell cultured in the presence of EGF for 24 hours on single active component nanoring patterns. Fibronectin, cortactin, actin, mmp and merge images are represented in panels. Box in Figure 3.51 is magnified in Figure 3.52.

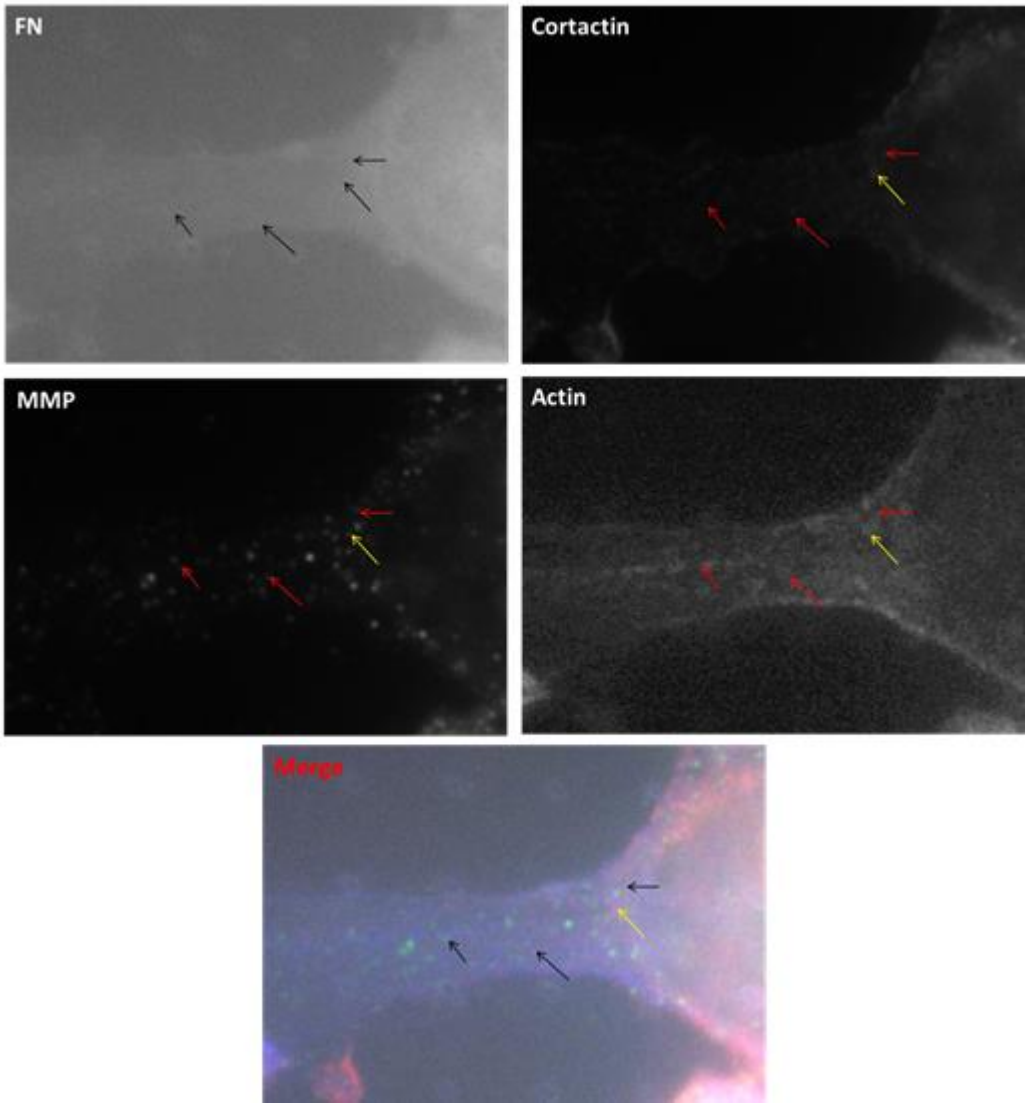

Figure 3.52. Magnification of MMPs transportation associated area of Figure 3.51.

This figure shows at high magnification the left cell area of Figure 3.51. Red arrows show transportation of mmp on actin, yellow arrows show pre-invadopodia positive for cortactin and actin. In merge image yellow arrows show pre-invadopodia and black arrows show transportation of mmp on actin.

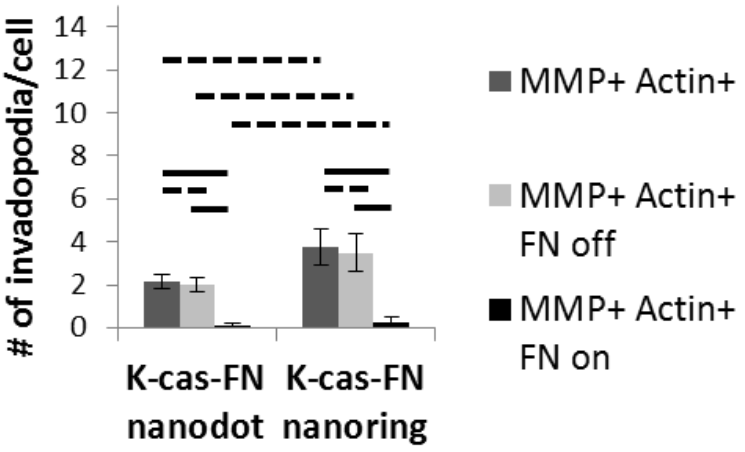

Figure 3.53. Quantitative distribution of transportation of mmps on K-casein-Fibronectin nanodot and K-casein-Fibronectin nanoring patterns.

MMP+ Actin+ shows all mmps are transported on actin in MDA-MB-231 breast cancer cells, MMP+ Actin+ FN on shows transportation of mmps on actin on nanopatterns, MMP+ Actin+ FN off shows transportation of mmps on actin between nanopatterns. Horizontal straight lines show the statistical difference is $p<0.05$ at one tail level while horizantal dotted lines show the statistical difference is $p<0.05$ at two tail level.

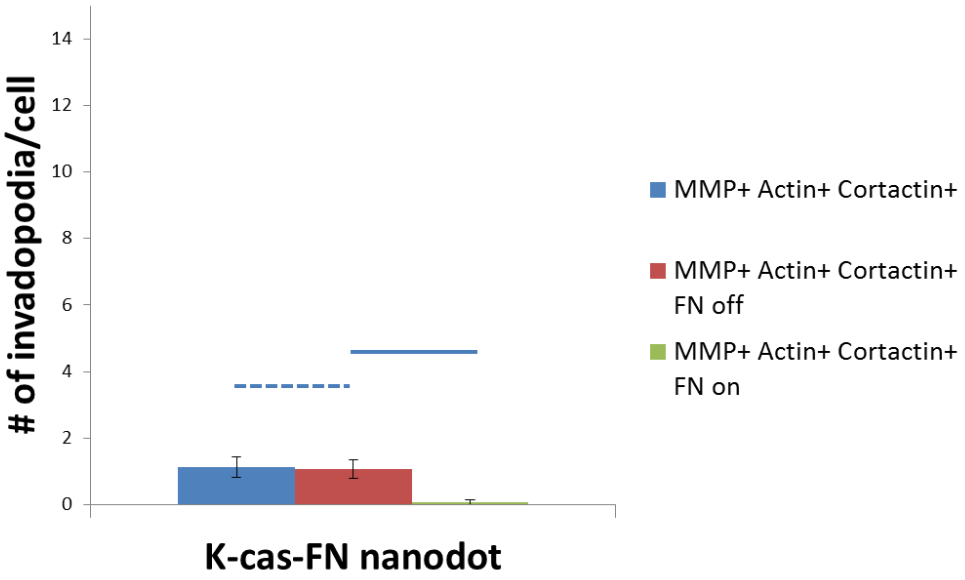

Figure 3.54. Quantitative distribution of invadopodia positive for cortactin, actin and mmp on K-casein-Fibronectin nanodot patterns.

MMP+ Actin+ Cortactin+ shows all invadopodia in MDA-MB-231 breast cancer cells, MMP+ Actin+ Cortactin+ FN on shows invadopodia on nanopatterns, MMP+ Actin+ Cortactin+ FN off shows invadopodia between nanopatterns. Horizontal straight lines show the statistical difference is $p<0.05$ at one tail level while horizantal dotted lines show the statistical difference is $p<0.05$ at two tail level. There is a difference between formed invadopodia on fibronectin nanopatters and between nanopatterns. Cells prefer to form invadopodia between fibronectin nanopatterns rather than on fibronectin nanopatterns.

3.7.3. Distribution of MMPs Transportation on Actin in Cancer Cells Cultured in The Presence of EGF for 24 hours on Double Active Component Nanopatterns

3.7.3.1. Distribution of MMPs Transportation on Actin in Cancer Cells Cultured in The Presence of EGF for 24 hours on Double Active Component Nanodot Patterns

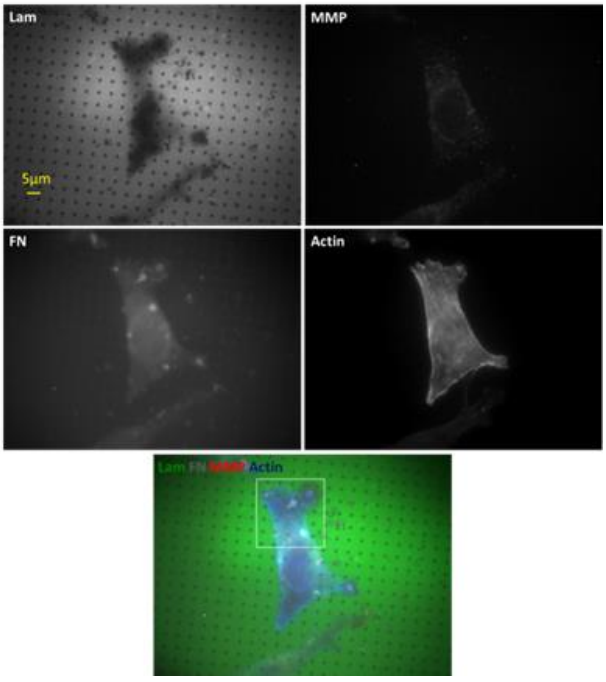

Figure 3.55. Transported MMPs on actin in a cell cultured in the presence of EGF for 24 hours on double active component nanodot patterns.

This figure shows a representative cell cultured in the presence of EGF for 24 hours on double active component nanodot patterns. Fibronectin, laminin, actin, mmp and merge images are represented in panels. Box in Figure 3.56 is magnified in Figure 3.57.

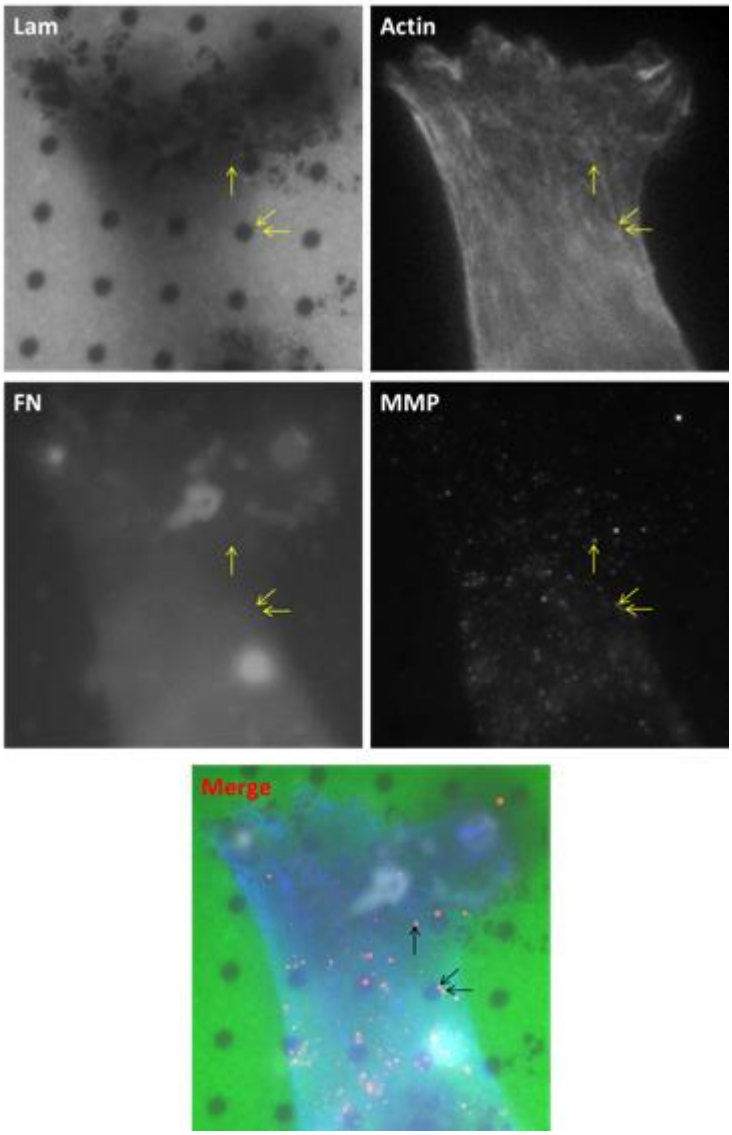

Figure 3.56. Magnification of transported MMPs associated area of Figure 3.55.

This figure shows at high magnification a upper cell area of Figure 3.55. Yellow and black arrows show transportation of mmps on actin. There are degradations on laminin surface. We can say that some invadopodia transform into mature invadopodia so they can realize matrix degradation.

3.7.4. Distribution of MMPs Transportation on Actin in Cancer Cells Cultured in The Presence of EGF for 24 hours on Double Active Component Nanoring Patterns

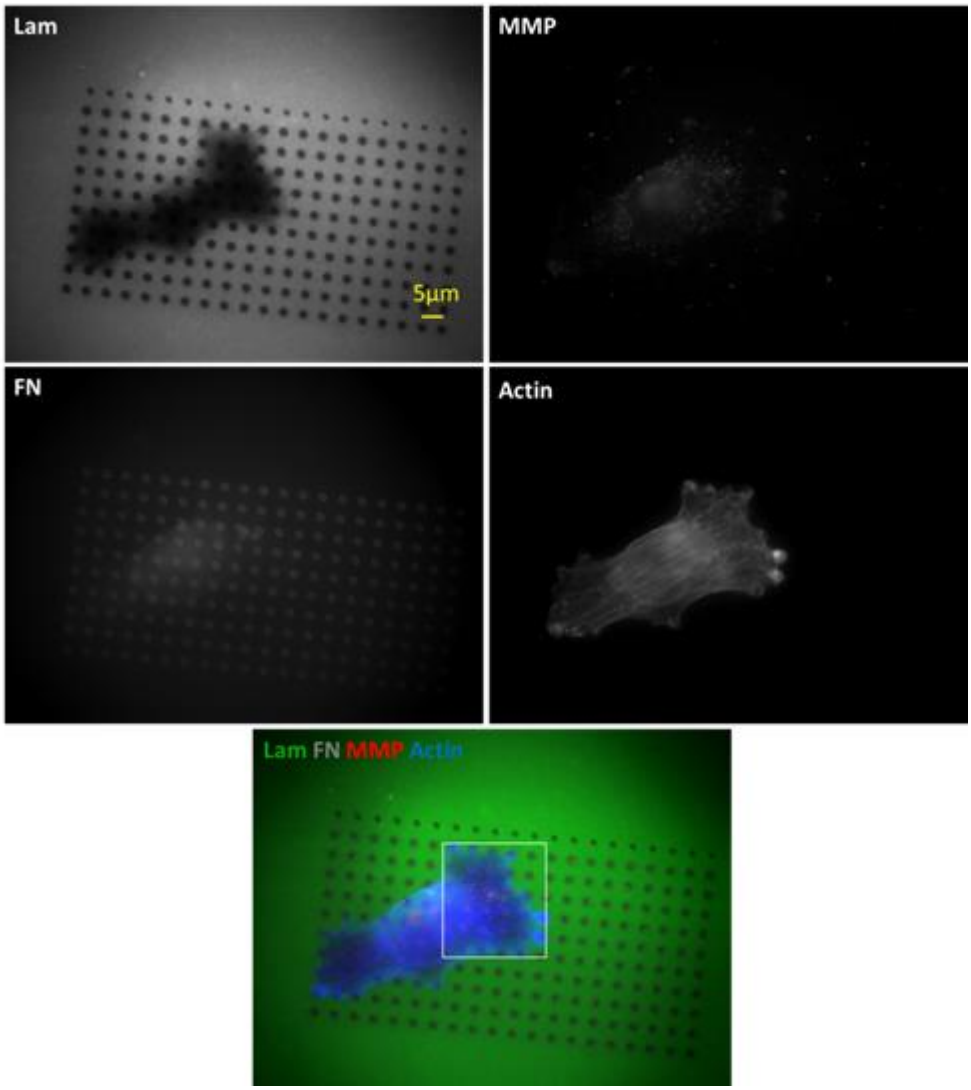

Figure 3.57. Transportation of MMPs on actin in a cell cultured in the presence of EGF for 24 hours on double active component nanoring patterns.

This figure shows a representative cell cultured in the presence of EGF for 24 hours on double active component nanoring patterns. Fibronectin, laminin, actin, mmp and merge images are represented in panels. Box in Figure 3.57 is magnified in Figure 3.58.

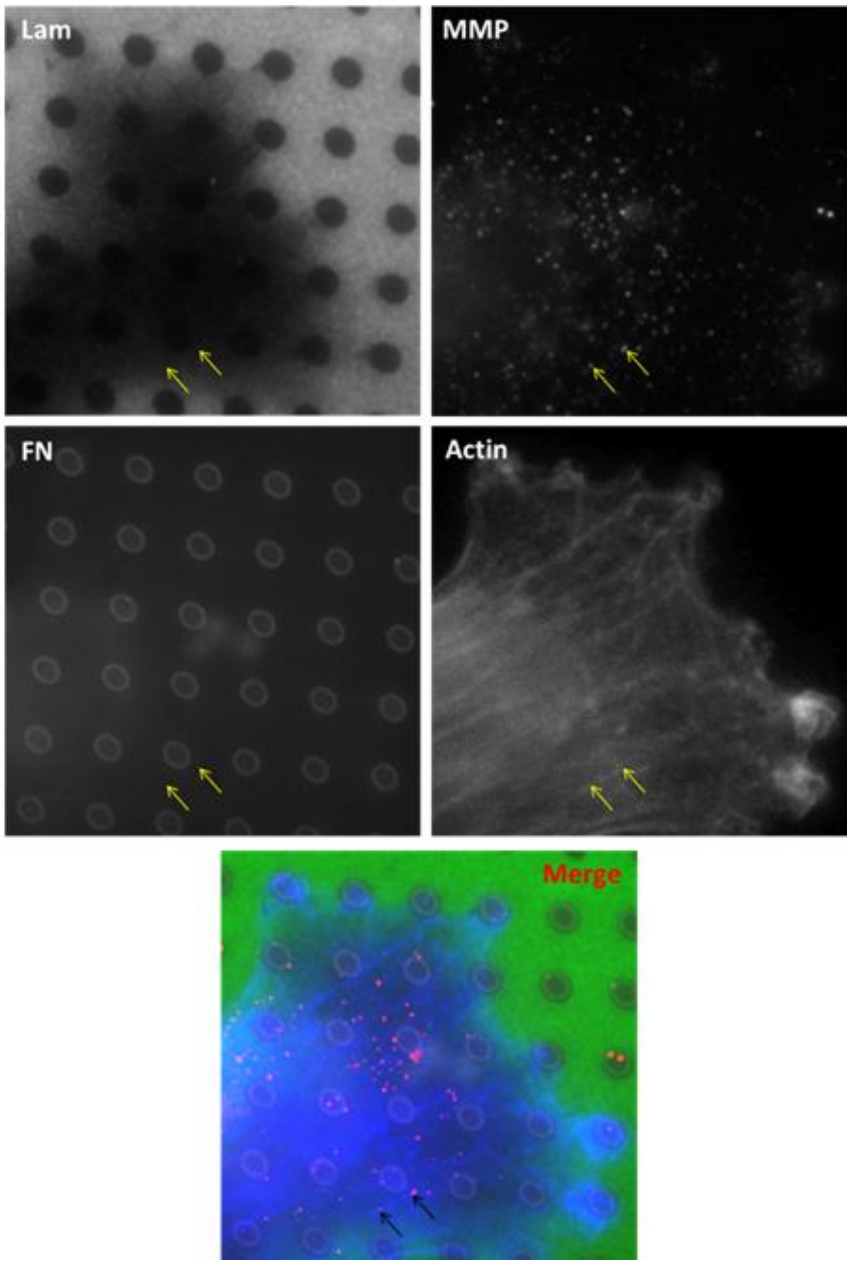

Figure 3.58. Magnification of MMPs transportation associated area of Figure 3.57.

This figure shows at high magnification a upper cell area of Figure 3.57. Yellow and black arrows show transportation of mmps on actin. There are degradations on laminin surface. We can say that some invadopodia transform into mature invadopodia so they can realize matrix degradation.

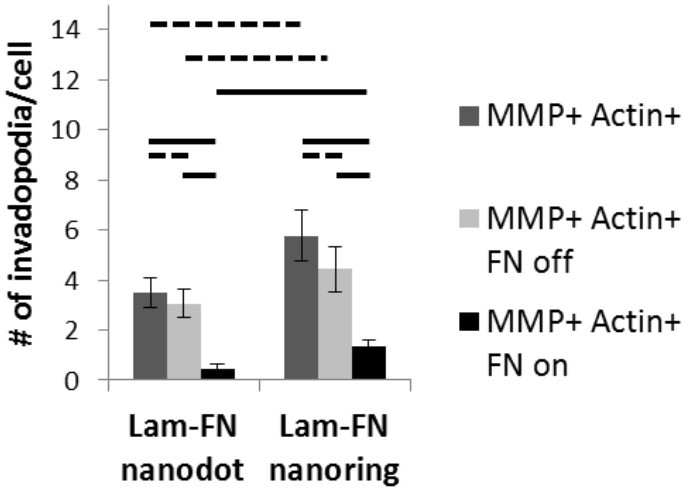

Figure 3.59. Quantitative distribution of transported mmps on actin on Laminin-Fibronectin nanodot and nanoring patterns.

MMP+ Actin+ Cortactin+ shows all mmps were transported on actin in MDA-MB-231 breast cancer cells, MMP+ Actin+ Cortactin+ FN on shows transportation of mmps on nanopatterns, MMP+ Actin+ Cortactin+ FN off shows transportation of mmps between nanopatterns. Horizontal straight lines show the statistical difference is $p<0.05$ at one tail level while horizantal dotted lines show the statistical difference is $p<0.05$ at two tail level. Number of mmps were transported on actin on nanoring patterns is more than on nanodot patterns. Cells prefer to transport mmps between fibronectin nanopatterns rather than on fibronectin nanopatterns for both patterns.

3.8. Distribution of Invadopodia on Gradient Nanopatterns

Polarization of invadopodia was analyzed in MDA-MB-231 breast cancer cells cultured in the presence of EGF for 24 hours on gradient patterns. Nanopatterns spasings were changing from 1μm to 10μm.

3.8.1. Distribution of Pre-invadopodia on Single Active Component Gradient Nanopatterns

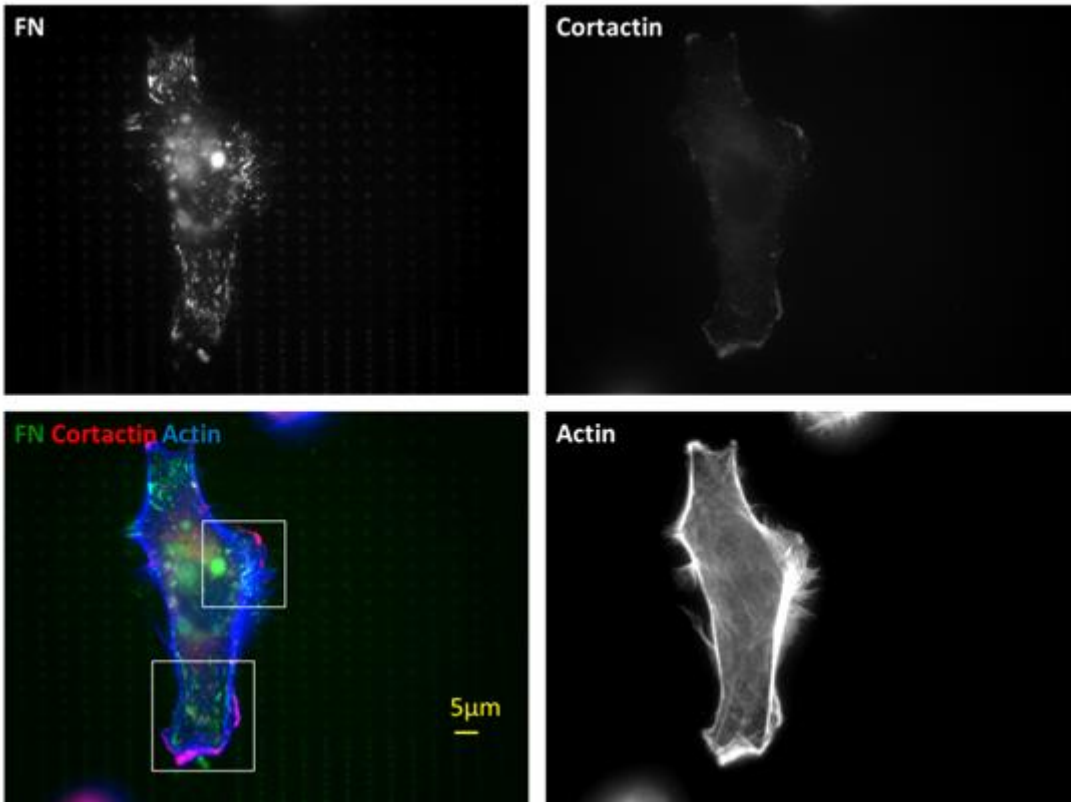

Figure 3.60. Pre-invadopodia in a cancer cell on single active component gradient nanopatterns.

This figure shows a representative cell cultured in the presence of EGF for 24 hours on single active component gradient nanopatterns. Fibronectin, actin, cortactin and merge images are represented in panels. Boxes in Figure 3.60 is magnified in Figure 3.61.

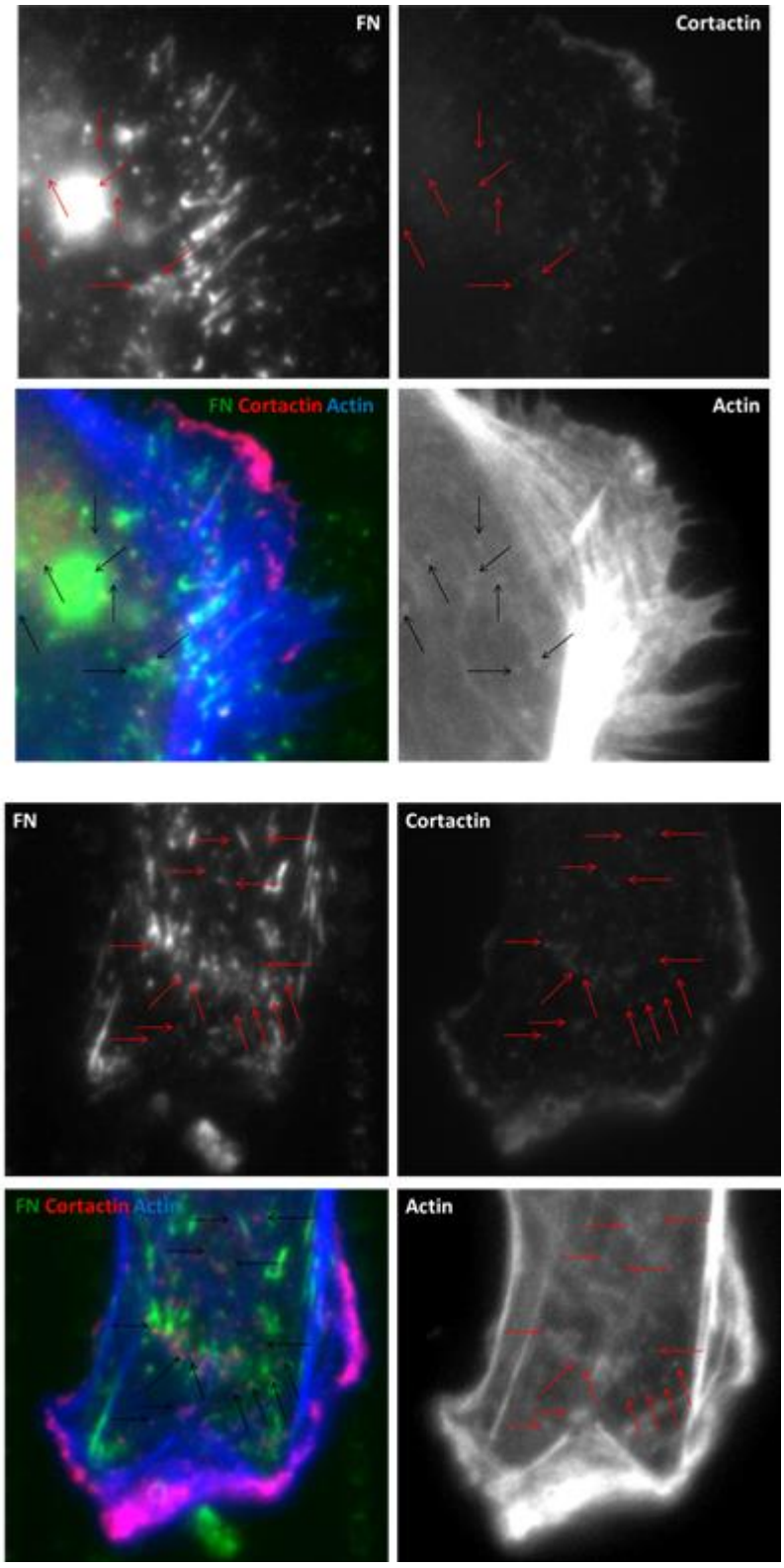

Figure 3.61. Magnification of pre-invadopodia associated areas of Figure 3.60.

First set of four images shows at high magnification the middle cell area andsecond set of four images shows the lower cell area of Figure 3.63. Black and red arrows show pre-invadopodia positive for cortactin and actin.

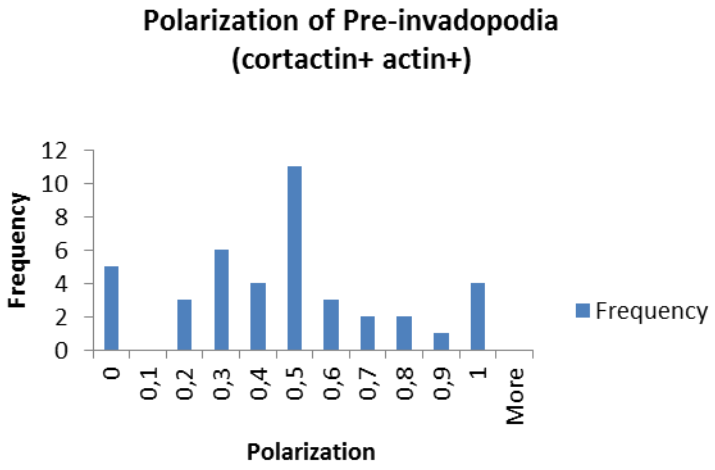

Figure 3.62. Polarization of pre-invadopodia in breast cancer cells on single active component gradient nanopatterns.

In the graph, 0.5 shows there is not polarization and 0.5-1.0 shows there is a polarization in same direction of gradient patterns. 0.0-0.5 shows there is not a polarization in same direction of gradient nanopatterns.

41 MDA-MB-231 breast cancer cells were used to polarization analyze for pre-invadopodia positive for cortactin and actin. There are high density of cells formed pre-invadopodia at minimum 1 μm and maximum 3 μm spacingson gradient patterns. We see there is not a polarization in same direction of gradient patterns for pre-invadopodia. This means number of pre-invadopodia is increasing in the gradient area where nanopatterns' spacings are increasing.

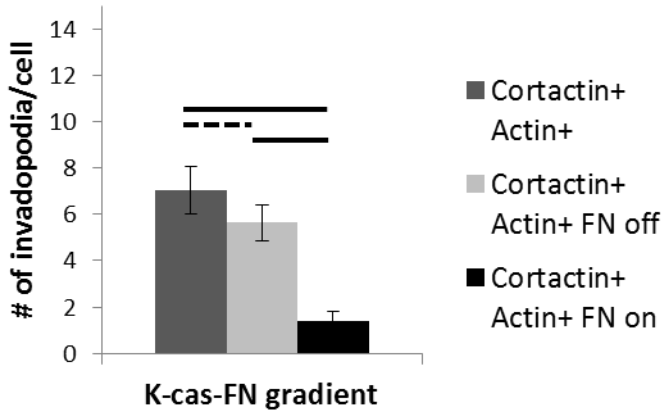

Figure 3.63. Quantitative distribution of pre-invadopodia per cell in cancer cells on single active component gradient nanopatterns.

Cortactin+ Actin+ shows all pre-invadopodia in MDA-MB-231 breast cancer cells, Cortactin+ Actin+ FN on shows pre-invadopodia formed on nanopatterns, Cortactin+ Actin+ FN off shows pre-invadopodia formed between nanopatterns. Horizontal straight lines show the statistical difference is $p<0.05$ at one tail level while horizantal dotted lines show the statistical difference is $p<0.05$ at two tail level. Cells prefer to form pre-invadopodia between gradient nanopatterns. There is a difference between formed pre-invadopodia on fibronectin nanopatterns and beetween fibronectin nanopatterns.

3.8.1.1. Distribution of MMPs were Transported on Actin on Single Active Component Gradient Nanopatterns

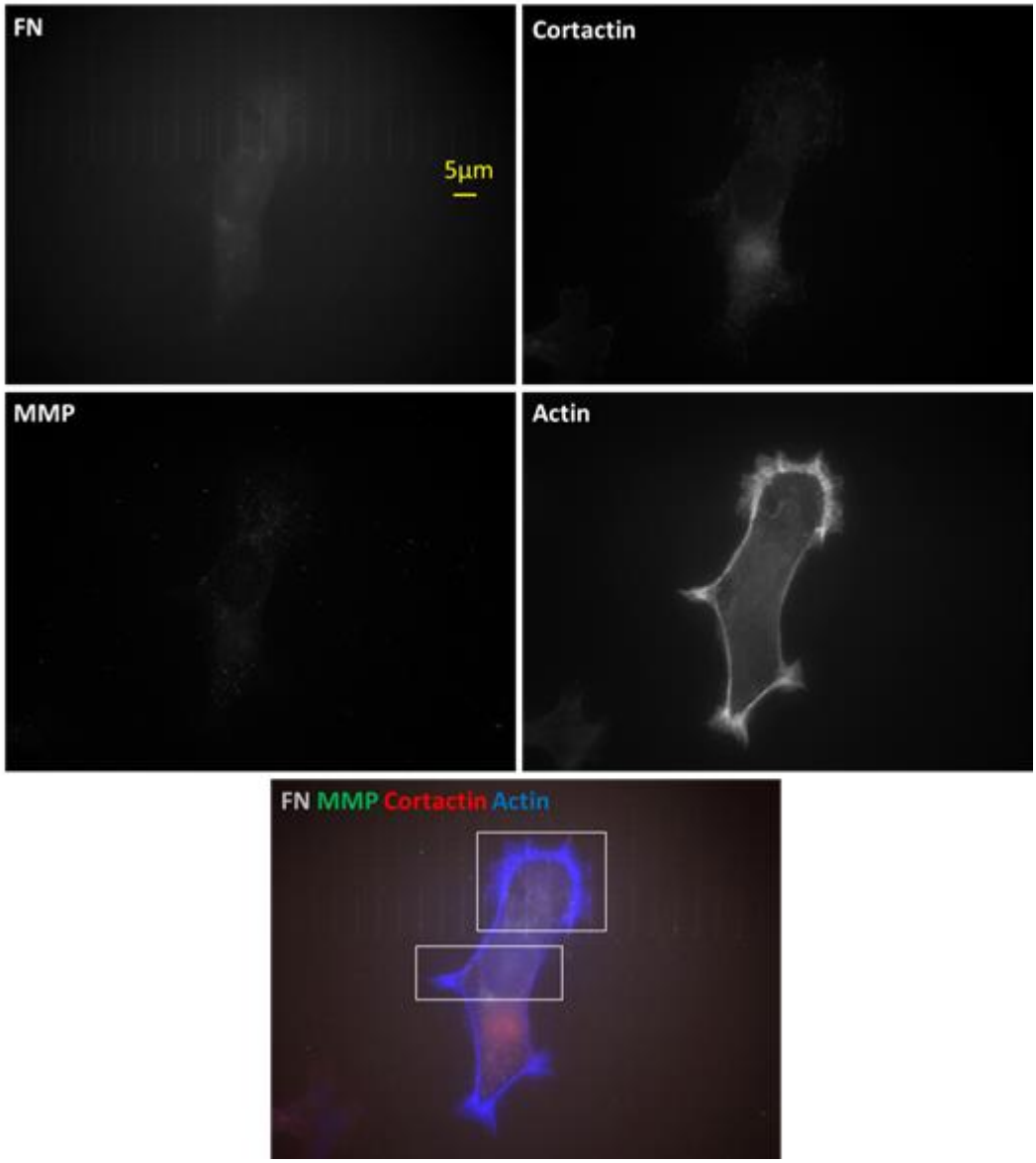

Figure 3.64. Transportation of MMPs on actin in a cell cultured in the presence of EGF for 24 hours on single active component gradient nanopatterns.

This figure shows a representative cell cultured in the presence of EGF for 24 hours on single active component gradient nanopatterns. Fibronectin, actin, cortactin, mmp and merge images are represented in panels. Boxes in Figure 3.64 is magnified in Figure 3.65.

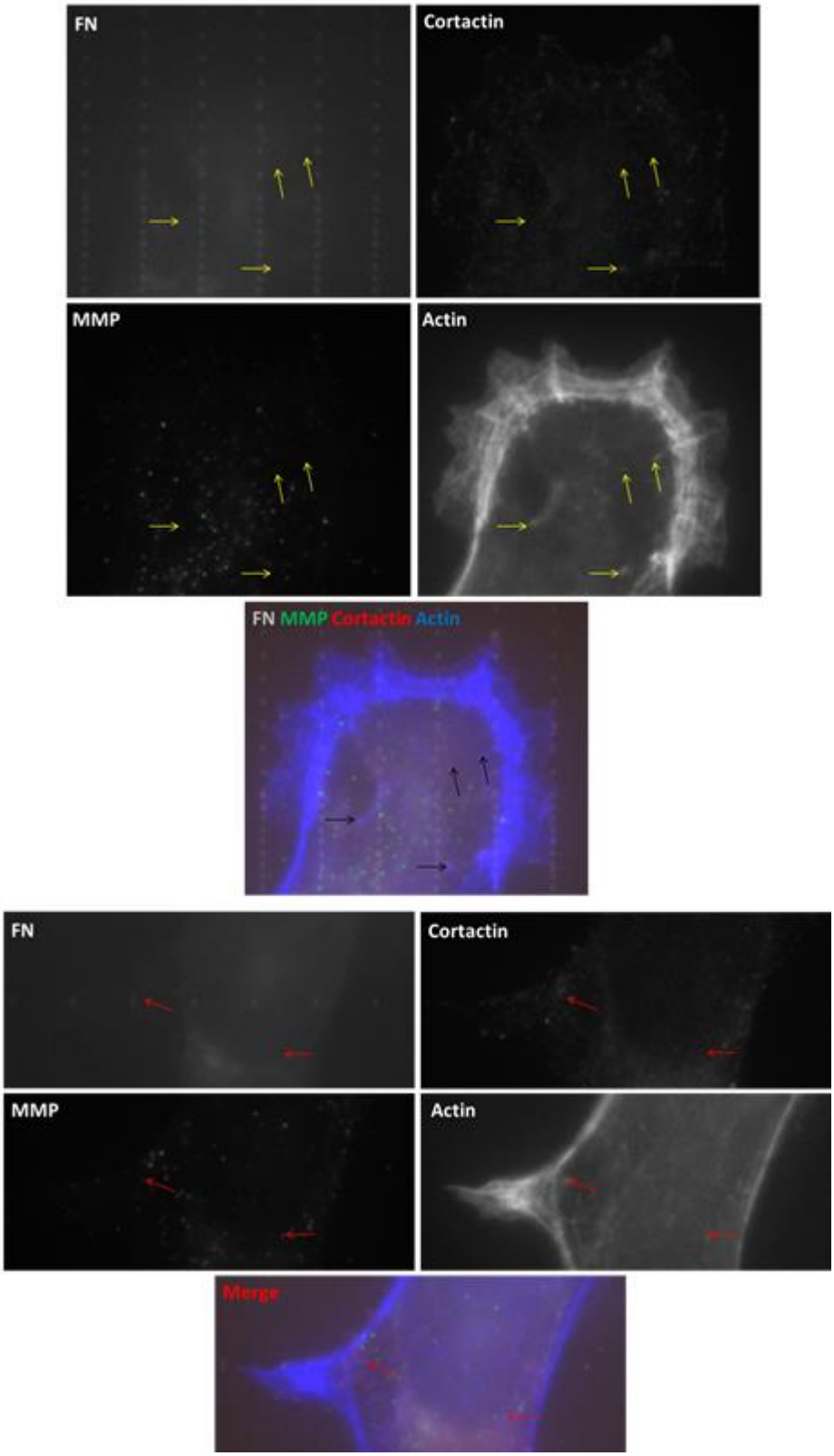

Figure 3.65. Magnification of invadopodia associated areas of Figure of 3.64.

First set of four images shows at high magnification the upper cell area and second set of four images shows the middle cell area of Figure 3.64. Yellow and black arrows show transported mmps on actin in first image set. Red arrows show transported MMPs on actin in second image set. Invadopodia positive for cortactin, actin and mmp were not observed on single active component gradient nanopatterns.

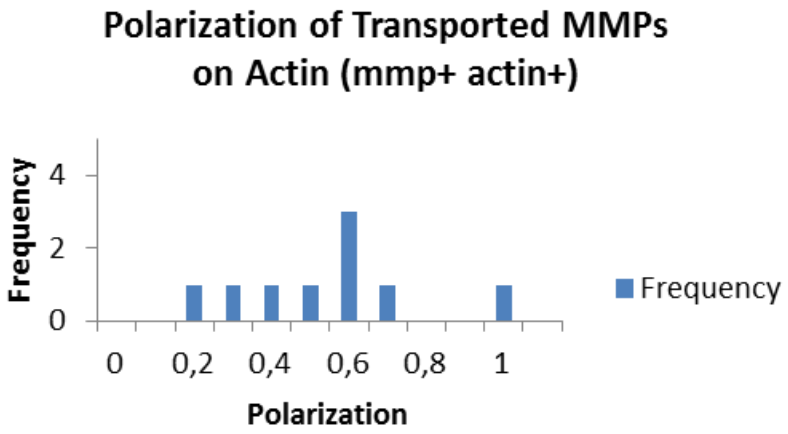

Figure 3.66. Polarization of transported MMPs on actin on single active component gradient nanopatterns.

In this graph, 0.5 shows there is not polarization and 0.5-1.0 shows there is a polarization in same direction of gradient patterns. 0.0-0.5 shows there is not a polarization in same direction of gradient nanopatterns.

9 MDA-MB-231 breast cancer cells were used to polarization analyze for transported mmps on actin. There are high density of cells transported mmps at minimum 1 μm and maximum 3 μm spacingson gradient patterns. We see there is not a polarization in same direction of gradient patterns for mmps transportation. This means number of pre-invadopodia is increasing in the gradient area where nanopatterns' spacings are decreasing.

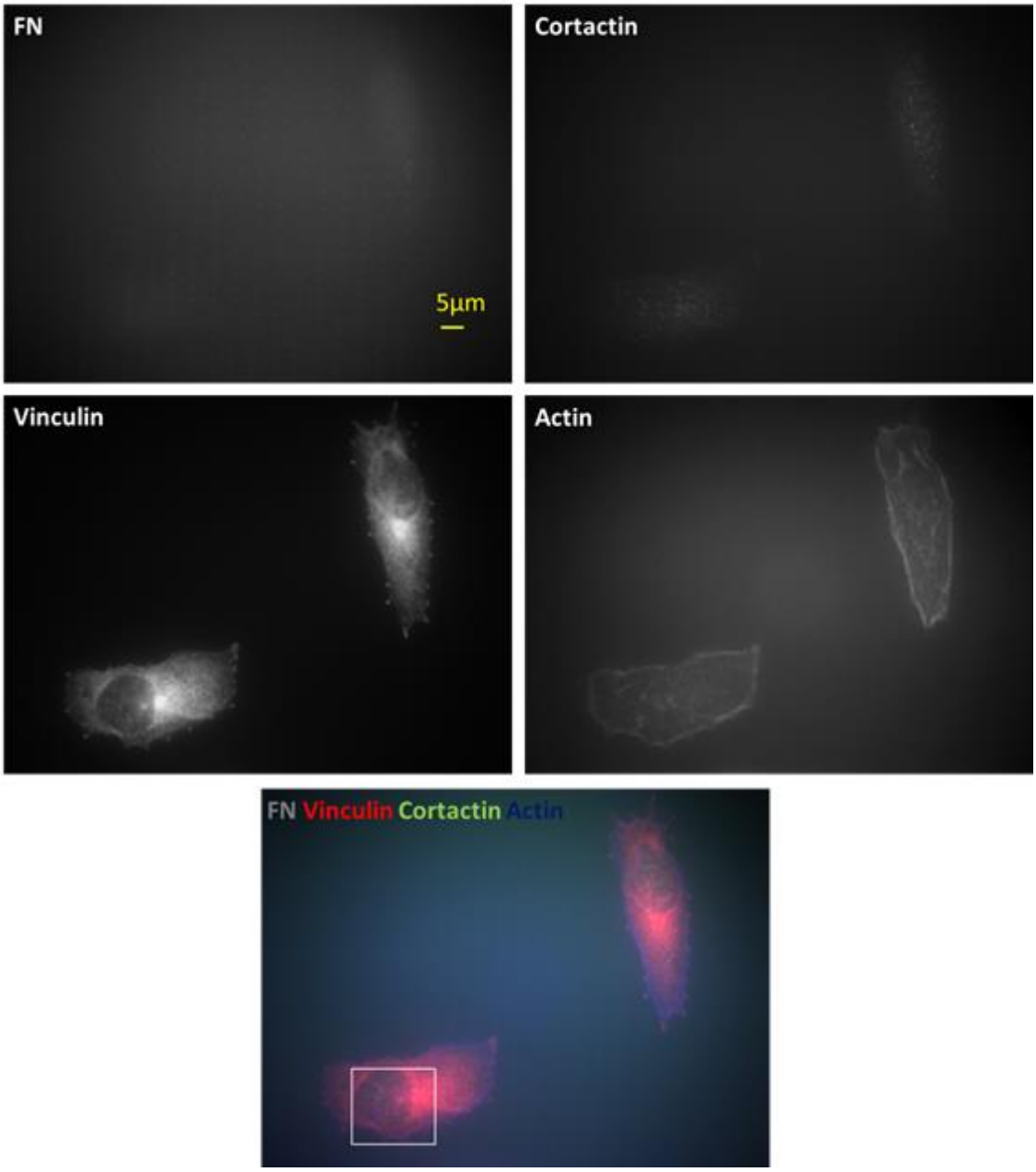

Figure 3.67. Pre-invadopodia and focal adhesions in a cell cultured in the presence of EGF for 24 hours on single active componenet gradient nanopatterns.

This figure shows a representative cell cultured in the presence of EGF for 24 hours on single active component gradient patterns. Fibronectin, actin, cortactin, vinculin and merge images are represented in panels. Boxes in Figure 3.67 is magnified in Figure 3.68.

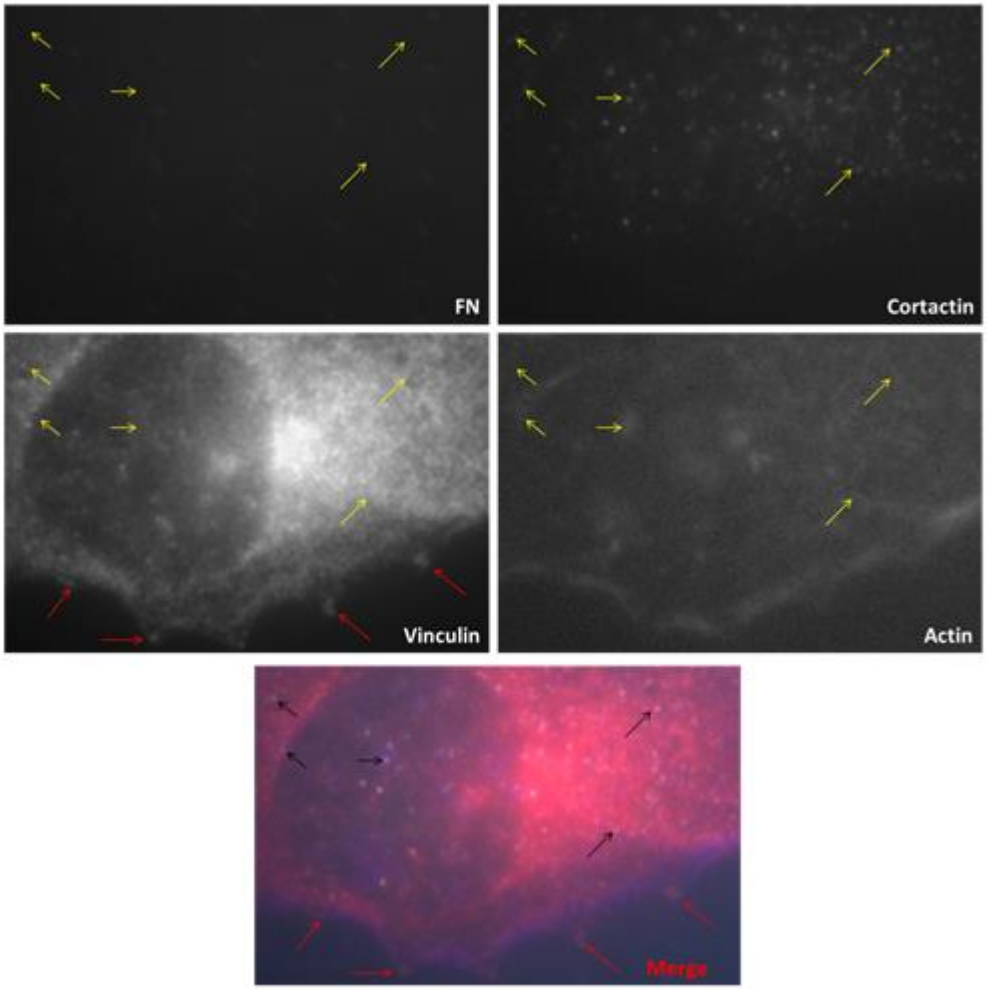

Figure 3.68. Magnification of invadopodia and focal adhesions associated area of Figure 3.67.

This figure shows at high magnification the middle cell area and of Figure 3.67. Yellow and black arrows show pre-invadopodia. Red arrows show focal adhesions. Pre-invadopodia prefer to form invadopodia between fibronectin gradient nanopatterns. There is no colocalization for focal adhesions and pre-invadopodia.

3.8.2. Distribution of Pre-invadopodia on Double Active Component Gradient Nanopatterns

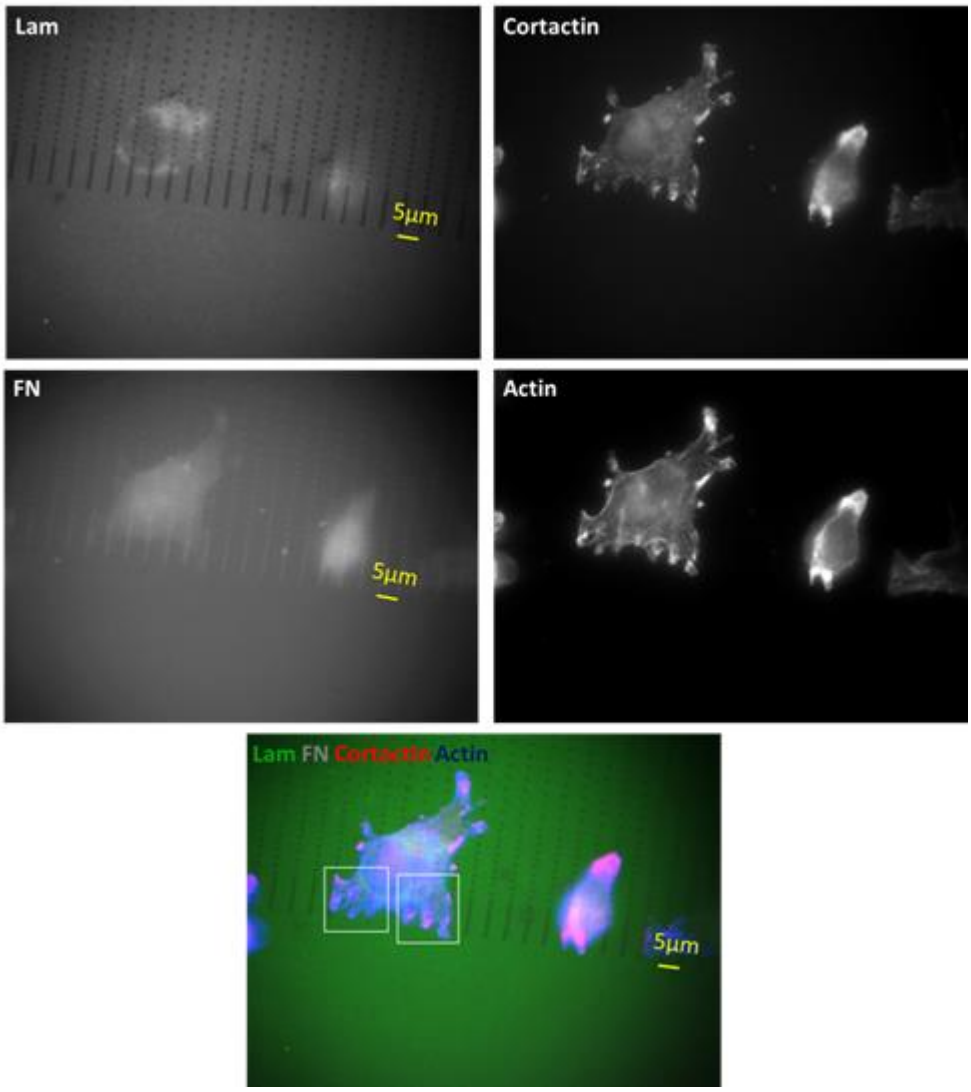

Figure 3.69. Distribution of pre-invadopodia per cell on double active component gradient nanopatterns.

This figure shows a representative cell cultured in the presence of EGF for 24 hours on double active component gradient nanopatterns. Fibronectin, laminin, cortactin, actin and merge images are represented in panels. Boxes in Figure 3.69 is magnified in Figure 3.70 and Figure 3.71.

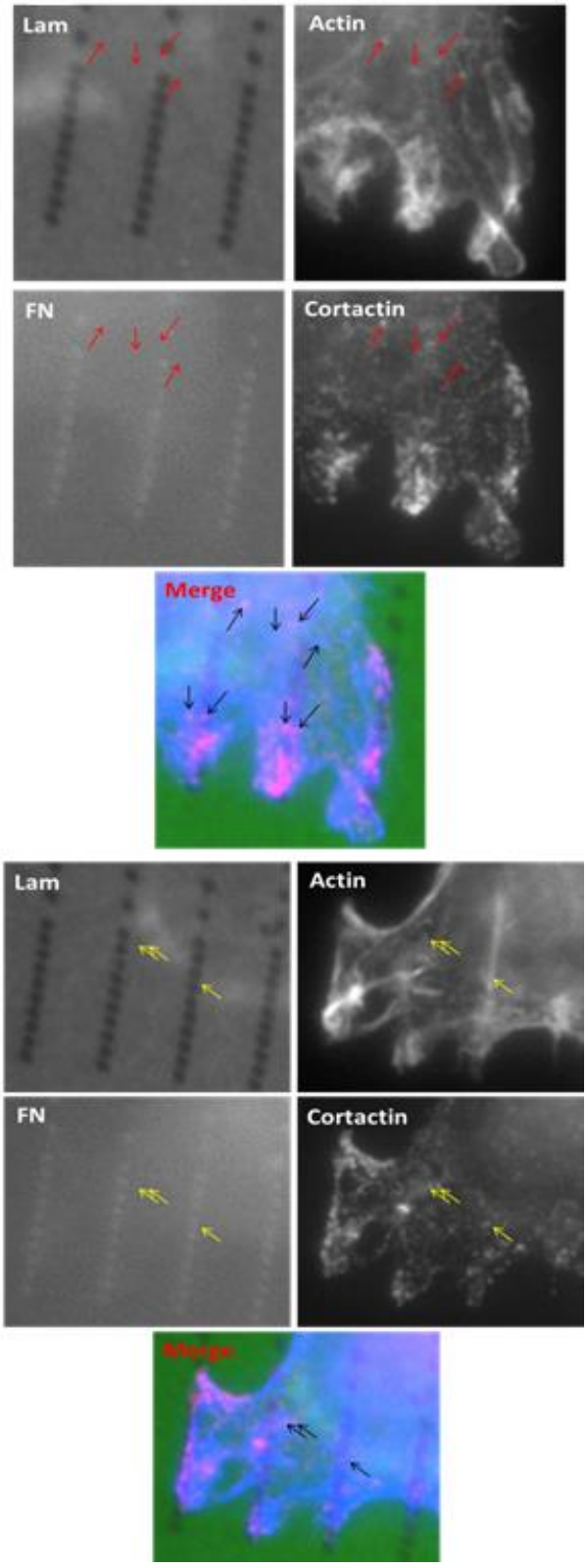

Figure 3.70. Magnification of invadopodia associated areas of Figure 3.69.

First set of five images shows at high magnification lower right cell area and second set of five images shows at high magnification lower left cell area of Figure 3.69. Black, red arrows in first set and black, yellow arrows show pre-invadopodia positive for cortactin and actin in second set.

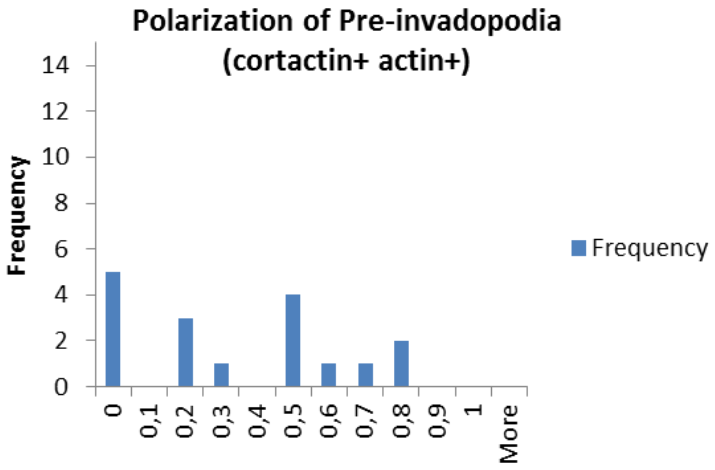

Figure 3.71. Polarization of pre-invadopodia on double active component gradient nanopatterns.

In this graph, 0.5 shows there is not polarization and 0.5-1.0 shows there is a polarization in same direction of gradient patterns. 0.0-0.5 shows there is not a polarization in same direction of gradient nanopatterns.

17 MDA-MB-231 breast cancer cells were used to polarization analyze for pre-invadopodia positive for cortactin and actin. There are high density of cells formed pre-invadopodia at minimum-maximum 1-2 μm and 1-3μm interval on gradient patterns. We see there is not a polarization in same direction of gradient patterns for pre-invadopodia. This means number of pre-invadopodia is increasing in the gradient area where nanopatterns spacingsare increasing.

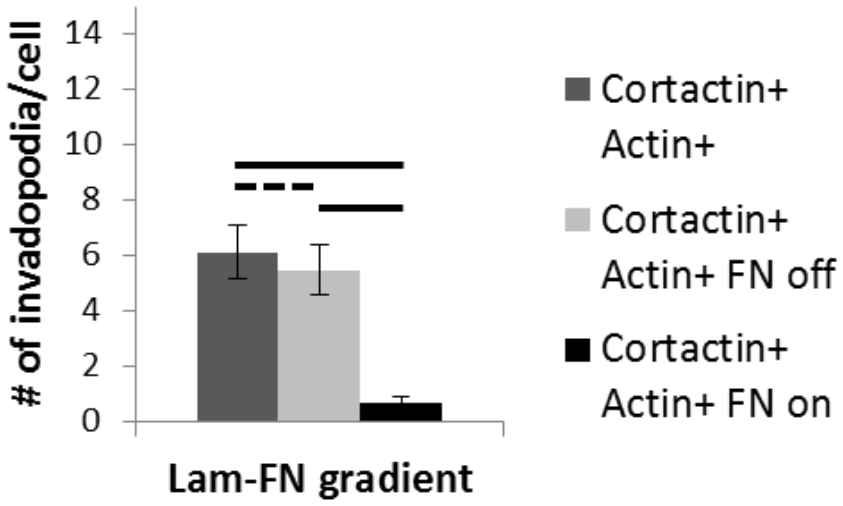

Figure 3.72. Quantitative distribution of pre-invadopodia per cell on double active component gradient nanopatterns.

Cortactin+ Actin+ shows all pre-invadopodia in MDA-MB-231 breast cancer cells, Cortactin+ Actin+ FN on shows pre-invadopodia formed on nanopatterns, Cortactin+ Actin+ FN off shows pre-invadopodia formed between nanopatterns. Horizontal straight lines show the statistical difference is $p<0.05$ at one tail level while horizantal dotted lines show the statistical difference is $p<0.05$ at two tail level. Cells prefer to form pre-invadopodia between gradient nanopatterns. There is a difference between formed pre-invadopodia on fibronectin nanopatterns and beetween fibronectin nanopatterns.

3.8.2.1. Distribution of MMPs were Transported on Actin on Double Active Component Gradient Nanopatterns

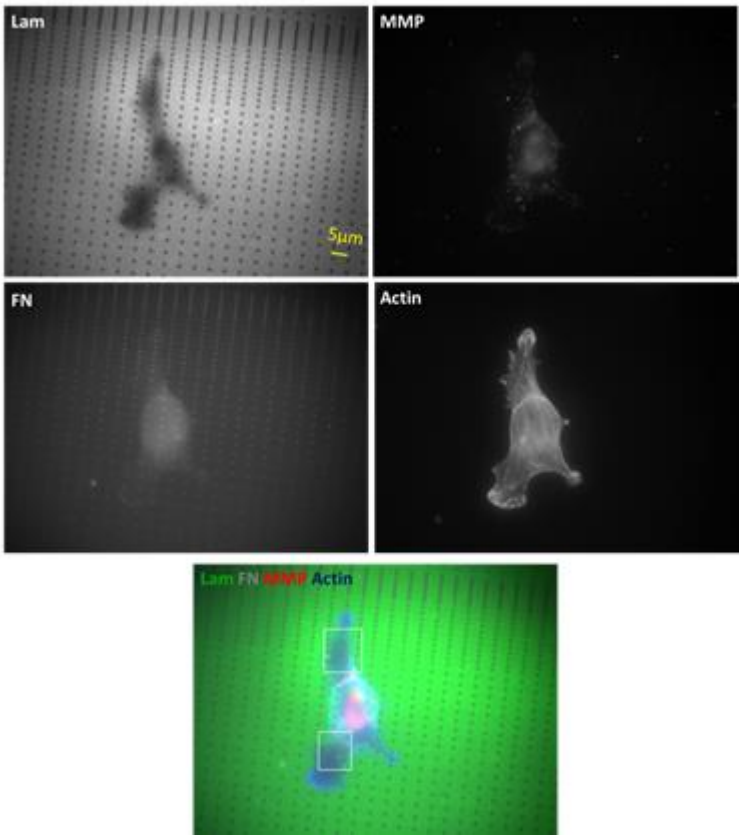

Figure 3.73. Transportation of MMPs on actin in a cell cultured in the presence of EGF for 24 hours on double active component gradient nanopatterns.

This figure shows a representative cell cultured in the presence of EGF for 24 hours on single active component gradient patterns. Laminin, fibronectin, actin, mmp and merge images are represented in panels. Boxes in Figure 3.73 is magnified in Figure 3.74.

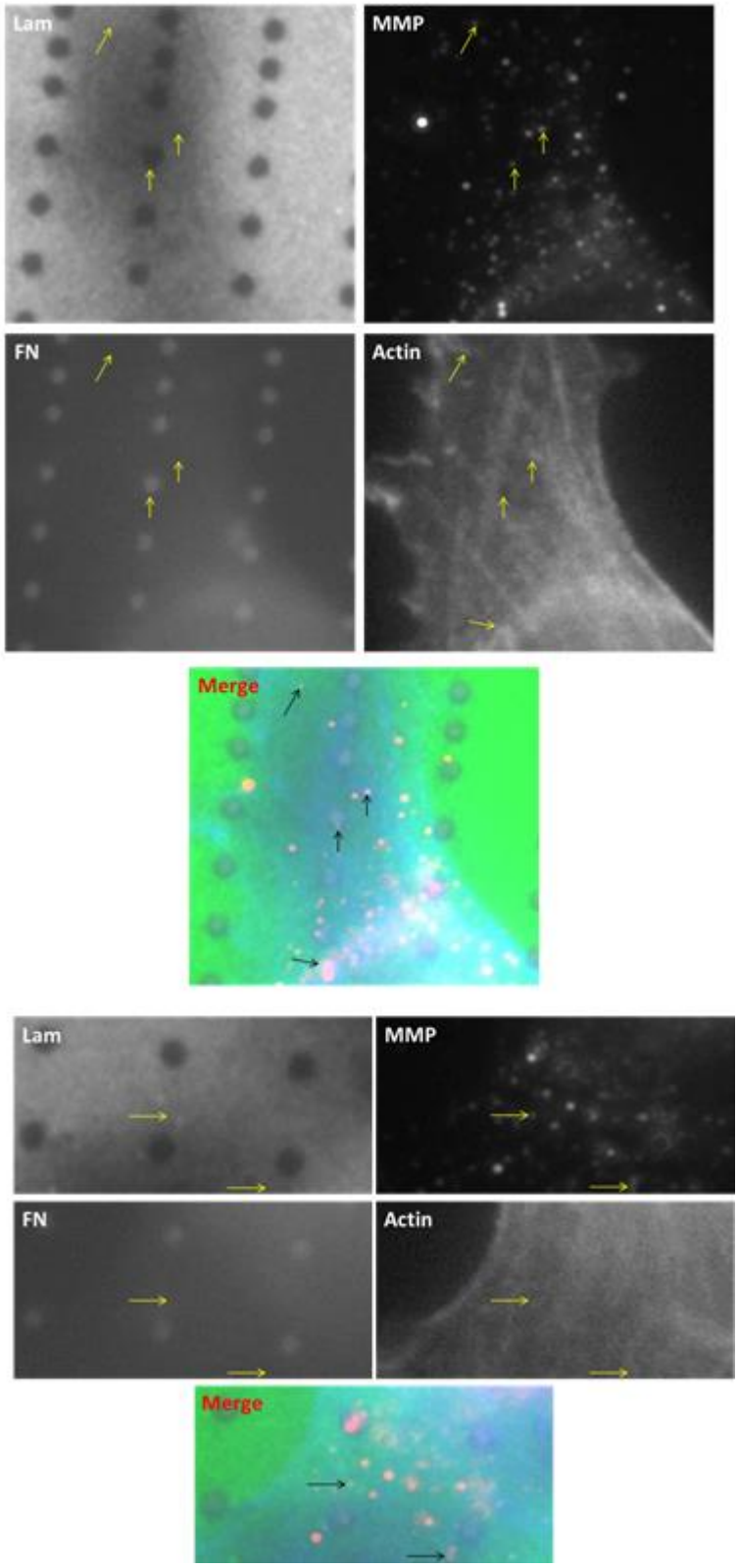

Figure 3.74. Magnification of transported MMPs asociated areas of Figure 3.73.

First set of five images shows at high magnification the upper cell area and second set of five images shows at high magnification the lower cell area of Figure 3.73. Yellow and black arrows show transported mmps on actin. There are degradations on laminin surface. We can say that some invadopodia transform into mature invadopodia so they can realize matrix degradation.

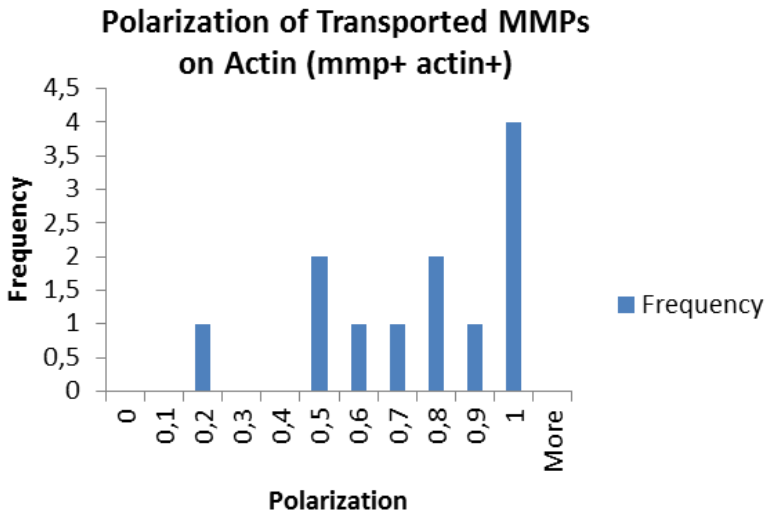

Figure 3.75. Polarization of transported MMPs on actin on double active component gradient nanopatterns.

In this graph, 0.5 shows there is not polarization and 0.5-1.0 shows there is a polarization in same direction of gradient patterns. 0.0-0.5 shows there is not a polarization in same direction of gradient nanopatterns.

12 MDA-MB-231 breast cancer cells were used to polarization analyze for transported mmps on actin. There are high density of cells transported mmps at minimum 1 μm and maximum 3 μm interval on gradient patterns. We see there is a polarization in same direction of gradient patterns for mmps transportation. This means number of pre-invadopodia are increasing in the gradient area where nanopatterns spacings are increasing. Invadopodia prefer to transport MMPs to the area which has high density for fibronectin.

CHAPTER 4

CONCLUSION

In this study, fibronectin, laminin proteins were used to coat silicon surfaces. EBL technique was used to create nanopatterns on these protein coated surfaces. Therefore mimic of cell microenviroment was provided and invadopodia formation in MDA-MB-231 breast cancer cells were examined.

Fibronectin and laminin coated surfaces were used as positive control while K-casein coated surfaces were used as negative control. One component experiments were performed with created fibronectin nanopatterns on K-casein coated surface and two component experiments were performed with fibronectin nanopatterns on laminin coated surface. Silicon surfaces were used after functionalization of surfaces was realized by APTES and gluteraldehyde for protein coating. Laminin is more degradable than fibronectin so laminin coated surfaces were used in 1-2 weeks. The most suitable microenviroment was obtained on surfaces had fibronectin nanopatters on laminin coated surface for two component experiments.

Cells adhesions weren't observed on K-casein control surfaces, but increment of invadopodia was observed on fibronectin control surfaces according to duration of cell culture (0 min, 10 min, 4 hours, 24 hours) in the presence of EGF. Number of invadopodia on laminin control surfaces was observed more than fibronectin surfaces. The absence of colocalization of focal adhesions and invadopodia were demonstrated in experiments were performed on fibronectin control, single and double component nanodot/nanoring patterns surfaces. This means invadopodia do not need focal adhesions during formation process. Cells prefer to form invadopodia between fibronectin nanopatterns rather than on fibronectin nanopatterns for bothsingle and double component experiments. These results indicate that localized cell adhesion is not required for invadopodia formation. Total number of pre-invadopodia per cell on nanodot patterns was observed more than nanoring patterns on both single and double active component.

Invadopodia positive for cortactin, mmp and actin were not observed on single active nanoring patterns surface. Reverse direction polarization was observed for pre-invadopodia on single and double active component gradient nanopatterns surface.

Cells prefer maximum 8 μm spacing to form invadopodia and 3 μm spacing to transport MMPs on actin on single active component gradient naopatterns. Cells prefer maximum 6 μm spacing to form invadopodia and 4 μm spacing to transport MMPs on actin on double active component gradient naopatterns. These results show cells prefer to form invadopodia in more narrow spacings at the transition from pre-invadopodia to mature invadopodia.

Degradations were observed on laminin, fibronectin and two component surfaces. According to these results we can say some invadopodia transformed into mature invadopodia and matrix degradations were realized using MMPs actively.

In conclusion, there are still debates on whether podosomes and invadopodia are different structure or have ability to transform into each other. This mentioned structure can be a dynamic structure which cells need to have during the development process and then transform into another structure leads to metastasis. If there is a dynamic structure, this transformation between podosomes and invadopodia or between pre-invadopodia and mature invadopodia can be blocked creating microenvironments are composed of different protein combinations. Intervention to metastasis even cancer can be provided immediately thanks to microenvironment associated works can clarify probably transformations.

REFERENCES

Alam, N., H. L. Goel, M. J. Zarif, J. E. Butterfield, H. M. Perkins, B. G. Sansoucy, T. K. Sawyer and L. R. Languino (2007). The integrin - growth factor receptor duet. Journal of Cellular Physiology 213(3): 649-653.

Artym, V. V., Y. Zhang, F. O. Seillier-Moiseiwitsch, K. M. Yamada and S. C. Mueller (2006). Dynamic interactions of cortactin and membrane type 1 matrix metalloproteinase at invadopodia: Defining the stages of invadopodia formation and function. Cancer Research 66(6): 3034-3043.

Ayala, I., M. Baldassarre, G. Caldieri and R. Buccione (2006). Invadopodia: A guided tour. European Journal of Cell Biology 85(3-4): 159-164.

Ayala, I., G. Giacchetti, G. Caldieri, F. Attanasio, S. Mariggio, S. Tete, R. Polishchuk, V. Castronovo and R. Buccione (2009). Faciogenital dysplasia protein fgd1 regulates invadopodia biogenesis and extracellular matrix degradation and is up-regulated in prostate and breast cancer. Cancer Research 69(3): 747-752.

Baldassarre, M., A. Pompeo, G. Beznoussenko, C. Castaldi, S. Cortellino, M. A. McNiven, A. Luini and R. Buccione (2003). Dynamin participates in focal extracellular matrix degradation by invasive cells. Molecular Biology of the Cell 14(3): 1074-1084.

Beaty, B. T., V. P. Sharma, J. J. Bravo-Cordero, M. A. Simpson, R. J. Eddy, A. J. Koleske and J. Condeelis (2013). Beta 1 integrin regulates arg to promote invadopodial maturation and matrix degradation. Molecular Biology of the Cell 24(11): 1661-1675.

Blouw, B., D. F. Seals, I. Pass, B. Diaz and S. A. Courtneidge (2008). A role for the podosome/invadopodia scaffold protein tks5 in tumor growth in vivo. European Journal of Cell Biology 87(8-9): 555-567.

Bowden, E. T., E. Onikoyi, R. Slack, A. Myoui, T. Yoneda, K. M. Yamada and S. C. Mueller (2006). Co-localization of cortactin and phosphotyrosine identifies active invadopodia in human breast cancer cells. Experimental Cell Research 312(8): 1240-1253.

Bravo-Cordero, J. J., L. Hodgson and J. Condeelis (2012). Directed cell invasion and migration during metastasis. Current Opinion in Cell Biology 24(2): 277-283.

Bravo-Cordero, J. J., M. Oser, X. M. Chen, R. Eddy, L. Hodgson and J. Condeelis (2011). A novel spatiotemporal rhoc activation pathway locally regulates cofilin activity at invadopodia. Current Biology 21(8): 635-644.

Buccione, R., G. Caldieri and I. Ayala (2009). Invadopodia: Specialized tumor cell structures for the focal degradation of the extracellular matrix. Cancer and Metastasis Reviews 28(1-2): 137-149.

Buday, L. and J. Downward (2007). Roles of cortactin in tumor pathogenesis. Biochimica Et Biophysica Acta-Reviews on Cancer 1775(2): 263-273.

Caldieri, G., I. Ayala, F. Attanasio and R. Buccione (2009). Cell and molecular biology of invadopodia. International review of cell and molecular biology, vol 275. K. W. Jeon. **275:** 1-34.

Carpenter, G. and S. Cohen (1990). Epidermal growth-factor. Journal of Biological Chemistry 265(14): 7709-7712.

Clark, E. S., B. Brown, A. S. Whigham, A. Kochaishvili, W. G. Yarbrough and A. M. Weaver (2009). Aggressiveness of hnscc tumors depends on expression levels of cortactin, a gene in the 11q13 amplicon. Oncogene 28(3): 431-444.

Cohen, S. (1962). Isolation of a mouse submaxillary gland protein accelerating incisor eruption and eyelid opening in the new-born animal. Journal of Biological Chemistry 237: 1555-1562.

DesMarais, V., H. Yamaguchi, M. Oser, L. Soon, G. Mouneimne, C. Sarmiento, R. Eddy and J. Condeelis (2009). N-wasp and cortactin are involved in invadopodium-dependent chemotaxis to egf in breast tumor cells. Cell Motility and the Cytoskeleton 66(6): 303-316.

Gil-Henn, H., A. Patsialou, Y. Wang, M. S. Warren, J. S. Condeelis and A. J. Koleske (2013). Arg/abl2 promotes invasion and attenuates proliferation of breast cancer in vivo. Oncogene 32(21): 2622-2630.

Gilcrease, M. Z. (2007). Integrin signaling in epithelial cells. Cancer Letters 247(1): 1-25.

Gimona, M. and R. Buccione (2006). Adhesions that mediate invasion. International Journal of Biochemistry & Cell Biology 38(11): 1875-1892.

Gimona, M., R. Buccione, S. A. Courtneidge and S. Linder (2008). Assembly and biological role of podosomes and invadopodia. Current Opinion in Cell Biology 20(2): 235-241.

Gligorijevic, B., J. Wyckoff, H. Yamaguchi, Y. R. Wang, E. T. Roussos and J. Condeelis (2012). N-wasp-mediated invadopodium formation is involved in intravasation and lung metastasis of mammary tumors. Journal of Cell Science 125(3): 724-734.

Harris, R. C., E. Chung and R. J. Coffey (2003). Egf receptor ligands. Experimental Cell Research 284(1): 2-13.

Kessenbrock, K., V. Plaks and Z. Werb (2010). Matrix metalloproteinases: Regulators of the tumor microenvironment. Cell 141(1): 52-67.

Labernadie, A., C. Thibault, C. Vieu, I. Maridonneau-Parini and G. M. Charriere (2010). Dynamics of podosome stiffness revealed by atomic force microscopy. Proceedings of the National Academy of Sciences of the United States of America 107(49): 21016-21021.

Leight, J. L., D. L. Alge, A. J. Maier and K. S. Anseth (2013). Direct measurement of matrix metalloproteinase activity in 3d cellular microenvironments using a fluorogenic peptide substrate. Biomaterials 34(30): 7344-7352.

Lewis, S., A. Locker, J. H. Todd, J. A. Bell, R. Nicholson, C. W. Elston, R. W. Blamey and I. O. Ellis (1990). Expression of epidermal growth-factor receptor in breast-carcinoma. Journal of Clinical Pathology 43(5): 385-389.

Li, R. H., G. Li, L. Deng, Q. L. Liu, J. Dai, J. Shen and J. Zhang (2010). Il-6 augments the invasiveness of u87mg human glioblastoma multiforme cells via up-regulation of mmp-2 and fascin-1. Oncology Reports 23(6): 1553-1559.

Linder, S. (2009). Invadosomes at a glance. Journal of Cell Science 122(17): 3009-3013.

Linder, S. and M. Aepfelbacher (2003). Podosomes: Adhesion hot-spots of invasive cells. Trends in Cell Biology 13(7): 376-385.

Linder, S., C. Wiesner and M. Himmel (2011). Degrading devices: Invadosomes in proteolytic cell invasion. Annual review of cell and developmental biology, vol 27. R. Schekman, L. Goldstein and R. Lehmann. **27:** 185-211.

Lizarraga, F., R. Poincloux, M. Romao, G. Montagnac, G. Le Dez, I. Bonne, G. Rigaill, G. Raposo and P. Chavrier (2009). Diaphanous-related formins are required for invadopodia formation and invasion of breast tumor cells. Cancer Research 69(7): 2792-2800.

MacGrath, S. M. and A. J. Koleske (2012). Cortactin in cell migration and cancer at a glance. Journal of Cell Science 125(7): 1621-1626.

Mader, C. C., M. Oser, M. A. O. Magalhaes, J. J. Bravo-Cordero, J. Condeelis, A. J. Koleske and H. Gil-Henn (2011). An egfr-src-arg-cortactin pathway mediates functional maturation of invadopodia and breast cancer cell invasion. Cancer Research 71(5): 1730-1741.

Magalhaes, M. A. O., D. R. Larson, C. C. Mader, J. J. Bravo-Cordero, H. Gil-Henn, M. Oser, X. M. Chen, A. J. Koleske and J. Condeelis (2011). Cortactin phosphorylation regulates cell invasion through a ph-dependent pathway. Journal of Cell Biology 195(5): 903-920.

Massague, J. and A. Pandiella (1993). Membrane-anchored growth-factors. Annual Review of Biochemistry 62: 515-541.

McNiven, M. A. (2013). Breaking away: Matrix remodeling from the leading edge. Trends in Cell Biology 23(1): 16-21.

Memon, A. A., B. S. Sorensen and E. Nexo (2006). The epidermal growth factor family has a dual role in deciding the fate of cancer cells. Scandinavian Journal of Clinical & Laboratory Investigation 66(7): 623-630.

Moro, L., L. Dolce, S. Cabodi, E. Bergatto, E. B. Erba, M. Smeriglio, E. Turco, S. F. Retta, M. G. Giuffrida, M. Venturino, J. Godovac-Zimmermann, A. Conti, E. Schaefer, L. Beguinot, C. Tacchetti, P. Gaggini, L. Silengo, G. Tarone and P. Defilippi (2002).

Integrin-induced epidermal growth factor (egf) receptor activation requires c-src and p130cas and leads to phosphorylation of specific egf receptor tyrosines. Journal of Biological Chemistry 277(11): 9405-9414.

Mueller, S. C., G. Ghersi, S. K. Akiyama, Q. X. A. Sang, L. Howard, M. Pineiro-Sanchez, H. Nakahara, Y. Yeh and W. T. Chen (1999). A novel protease-docking function of integrin at invadopodia. Journal of Biological Chemistry 274(35): 24947-24952.

Oser, M., A. Dovas, D. Cox and J. Condeelis (2011). Nck1 and grb2 localization patterns can distinguish invadopodia from podosomes. European Journal of Cell Biology 90(2-3): 181-188.

Oser, M., C. C. Mader, H. Gil-Henn, M. Magalhaes, J. J. Bravo-Cordero, A. J. Koleske and J. Condeelis (2010). Specific tyrosine phosphorylation sites on cortactin regulate nck1-dependent actin polymerization in invadopodia. Journal of Cell Science 123(21): 3662-3673.

Oser, M., H. Yamaguchi, C. C. Mader, J. J. Bravo-Cordero, M. Arias, X. M. Chen, V. DesMarais, J. van Rheenen, A. J. Koleske and J. Condeelis (2009). Cortactin regulates cofilin and n-wasp activities to control the stages of invadopodium assembly and maturation. Journal of Cell Biology 186(4): 571-587.

Packard, B. Z., V. V. Artym, A. Komoriya and K. M. Yamada (2009). Direct visualization of protease activity on cells migrating in three-dimensions. Matrix Biology 28(1): 3-10.

Ruoslahti, E., Y. Yamaguchi, A. Hildebrand and W. A. Border (1992). Extracellular-matrix growth-factor interactions. Cold Spring Harbor Symposia on Quantitative Biology 57: 309-315.

Sabeh, F., R. Shimizu-Hirota and S. J. Weiss (2009). Protease-dependent versus -independent cancer cell invasion programs: Three-dimensional amoeboid movement revisited. Journal of Cell Biology 185(1): 11-19.

Sainsbury, J. R. C., A. J. Malcolm, D. R. Appleton, J. R. Farndon and A. L. Harris (1985). Presence of epidermal growth-factor receptor as an indicator of poor prognosis in patients with breast-cancer. Journal of Clinical Pathology 38(11): 1225-1228.

Schoumacher, M., R. D. Goldman, D. Louvard and D. M. Vignjevic (2010). Actin, microtubules, and vimentin intermediate filaments cooperate for elongation of invadopodia. Journal of Cell Biology 189(3): 541-556.

Seals, D. F., E. F. Azucena, I. Pass, L. Tesfay, R. Gordon, M. Woodrow, J. H. Resau and S. A. Courtneidge (2005). The adaptor protein tks5/fish is required for podosome formation and function, and for the protease-driven invasion of cancer cells. Cancer Cell 7(2): 155-165.

Sharma, V. P., R. Eddy, D. Entenberg, M. Kai, F. B. Gertler and J. Condeelis (2013). Tks5 and ship2 regulate invadopodium maturation, but not initiation, in breast carcinoma cells. Current Biology 23(21): 2079-2089.

Singh, A. B. and R. C. Harris (2005). Autocrine, paracrine and juxtacrine signaling by egfr ligands. Cellular Signalling 17(10): 1183-1193.

Stylli, S. S., A. H. Kaye and P. Lock (2008). Invadopodia: At the cutting edge of tumour invasion. Journal of Clinical Neuroscience 15(7): 725-737.

Stylli, S. S., T. T. I. Stacey, A. H. Kaye and P. Lock (2012). Prognostic significance of tks5 expression in gliomas. Journal of Clinical Neuroscience 19(3): 436-442.

Taipale, J. and J. KeskiOja (1997). Growth factors in the extracellular matrix. Faseb Journal 11(1): 51-59.

Thery, M., V. Racine, M. Piel, A. Pepin, A. Dimitrov, Y. Chen, J. B. Sibarita and M. Bornens (2006). Anisotropy of cell adhesive microenvironment governs cell internal organization and orientation of polarity. Proceedings of the National Academy of Sciences of the United States of America 103(52): 19771-19776.

Wang, W. G., S. Goswami, K. Lapidus, A. L. Wells, J. B. Wyckoff, E. Sahai, R. H. Singer, J. E. Segall and J. S. Condeelis (2004). Identification and testing of a gene expression signature of invasive carcinoma cells within primary mammary tumors. Cancer Research 64(23): 8585-8594.

Wang, W. G., J. B. Wyckoff, S. Goswami, Y. R. Wang, M. Sidani, J. E. Segall and J. S. Condeelis (2007). Coordinated regulation of pathways for enhanced cell motility and chemotaxis is conserved in rat and mouse mammary tumors. Cancer Research 67(8): 3505-3511.

Yamada, K. M. and S. Even-Ram (2002). Integrin regulation of growth factor receptors. Nature Cell Biology 4(4): E75-E76.

Yamaguchi, H. (2012). Pathological roles of invadopodia in cancer invasion and metastasis. European Journal of Cell Biology 91(11-12): 902-907.

Yamaguchi, H., M. Lorenz, S. Kempiak, C. Sarmiento, S. Coniglio, M. Symons, J. Segall, R. Eddy, H. Miki, T. Takenawa and J. Condeelis (2005). Molecular mechanisms of invadopodium formation: The role of the n-wasp-arp2/3 complex pathway and cofilin. Journal of Cell Biology 168(3): 441-452.

Yilmaz, M. and G. Christofori (2009). Emt, the cytoskeleton, and cancer cell invasion. Cancer and Metastasis Reviews 28(1-2): 15-33.

Yu, X. Z. and L. M. Machesky (2012). Cells assemble invadopodia-like structures and invade into matrigel in a matrix metalloprotease dependent manner in the circular invasion assay. Plos One 7(2).

Yu, X. Z., T. Zech, L. McDonald, E. G. Gonzalez, A. Li, I. Macpherson, J. P. Schwarz, H. Spence, K. Futo, P. Timpson, C. Nixon, Y. F. Ma, I. M. Anton, B. Visegrady, R. H. Insall, K. Oien, K. Blyth, J. C. Norman and L. M. Machesky (2012). N-wasp coordinates the delivery and f-actin-mediated capture of mt1-mmp at invasive pseudopods. Journal of Cell Biology 199(3): 527-544.